LASER DENSIFICATION OF GEL SILICA GALSSES AND OPTICAL APPLICATIONS

BY

TAIPAU CHIA

A DISSERTATION PRESENTED TO THE GRADUATE SCHOOL
OF THE UNIVERSITY OF FLORIDA IN PARTIAL FULFILLMENT
OF THE REQUIREMENTS FOR THE DEGREE OF
DOCTOR OF PHILOSOPHY

UNIVERSITY OF FLORIDA

1992

Copyright 1992

by

Tsipau Chua

To my husband, Shanshan, and my parents

with gratitude for their constant support

ACKNOWLEDGEMENTS

This dissertation would not have been possible without the assistance of many I wish to express my sincere appreciation to the chairman of my committee, Dr L. L. Hench, for his guidance and invaluable suggestions during the experimental part of this work and the preparation of the manuscript. I would also like to thank the other members of my committee Dr D E Clark, Dr C K Hsieh, Dr R E Hummel and Dr J H Simmons, for their continued encouragement and suggestions.

Special thanks go to Dr.J K West, who always had time to discuss the research problems and provided continued interest throughout this research project. I wish to thank Guy P La Torre for his patience and the technical assistance during the work. I would also like to express my sincere gratitude to Chaobin Qin who offered great support in writing the programs of the thermal model Additional thanks go to all my friends and colleagues for their ever-present assistance.

Appreciation is also extended to my host friend Frances Fabrick for her continued encouragement. My best friends Drs G Shieh and S Jan offer invaluable support during my stay in the United States.

I especially wish to thank my husband for his continued support and encouragement during our graduate studies and to my parents and my parents in-law who have always encouraged me to pursue further education

Financial support from the Air Force Office of Scientific Research under contract number F49620-88 C 0073, GelTech Inc contract number 4910-4509-322 12 is gratefully acknowledged

TABLE OF CONTENTS

ACKNOWLEDGEMENTS iv

LIST OF TABLES ix

LIST OF FIGURES x

KEY TO SYMBOLS xvii

ABSTRACT xix

CHAPTER

1 INTRODUCTION 1
  1 1 Background 1
  1 2 Advantages of Laser Densification of Gel-Silica Glasses 2
  1 3 Introduction 3
    1 3 1 Motivations of This Study 3
    1 3 2 Objectives 4
    1 3 3 Introduction 5

2 LITERATURE REVIEW 8
  2 1 Sol-Gel Processing 8
    2 1 1 Historical Sketch 8
    2 1 2 Review of Sol-Gel Processing and Science 10
    2 1 3 Optical Applications of Sol-Gel Glasses 13
  2.2 Heat Treatment on Glasses by using a CO_2 Laser 24
  2.3 Microlenses 26
    2 3.1 Review of Optical Information Processing 26
    2 3 2 Review of Microlenses 28
    2 3 3 Ray Theory of a Planar Gradient-index Microlenses 34
    2 3 4 Geometry of Waveguide Geodesic Microlenses 38
    2.3 5 Applications of Microlenses 40
      (a)Integrated Optics 40
      (b)Micro-optics 42
      (c)Stacked Planar Optics 45
  2 4 Review of FTIR 50

3 PROCESSING AND PROPERTIES OF GEL-SILICA GLASSES 58
  3 1 Introduction 58
    3 1 1 Goals of Sol-Gel Processing 58
    3.1 2 Properties of Furnace Densified Gel-Silica Glass 60
  3.2 Preparation of Type VI Gel-Silica Glasses 61

Properties of Gel-Silica Glasses by Furnace Densification 67
3.3 Physical properties 67
3.3.1 Bulk Density and Pore Texture Analysis 67
3.3.2 Results and Discussions 71
3.3.3 Conclusions 74
3.4 Thermal Property 74
3.4.1 Dilatometer Analysis 74
3.5 Mechanical Property 78
3.5.1 Load/Size Effect in Microhardness 78
3.5.2 Microhardness Analysis 83
3.6 Optical Properties 87
3.6.1 UV/VIS/NIR Spectroscopy 87
3.6.2 FTIR Reflectance Spectroscopy 90
3.6.3 FTIR Reflectance Microspectra Analysis 91
3.6.4 Refractive Index Analysis at 0.633 µm 95
3.6.5 Refractive Index Analysis at 3.57 µm 100
3.6.6 Composite Diagram of the PMP and Refractive Index 102
3.7 Conclusions 106

4. LASER DENSIFICATION OF GEL-SILICA GLASS 108
4.1 Introduction 108
4.2 Method of Laser Densification 110
4.2.1 Method of Laser Densification 110
4.3.2 Methods of Characterization 113
4.3 Results 116
4.3.1 Bulk Density Effects on Laser Densification 116
4.3.2 Surface Investigation of Heat Affected Zone 120
4.3.3 Cross Section Investigation of Heat Affected Zone 132
4.3.4 Stability after Laser Densification 137
4.3.5 Comments on Previous Work[Slo90] 138
4.3.6 Mechanisms of the Instability 141
4.4 Mechanisms of Laser Induced Densification 142
4.5 Conclusions 146

5. APPLICATIONS IN OPTICS 148
5.1 Introduction 148
5.2 Advantages of Laser Densification 152
5.3 Geodesic Microlenses(M-I) 153
5.4 Planar GRIN Microlenses 156
5.5 Theoretical Analysis 159
5.5.1 Theoretical Analyses 159
5.5.2 Comparisons 164
5.6 Negative Microlenses(M-III) 165
5.7 Multimode GRIN Channel Waveguide 169
5.8 Conclusions 170

6 CHARACTERIZATIONS OF LASER DENSIFICATION OPTICS 172
6.1 Introduction 172
6.2 Characterization Methods 173
6.2.1 Characterization Methods of the M-II Microlenses 173
6.2.2 Characterization Method of the M-III Microlenses 177
6.3 Characterization Results and Discussion 179

6 3 1 Surface IR Spectra Analysis 179
6 3 2 IR Spectra Analysis of the Cross Section 183
6 3 3 Index Profile 187
6 3 4 Optical Properties of M-II Microlenses 189
6.3 5 Profile of the Focused Spot 195
6 3 6 Characterization of the M-III Microlenses 195
6 4 Conclusions 198

7 LASER DENSIFICATION MODELINGs 200
7 1 Thermal Model of a Laser Densifiod Track 200
7 1 1 Abstract 200
7 1.2 Introduction 200
7 1 3 Formulation of the Physical Model 201
7 1 4 Results and Discussion 205
7 1 5 Conclusions 214
7.2 Thermal Model of a Laser Densified Spot 214
7 2.1 Introduction 214
7 2 2 Computation Method 216
7 2 3 Computation Results 221
7 2 4 Comparisons 240
7 2.5 Conclusions 248

8 SUMMARY AND CONCLUSIONS 249
8 1 Summary 249
8 2 Conclusions 253

APPENDIX 257

A KRAMERS-KRONIG METHOD 257
B COMPUTER PROGRAM OF THE LASER DENSIFICATION MODELING 260

LIST OF REFERENCES 276

BIOGRAPHICAL SKETCH 288

LIST OF TABLES

Table — Page

2 1 Materials, fabrication methods, and properties of different types of optical microlens 33

2 2 Assignments of molecular vibration modes of the silica glass 52

3 1 Degree of densification and corresponding refractive indices and index change at 0 633 μm of gel silica glasses 97

4 1 Laser densification conditions of the three points within envelop C of Figure 4 5 119

6 1 Optical properties of the GRIN planar gel silica microlenses 193

6 2 Optical property of the negative microlens at various processing parameters 197

7 1 Calculational variables and values 204

7 2 Calculated variables, sample specifications, and property values 225

LIST OF FIGURES

Figure Page

2.1 A flow chart of sol-gel processing steps 11

2.2 The light ray trajectory in a GRIN medium, after [Iga84] 35

2.3 Ray trajectory in a three-dimension DI medium, a planar microlens Region I is an index distributed region and II a uniform one, after [Iga84] 36

2.4 Cross section view of a typical geodesic lens 39

2.5 Integrated optical microlens, after [Fei88][Car91] 41

2.6 A radio-frequency spectrum analyzer, after [Hut87] 43

2.7 Micro optical lenses 44

2.8 Microlens array used in the optical computer, after [Fei88][Ham90a] 46

2.9 A planar GRIN microlens array 47

2.10 Stacking of planar optical devices, after [Iga84] 48

2.11 Schematics of longitudinal-optic and transverse-optic lattice vibration modes of a monoatomic chain of atoms 54

2.12 Schematics of local vibrational motions of asymmetrical stretching and symmetrical stretching of the oxygen atoms with respect to the silicon atom in amorphous silica, after Kirk[Kir88] 55

3.1 Process sequence of gel-silica glass(pore radius= 1.2 nm) with scaled structural characteristics 62

3.2 Schematic of the aging schedule for a pure gel-silica monolith 63

3.3 Schematic of the drying schedule for a pure gel silica monolith 64

3.4 Schematic of the thermal stabilization schedule for pure gel-silica optical substrates 66

3.5 Typical chemical stabilization and densification schedule for gel-silica glass optical substrates 68

3.6 Pore volumes and bulk densities of gel-silica glasses at increasing densification temperature 72

3.7 Surface area and pore radii of gel-silica glasses at increasing densification temperature 73

3.8 Dilatometric behavior of gel silica glasses exposed to ambient atmosphere. ... 76

3.9 Schematic of ISE effect in solids, illustrating the ISE boundary, after [Li91] 80

3.10 A relationship between the measured microhardness of a partially densified gel-silica glass with increasing indentation load 84

3.11 Vickers hardness number of gel-silica glasses at increasing densification temperature 85

3.12 Vickers hardness number of gel-silica glasses at increasing bulk density 86

3.13 UV/VIS/NIR transmission of (a) a Type VI porous gel-silica glass and (b) a Type V full density gel-silica glass 89

3.14 Normal reflectance micro-spectra of four gel-silica glasses at increasing densification temperatures 93

3.15 A relationship between the refractive indices at 0.633 μm and the bulk densities of the gel-silica glasses, densification temperatures are indicated 98

3.16 Index of refraction versus density for silica gels, gel-silica glasses, and crystallines phases, after [Hen90] 99

3.17 A typical normal infrared reflectance micro-spectrum(a), a transformed refractive index spectrum(b) and a transformed absorbance spectrum(c) of a Type V gel silica glass 101

3.18 Refractive indices at 3.57 μm(line 1) and at 0.633 μm(line 2) of gel silica glasses at increasing degree of densification 103

3.19 Peak maximum position(PMP at left side) of gel silica glass substrates with different bulk densities densified at different temperatures G1(180°C), G2(800°C), G3(1000°C), G4(1150°C), and refractive index n at 0.633 μm(at right side) of A1(180°C), A2(615°C), A3(900°C), and G4(1150°C) 105

4.1 Process sequence of treatment of gel-silica sample prior to laser densification 111

4.2 Instrumental arrangement of laser densification on gel silica glasses 112

4.3 Corresponding CO_2 laser energy at varied pulse widths and power settings 114

4.4 Energy profile of the CO_2 laser used in this study 115

4.5 Laser densification conditions of the gel samples with different starting densities Corresponding surface profiles of points 1 2, and 3 are also shown above 117

4.6 Comparisons of laser densified spot sizes of a dry gel and a partially densified gel at different pulse widths 122

4.7 Appearance of a laser densified spot on a dry gel 123

4.8 Appearance of laser densified spots on gel samples with different starting densities 124

4.9 Surface VHN profile of a laser densified spot on a gel sample, laser densification conditions are also indicated 125

4.10 Surface VHN profile of a laser densified spot on a gel-silica sample(A5), laser densification conditions are also indicated 127

4.11 Surface VHN profile of a laser densified spot on a gel-silica sample(A6), laser densification conditions are also indicated 128

4.12 Schematic of micro-FTIR investigation on a laser densified spot(upper) and the corresponding PMP profile(lower) with indicated laser densification conditions of this spot 130

4.13 Appearance of surface (a) and cross section(b) and (c) of laser densified spots on a gel silica sample 133

4.14 Cross section VHN profile of a laser densified spot on a gel silica sample, laser densification conditions are also indicated 134

4.15 Schematic of micro-FTIR investigation on the cross section of a laser densified spot(upper) and the corresponding PMP profile(lower) with indicated laser densification conditions of this spot 136

4.16 Stability of surface VHN profile of a laser densified spot on a gel sample measured at different times after the laser densification(Track 1, 2 and 3), laser densification conditions of this spot are also indicated 139

4.17 Schematic of permanent shrinkage mechanism. condensation of neighboring silanol groups on pore surface resulting in pore closure and densification 143

4.18 Structure characteristics before and after laser densification of a Type VI gel silica glass 145

5.1 Three types of microlenses M-I, M-II, M-III produced by laser irradiation on gel-silica glasses 149

5.2 Diverged optical rays by a M-I compound lens, the optical ray(dashed lines) are deflected in a wider angle if a GRIN region does not exist 151

5.3 Instrumental arrangements(a) for the observation of focusing phenomenon of a M-I geodesic microlens the result is shown in (b) 155

5.4 A M II microlens produced after polishing the diameter is ~ 800μm 157

5.5 Focusing phenomenon of arrays of the M II GRIN planar microlens on a porous gel silica sample The result is shown in (b) 158

5.6 Magnification of a character s using a gel-silica M-II GRIN planar microlens on a porous gel-silica substrate 160

5.7 Relationships between the index change(Δn) and the calculated focal length and the nominal numerical aperture of lenses 162

5.8 Relationships between the radius(=a), GRIN depth(=d), and the calculated focal length of lenses 163

5.9 Focusing phenomenon of a M-III negative microlens arrays on a silica substrate, the focusing phenomenon is due to a diffraction effect 167

5.10 Images of a lamp source of a microscope(b) formed by three negative negative microlenses on a silica substrate observed using a microscope(a) 168

6.1 Instrumental arrangement for the measurement of the focal length of the GRIN planar gel silica microlens 175

6.2 Instrumental arrangement for the measurement of the coupling efficiency of the GRIN planar gel silica microlens 176

6.3 Cross section of a negative microlens made by laser heating on the surface of a pure silica glass 178

6.4 Method of obtaining IR reflectance spectra across a laser densified spot using FTIR microspectroscopy(a) and the results(b), the asymmetric and symmetric stretching vibrations of Si-O-Si bonds are indicated 180

6.5 Comparisons of the micro-FTIR spectrum of a Type V full density gel silica glass(a) and the spectrum of the middle of the laser densified spot(b) 182

6.6 Method of obtaining IR reflectance spectra across the cross section of a laser densified spot at the same depth using FTIR microspectroscopy 184

6.7 Results of the micro-IR spectra along the cross section of the laser densified spot, the peak maximum positions of the asymmetric(left) and symmetric(right) stretching vibration modes are indicated 185

6.8 The profile of the peak maximum positions on the cross section of the laser densified at the same depth, corresponding numbers of the investigated area are indicated 186

6.9 The refractive index profile on the surface of the laser densified spot at 0.633 μm, corresponding numbers of the investigated area are indicated 188

6.10 The refractive index profile on the surface of the laser densified spot at 3.57 μm, corresponding numbers of the investigated area are indicated 190

6.11 Properties of the gel-silica glasses with increasing bulk density 191

6.12 The effect of the index change on the nominal numerical aperture 194

6.13 The intensity profile of the focused spot formed by a GRIN planar gel-silica microlens 196

7.1 Physical system of laser densification under investigation 202

7.2 Relative temperature profiles at different heat diffusivities 206

7.3 Relative temperature profiles at different heat transfer coefficients 207

7.4 Relative temperature profiles at different laser power settings 208

7.5 Relative temperature profiles at different travelling velocities 209

7.6 Three-dimensional temperature distribution on X-Z plane 211

7.7 Three-dimensional temperature distribution on Y-Z plane 212

7.8 Convergence of the solution of equation (7.2) 213

7.9 A fictitious exact solution and an approximate solution from a finite-difference method, after [Shi84] 217

7.10 A mesh structure of the glass substrate designed for the computations of the three-dimension temperature distribution by laser irradiation, each point in the mesh represents a data point 218

7.11 A three-dimensional temperature profile produced by laser irradiation on the surface of a silica glass, with more than 1000 data points per volume 220

7.12 Physical system of laser densification under investigation 222

7.13 Schematic of the heat affected zone and the temperature profiles on the surface (a) and the x-cross section(b) of a laser irradiated spot 223

7.14 A relationship between the calculated maximum temperature and the time step 224

7.15 Surface temperature profiles on the X Y plane at different time steps 227

7.16 Temperature profiles on the cross section of a laser irradiated region at different time steps 228

7.17 A three-dimensional diagram shows the temperature profile on the surface of a laser densified spot, dimensions and temperature range are also indicated 229

7.18 A contour map of the temperature profile on the surface of a laser densified spot, dimensions and temperature range are also indicated 230

7.19 A three-dimensional diagram shows the temperature profile on the cross section of a laser densified spot, dimensions and temperature range are also indicated 232

7.20 A contour map of the temperature profile on the cross section of a laser densified spot, dimensions and temperature range are also indicated 233

7.21 The calculated heating and cooling curves by laser irradiation on a pure silica glass 234

7.22 The temperature profiles on the surface of the glass substrate upon heating 236

7.23 The temperature profiles on the surface of the glass substrate upon cooling 237

7.24 The temperature profiles on the cross section of the glass substrate upon heating 238

7.25 The temperature profiles on the cross section of the glass substrate upon cooling 239

7.26 Comparison of the calculated temperature profile with the VHN profile on the surface along the diameter of the laser densified spot as shown in (a), normalized temperature and VHN varied with position are shown in (b) 241

7.27 Comparison of the calculated temperature profile with the PMP profile on the surface along the diameter of the laser densified spot as shown in (a), normalized temperature and PMP varied with position are shown in (b) 243

7.28 Comparison of the calculated temperature profile with the VHN profile in the middle and along the cross section of the laser densified spot as shown in (a), normalized temperature and VHN varied with position are shown in (b) 244

7 29 Comparison of the calculated temperature profile with the PMP profile in the middle along the cross section of the laser densified spot as shown in (a), normalized temperature and PMP varied with position are shown in (b) 246

7 30 Comparison of the calculated temperature profile with the PMP profile along the cross section at the same depth of the laser densified spot as shown in (a) normalized temperature and PMP varied with position are shown in (b) 247

Key to Symbols

AS	Asymmetric Stretching vibration of Si-O-Si
BD	Bulk Density of the gel sample
BET	A gas adsorption analysis developed by Brunauer, Emmett and Teller[Bru38]
DI	Deionized water
DSC	Differential Scanning Calorimeter
DTA	Differential Thermal Analyzer
FDR	Full Dense Region of the laser densified gel silica glass, region with VHN ~ 812±18
FL	Focal length of an optical lens
GRIN	Gradient refractive index
HAZ	Heat Affected Zone, region with VHN > VHN of the substrate
INDO	Intermediate Neglect of Differential Overlap molecular orbital theory
IR	Infrared spectrum
ISE	Indentation load/size effect
k	Wavenumber(1/cm)
LDC	Laser Densification Conditions including L1, L2(inches), pulse width(sec) and power(mA)
LIS	A spot produced by laser irradiation
LO	Longitudinal-Optical, Maxwellian electric polarization is parallel to the propagation vector of the IR wave[Gal83]
MCVD	Modified Chemical Vapor Deposition
n	Refractive index

NA	Numerical Aperture of an optical lens
NBO/BO	Ratio of non-bridging oxygen (NBO i e SiOH) to bridging oxygen bonds (BO i e Si-O-Si)
NBS	National Bureau Standard
NIR	Near Infrared
NIST	National Institute of Standards and Technology
PMP	Peak Maximum Position(1/cm)
PSR	Proportional Specimen Resistance in microhardness theory[Li91]
SD	Starting Density, initial bulk density of the gel substrate before laser irradiation
SS	Symmetric Stretching vibration of Si O-Si
T_g	Glass transition temperature
TGA	Thermogravimetric analysis
TMOS	Tetramethoxysilane
TO	Transverse-Optical, Maxwellian electric polarization is transverse to the propagation vector of the IR wave[Gal83]
UV	Ultraviolet
VHN	Vickers Hardness Number
VHN_m	Vickers Hardness Number of a Type V gel silica glass ~812±18
VLSI	Very large Scale Integrated Circuit
ΔAS	Change in frequency Asymmetric Stretching vibration of Si-O-Si
ΔBD	Change in bulk density
Δn	Change in refractive index
ΔVHN	Change in Vickers hardness number

Abstract of Dissertation Presented to the Graduate School of the University of Florida in
Partial Fulfillment of the Requirements for the Degree of Doctor of Philosophy

LASER DENSIFICATION OF GEL SILICA GLASSES AND OPTICAL APPLICATIONS

BY

Tapas Chia

August, 1992

Chairman: Dr. Larry L. Hench
Major Department: Materials Science and Engineering

The goals of this study are to densify locally Type VI porous gel silica glasses using a CO_2 laser, characterize the properties of laser densified regions and explore optical applications such as gradient refractive index(GRIN) microlenses, geodesic microlenses and micro-optical arrays.

Ranges of substrate density from 1.15 g/c.c. to 2.15 g/c.c were studied and densities of > 1.8 g/c.c. produced stable optical elements and achieved a full density region of 2.2 g/c.c. The laser irradiated region has a higher refractive index than the gel silica substrate(Δn=0.01 to 0.09) and can be used to manipulate optical rays for focusing or imaging or function as GRIN micro-optical and integrated-optical components. Characterization of the surface and the cross section of the laser densified region includes microhardness measurement and micro-IR reflectance spectroscopy. It is demonstrated that micro-IR spectroscopy is a fast and nondestructive technique for characterization of GRIN optics. Optical properties of the laser densified spot are also analyzed. Quantitative analysis of focal length and numerical aperture are obtained using ray theory. A new method was developed for determining the refractive index of the porous gel silica glasses from reflectivity measurements.

The results of laser densification show the potential to replace the current complicated techniques and the capability of using laser processing to make micro-optical devices on the gel-silica substrates.

A novel technique, sol-gel processing, was used in this study for the preparation of the silica substrates for further laser densification. Type VI gel silica glass has a unique homogeneous pore texture with average pore radii of 1.2 nm. Properties of the furnace densified gel-silica glasses are characterized, and results are equivalent to laser densified glasses.

A new quantitative three-dimensional transient model was developed for the first time to simulate the temperature distributions of the laser densified track or spot. Temperature distributions are simulated using thermodynamic principle within a computational volume of 2x2x2 mm^3 with 1000 data points per volume. The governing differential equation of this thermal model was derived from the law of energy conservation and solved by using an Alternate Direction-Implicit(ADI) method. The calculated temperature distributions compared well with the property distributions of the laser densified spots.

CHAPTER 1
INTRODUCTION

1.1 Background

In 50s and 60s, the invention of transistor and integrated circuits stimulated the development the electronic communication systems. Today, the invention of the semiconductor laser and glass fiber not only replaces the wires but also promotes the development of optical computing or optical signal processing. The advantages of using optical computing include speed, low cost, compact size, direct image processing, immunity to electromagnetic interference, massive parallelism and connectivity. Optical signal processing often operates on two-dimensional inputs or in guided-wave optical technology, such as image processing, pattern recognition, and robotic vision. One of the attractive features of the optical signal processing is the high data rate operating with low power laser. Compared with the electronic data rate, optical data rate is 10^5 times higher.

The necessary devices used in optical computing or optical signal processing include couplers, waveguides, interconnects and microlens arrays. Current processing for satisfying the needs listed above have limitations. The limitations are related to the material processing available. The current fabrication processes are primarily chemical based, vapor phase or plasma based, and/or ion beam or molecular beam based processing. Therefore, there is a need for new, simple processing method to produce a new generation of optical components. This is especially the case for integrated optical systems which are compatible with fiber optics and can include non-linear optical switches, interconnects, filters, etc.

The opportunity now exists for a new approach to produce optical devices by combining the sol-gel processing of new optically transparent silica glasses with the laser processing of local densification of gel-silica glasses. Sol-gel processing has been recognized for producing pure silica glass with superior properties at lower processing temperature. Laser processing is introduced due to the speed and high degree of automation which the current complicated techniques cannot achieve. The other unique feature of laser written optical devices is the controllable dimensions(≤ 1.5 mm) and the ability to form complex patterns of laser irradiated regions

Examples of micro-optical components that can be made by using laser densification of gel-silica glasses are waveguides, negative microlenses, geodesic microlenses, GRIN(Gradient refractive index) planar microlenses and the arrays of all types of these microlenses

Thus, the goal of this work is to explore the optical applications of the laser densified elements in integrated optics or micro-optics developed by using modern technologies(sol-gel processing and laser processing) which have great potential to replace the current fabrication methods for micro-optical or integrated optical devices.

1.2 Advantages of Laser Densification of Gel-Silica Glasses

The advantages of using gel silica glasses as the substrates of the optical devices include

(a)High optical transmittance of Type V full density gel silica glass from wavelength of 180 to 3500 nm i e multichromatic source compatible and index matching with fiber optics,
(b)Homogeneous pore texture and
(c)Availability of further densifying the porous gel silica glass using laser heating

The advantages of using laser densification to make optical devices include
(a)A fast and clean technique,
(b)A contact free local treatment,
(c)Ease of fabrication and design,

(d)Introduction of GRIN optical devices,

(e)A high degree of automation and a good reproducibility of the process,

(f)A feasible alternative or addition to existing techniques, and

(g)A direct fabrication technique that simultaneously improves the optical performance of the laser irradiated area.

1.3 Introduction

1.3.1 Motivations of This Study

Sol-gel processing is an important new technique for making high purity silica substrates for optical applications. The surfaces and the interfaces of the gel-silica substrates can be controlled during earliest stage of formation[Hen84]. The volume fraction of porosity of the gel-silica glass decreases with accompanying increase in Index of refraction(n) at increasing densification temperatures. Type VI porous gel-silica glass has a unique homogeneous pore texture with average pore radii of 1.2 nm. The extremely small pores make it possible to control densification by an incident laser beam with high precision. Thus, this new Type VI gel-silica optical material is selected as the silica substrate in this study. The final product of the sol-gel processing is a Type V full density gel-silica glass which is structurally like a commercial pure silica glass and has superior thermal and optical properties[Muk88][Wan88][Hen88][Hen90a]

Both Type VI porous gel-silica glasses with intermediate values of n and Type V full density gel-silica glasses(bulk density=2.2 g/c.c. and n=1.46) can be made reliably. The difference in the refractive indices between Type VI and Type V gel-silica glasses stimulates the development of optical devices with a higher refractive index than the substrate. This concept becomes a reality by introducing a CO_2 laser to locally densify the Type VI porous gel-silica glasses.

Lasers are readily available, high technology tools for modifying the surface properties of the materials by direct heating. In this research work, the refractive index of the gel-silica substrate is increased by using a localized CO_2 laser heating. The silica substrate absorbs the laser energy very efficiently because the wavelength of the CO_2 laser is close to the Si-O-Si stretching vibration mode. Therefore, optical devices with higher refractive index such as microlens arrays can be directly 'written' on the surface of the porous gel silica substrates. The laser processing time of making one microlens is ~1.5 seconds in this work. Arrays of microlens can also be made by using a computer-controlled positioner to permit the translation of the gel silica sample in front of the laser beam.

The motivations of the study are to combine the modern technologies of sol gel processing and laser processing, use the laser densification to further densify the porous gel silica glasses locally, and consequently increase the index of refraction, and explore the optical applications of the laser densified gel silica glasses in the fields of micro-optics and integrated-optics.

1.3.2 Objectives

The goals of this study include

(a)Densify locally Type VI porous gel silica glasses using a CO_2 laser,

(b)Characterize the properties of laser densified regions,

(c)Characterize the furnace densified gel silica glasses at increasing densification temperature and compare the results with the properties of the laser densified region,

(d)Investigate the stability of the laser densified spot,

(e)Explore optical applications of the laser densified optical components such as GRIN microlenses, geodesic microlenses and micro-optical arrays, (f)Develop three-dimensional transient thermal models for the laser densification of the gel silica glasses.

1.3.3 Introduction

This dissertation is divided into eight chapters. Chapter 1 describes the background, advantages, and general introduction of this study. Chapter 2 covers the reviews of sol gel processing, laser processing and the extensive review of the optical microlenses. Chapter 3 describes the sol-gel processing and the characterization of furnace densified gel silica monoliths such as the physical, thermal, mechanical, and the optical properties. Thermal stabilization and chemical stabilization were used to obtain gel-silica substrates with high bulk densities. Requirements of Type VI gel silica glass for further laser densification are described.

Ranges of substrate density from 1.15 g/c.c. to 2.15 g/c.c. are discussed in Chapter 4. Previous study showed that relaxation of the laser densified region occurred after laser irradiation when a gel-silica glass with low bulk density(=1.56 g/c.c.) was used. Therefore, the effects of the bulk densities of the gel-silica glasses on the laser densification were studied. The maximum degree of densification of the porous gel silica glasses produced by the CO_2 laser heating was also investigated. The results showed that substrate densities of > 1.8 g/c.c. produced stable optical elements and achieved a full density region of 2.2 g/c.c. in the center of the laser densified spot. Characterization of the surface and the cross section of the laser densified region(~1.4 mm in diameter, 200 μm in depth) includes microhardness measurement and micro-IR reflectance spectroscopy. It is demonstrated that micro-IR spectroscopy is a fast and nondestructive technique for characterization GRIN optics. This technique allows an immediate investigation of the structural changes of the laser densified spots and tracks.

Characterization results of furnace densified gel-silica glasses discussed in Chapter 3 are equivalent to the properties of the laser densified glasses. Stability of the laser densified spot was investigated by monitoring the VHN profile at increasing time. Approaches of preventing water effect on laser densification are summarized. Mechanisms of laser densification of porous gel-silica glass are discussed. Structural model of a laser densified spot is also shown.

Schematics of the optical devices that can be made on gel silica substrates are illustrated in Chapter 5 which include a geodesic microlens, a compound microlens, a GRIN planar microlens, and negative microlens and microlens arrays. The function of the laser densified GRIN region include focusing, defocusing and imaging. Qualitative and theoretical analyses of the laser densified optics(i.e. the phenomena of focusing and imaging and the calculated focal length and nominal numerical aperture) are discussed. Advantages of the fabrication of optical components using laser heating are also summarized.

The optical properties of the laser densified spots are analyzed quantitatively in Chapter 6. The laser irradiated region has a higher refractive index than the gel-silica substrate(Δn=0.01 to 0.09). The laser induced index change ≤ 0.09 is higher than the index change(=0.05) of a GRIN rod made from sol-gel process[Yam90]. Characterization of the laser densified microlenses include IR reflectance spectra of the laser densified spot, surface index profiles, focal length, coupling efficiency, numerical aperture,and the profile of focused spot formed by a gel-silica GRIN planar microlens.

We know that the properties of the gel-silica glasses are strongly affected by the processing temperature, as discussed in Chapter 3. Thus, it is important to know the temperature distribution of the laser densified spot. Quantitative transient thermal models were developed to simulate the dynamic three-dimensional temperature distributions of the laser densified track or spot. For a laser densified spot, temperature distributions are simulated using thermodynamic principle within a computational volume of 2x2x2 mm^3.

with 1000 data points per volume. The governing equation of this thermal model is derived from the law of energy conservation. The equation was solved by using an Alternate Direct Implicit(ADI) method. The heating rate, cooling rate and the three-dimensional temperature distributions were obtained. The simulated temperature distributions from the thermal model of a laser densified spot compare well with the property distributions on the surface and the cross section of the laser densified region. Chapter 8 describes the summary and conclusions of this research work.

CHAPTER 2
LITERATURE REVIEW

2.1 Sol-Gel Processing

2.1.1 Historical Sketch

Interest in the sol-gel processing of inorganic ceramic and glass materials began as early as the mid 1800's with Ebelmen and Graham's studies on silica gels. There was little technological interest because long drying times for one year, or more, were necessary to obtain monolithic silica gels[Hen90b]. Roy and coworkers recognized the potential for achieving very high levels of chemical homogeneity in colloidal gels and used the sol-gel method in the 1950's and 1960's to synthesize many ceramic oxide composites from the melted gels, including compounds involving SiO_2, Rb_2O, Ga_2O_3, ThO_2, ZrO_2, etc., which were originally made for the phase equilibria studies[Roy56][Roy69]. Dislich made a borosilicate glass disk several centimeters in diameter at 620°C by hot pressing a gel powder prepared from metal alkoxides in 1971[Sak85].

According to Sakka, the revival of sol-gel process started with the works of Dislich and Roy around 1970 because there was rising demand for new materials used in energy, electronics, communications, and other high technology fields[Sak85]. Ulrich also pointed out that traditional approaches based on high temperature and sophisticated fabrication technologies impose a severe limit on producing glasses, etc., of high reliability which lead to unpredictable, catastrophic failures during use and inhibit the attainment of properties approaching the theoretical values in glass and glass ceramics[Ulr88]. Sol-gel processing, therefore, was developed to attain these objectives.

Since 1970, powders, fibers, grains, preform of optical fibers, and a variety of coatings and films have been developed[Dis83]. Yoldas succeeded in preparing large, and transparent monoliths of porous alumina by the sol gel method which aroused considerable interest[Yol75]. Zarzycki et al. demonstrated the production of large monolithic aerogels by hypercritical drying and discussed the crystallization behavior of the gels and glasses made from hot-pressed gels[Pha82][Zar84]. Yamane investigated the formation of monoliths from the sol-gel process by considering the effects of gelling temperature, catalyst on gelling time, and the densification temperature on the pore size distribution[Yam88]. Mackenzie indicated that sol gel process has the capability of preparation of new and/or improved optical materials and it permits the fabrication of optical components into shapes not easily achieved by other processing techniques[Mac90]. Hench and colleagues have developed various gel silica glasses[Wan88], TiO_2-containing gel silica glass[Che91], large pore gel-silica glass[Fos90], controlled texture by aging [Liu91], and doped gel silica glass[Hen90b]. Large monolithic xerogel silica glasses with high optical performance were successfully made by a reliable sol-gel process [Hen88]. There are also many published works that show the great strides in understanding the fundamental aspects of preparing homogeneous multicomponent ceramics from alkoxide-derived gels[Hen90b][Bri90].

To date, a full dense gel-silica glass can be made in days instead of a year. Manipulating the expected ultrastructure of the prepared materials become a reality through sol gel processing. Many new products through sol gel processing (starting from sol) bring a new era in the manufacture of ceramics, glasses, and composites which contrast to the traditional technology(from melt) since prehistory. Mackenzie discussed the fact that the sol-gel process has been increasingly employed in innovative applications in the past few years especially in the field of composites, porous solids and coatings[Mac88]. With the uniqueness and versatility of the sol gel process there is no doubt that it will be applied to more optical devices, components and other promising applications[Mac90]. Ulrich concluded that major advances in glass during the next several decades will require an emphasis which relates chemical processes to glass formation, the impact will be most evident on new materials and ultrastructural level composites fabricated by low temperature solution processes[Ulr85][Ulr88].

2.1.2 Review of Sol-Gel Processing and Science

In recent years, silica components meet very strict requirements in optical applications, like high purity, homogeneous ultrastructure, high optical performance, tailored porosity, controllable pore size and pore distribution[Muk88][Wan89]. It is recognized that using sol-gel processing is one of the approaches to control the surfaces and interfaces of materials during the earliest stages of formation[Hen84]. In order to provide a fundamental understanding of the sol gel science for optical applications, the following discussions focus on sol-gel processing, the resulting product of each processing step, and discuss the variables, mechanisms, modification approaches, models of densification, and advantages of the sol-gel processing.

Figure 2.1 shows the flow chart of sol-gel processing starting from the mixture of the sol. First, a sol is described as a colloidal suspension of solid particles in a liquid [Bri90] which is a mixture of precursors(e.g. organometallic compounds like tetramethoxysilane, TMOS), water, and acid catalyst. The precursors react readily with water through reactions termed as hydrolysis, alcohol condensation, and water condensation at the functional group level as shown below[Bri90].

hydrolysis

$$\equiv Si\text{-}OR + H_2O \Rightarrow HO\text{-}Si(OR)_3 + ROH \qquad (2.1)$$

alcohol condensation

$$\equiv Si\ OR + HO\text{-}Si\equiv \Rightarrow \equiv Si\ O\text{-}Si\equiv + ROH \qquad (2.2)$$

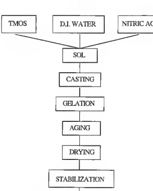

Figure 2.1 A flow chart of Sol-Gel processing steps.

water condensation

$$\equiv Si\ OH + HO\text{-}Si\equiv \Rightarrow \equiv Si\text{-}O\text{-}Si\equiv + H_2O \qquad (2.3)$$

R is an alkyl -OR represents the alkoxy group OH is a hydroxyl group and ROH is an alcohol. The hydrolysis is rapid and complete if the amount of water and catalyst is appropriately controlled. In an acidic environment, and below 4 moles of water per mole of TMOS, the branching of polymers increases with water content, i.e the gelling time is shortened and the viscosity is increased Above 4 moles of water, as a result of the dilution of polymers by excess water the gelling time is prolonged and the viscosity decreases[Miz85]

The pH of the catalyzed sol has strong effect on the structure of the gel At pH = 1, primarily linear or randomly branched polymers are formed. Discrete and more highly-branched polymeric clusters are formed at pH 7 and higher The different resulting structures of the polymers are due to the mechanisms of the hydrolysis involving electrophilic attack at low pH, hydrolysis and polymerization involving nucleophilic attack on silicon[Bri84] Other factors that might affect the hydrolysis and condensation reactions are solvent effects, spatial factors(complicated alkoxy group), and the inductive effect of methylethoxysilanes[Sak88][Bri88a][Bri88b][Bri88c][Bri90]

Other types of gels, multicomponent gels or large pore gels, can be made by adding different chemicals when preparing the mixture of the sol For example, foreign cations like Na may be added into the mixture to form a multicomponent gel silica glass. Adding HF into the sol or base catalyzed sol may result in a gel with large pore diameter (> 8 nm)

The gellation step leads to a wet gel with separated phase structures One phase is a continuous three-dimensional network similar to that in silica glass, but with OH groups on the pore surfaces. The second phase is a water alcohol solution in the pores[Rab85] The texture of the gel can still be modified after the gel point, although it is called a "frozen in" structure in order to increase the strength of the gels or create novel types of gels with tailored ultrastructures. For example, texture of the gels during the aging process is controllable after soaking in a NH_4OH solution. The pore shape, pore diameter(up to 38 nm) and porosity(up to 74%)can be tailored by aging time, aging temperature, and NH_4OH atmosphere treatments[Liu91]. These textural features of the aged gels remain after drying. Other examples of modifying the structures of the gels before drying are soaking, leaching, and inter-diffusion of index modifying cations in order to create GRIN gel-silica glass for optical applications[Yam90][Che90][Yam91].

The mechanisms involved in the aging process are condensation(chemical composition change), syneresis(physical dimension change) and Ostwald ripening(texture change)[Liu91]. The driving force for Ostwald ripening is lowering the solid/liquid interfacial energy by the growth of large particles at the expense of smaller ones. Large amounts of water, high pH, or high aging temperature of the gel environment actually speeds up the dissolution and redeposition of the polymers which result in extensive restructuring of the gel[Bri84]. Iler indicated that the rate of dissolution of amorphous silica increased linearly with increasing pH from 3 to 6, which is able to increase the coordination of silicon above four which weakens the surrounding siloxane bonds of the network[Ile79][Bri90]. These modifications result in lower microhardness and higher porosity of the dry gels.

The objective of the drying step is to eliminate the interstitial phase, water-based solution (aquagels) or alcoholic solution (alcogel) of the wet gel at a temperature up to 180°C under ambient atmosphere. The driving force of the drying step is to shrink to reduce the solid-liquid interfacial area (which is in the order of 400-800 m^2/g) and the reduction of chemical potential through condensation reactions[Sch86]. A dry gel, termed a xerogel, with higher mechanical strength is obtained after irreversible and sizable shrinkage(up to 50%)[Zar84]. An aerogel can be made by using hypercritical drying of the wet gel, without any shrinkage, which results in a solid with a density as low as 0.08 g/c.c.[Hen90b]

Real time monitoring the drying behavior of an alkoxide derived silica gel, studied by Wilson, showed that the drying process of the gel consists of three stages[Wil89a][Wil89b].

Stage I During which the greatest changes in volume weight and structure occur.

Stage II In which changes in weight and volume are small but large changes in optical characteristics are seen.

Stage III. In which there are no further dimensional changes, but there is a progressive loss of weight to the minimum attainable value.

These three stages are consistent with the drying stages discussed by Scherer and Brinker[Bri90]. Scherer showed detailed studies of drying behavior of the gel, including the causes of contraction, contributions of the capillary stress, the controlling factors of shrinkage rate, the quantitative model of stress and strain, and the drying models for a flat plate and a film on a rigid substrate[Sch86][Sch87a][Sch87b][Sch88].

The drying stage is one of the crucial stages to obtain a monolithic gel. During drying, a large stress is introduced and leads to catastrophic fracture if the drying process is improper. Scherer indicated that the development of stress in the gel depends on the relative rates of three independent processes: evaporation, viscous deformation of the solid, and flow of the liquid in the pores of the gel[Sch86]. A quantitative description of the stress during drying is also discussed by Zarzycki. The approaches to avoid cracking during drying are shown as follows[Zar84]:

(a)Increase the mechanical resistance of the gel by aging.

(b)Diminish the magnitude of capillary forces, especially generated from a gel with very small pores.

(c)Eliminate the capillary forces totally, e.g. using hypercritical drying to obtain an aerogel.

Various types of gels, containing transition metal or rare earth elements also can be made by soaking the dry gels in a solution with soluble cations[Wan88]

Dry gels have large surface area(>400 m^2/g) and very high concentration of silanols on the pore surface These features of the dry gels make them both thermally and environmentally unstable Dehydration of the dried gels termed stabilization, is required to overcome these instabilities and transform the gel into glass There are two types of stabilization, thermal stabilization(or thermal dehydroxylation) and chemical stabilization(or chemical dehydroxylation), both involving the reduction of the surface area, free volume and the concentration of the silanols while the gel becomes more highly crosslinked [Bri85a][Hen90b] During stabilization a process of gel to-glass conversion both chemical and structural transformations take place[Bri82] If the hydroxyls are not desorbed before pores close during densification, they will cause bloating or foaming when water expands within closed pores.

Thermal stabilization is used to reduce the surface area and the silanol concentration. The strength of the gel increases as the silica network is stiffened by condensing the internal hydroxyls[Sch86] However, it is difficult to maintain the monoliths and transparency by using only thermal stabilization to fully densify pure silica gels Chemical dehydroxylation is widely used to obtain the least concentration of silanols to compensate the deficiency of the thermal dehydroxylation[Miz84] Chemical stabilization has proved to be more effective in removing hydroxyl groups prior to consolidation[Bri90] The most effective chemicals used in surface dehydration of silica gels are $ClSi(CH_3)_3$, $SiCl_4$, Cl_2, and CCl_4 which react with the surface hydroxyl groups into the form of HCl and desorb from the the gel body at a temperature range of 400°C - 800°C when the pores are still connected[Sny66][Hen90a] However the use of chlorine compounds in dehydration can incorporate chlorine ions in the structure of the densified gel-silica glass One approach of dechlorination carried out in an oxygen atmosphere is useful as discussed by Susa et al.[Sus86]

Partially densified gels are lower in refractive index, chemical durability, strength, and modulus than those of the fully densified gel-silica glass[Bri90]. Further densification of a partially densified silica gel occurs between 1000°C to 1700°C which transforms them into glass, depending upon the radii of the pores and the surface area[Hen90a]. The silica gels with small pores (radius ~12Å) can be fully densified at a low temperature of ~ 1150°C. The gels with larger pores reach full density at higher densification temperatures, e.g. > 1150°C[Hen88][Hen90b]. Once the gel has been densified and heated above T_g, its structure and properties become indistinguishable from those of conventionally melted glass of the same composition[Bri85a][Bri85b][Bri85c].

Mechanisms involved in thermal stabilization of the silica gel have been summarized by Hair from combined infrared and gravimetric data. The amount of the physically adsorbed water and the silanol groups on the pore surface are changed with increasing temperature[Yon58][Hai67]. A summary of these changes is as follows:

(a) Physically adsorbed water is completely removed by pumping in vacuum at room temperature

(b) Surface silanol groups start to condense and eliminate water at about 170°C

(c) Dehydration is completely reversible up to about 400°C.

(d) Above 400°C, the dehydration is not reversible and the amount of chemisorption that can occur is an inverse function of the temperature of heat treatment.

(e) Above 850°C, no chemisorption of water can occur and the surface is hydrophobic

(f) Sintering starts to occur at 900°C and the predominant mechanism of sintering is viscous flow

In Scherer's studies, the porous glass contracts by ~1% with no change in pore volume on heating to 550°C, indicating that the skeletal density increases by ~3% as the hydroxyls are removed by condensation reactions[Sch86]. There is a concurrent increase of ~33% in the elastic modulus. Following heating to 800°C, the modulus is almost twice as large as it was initially. Above ~900°C, the pores begin to shrink by viscous sintering [Sch86].

Brinker and Scherer discuss the densification of the silica gels extensively[Bri90]. There are three mechanisms involved in the thermal stabilization of the silica gel heating up to ~ 800°C[Elm83][Bri90].

(a) Below 150°C, shrinkage and weight loss are caused by the desorption of water and alcohol.

(b) Between 150°C and ~525°C, shrinkage and weight loss are attributed primarily to the removal of organics(principally weight loss), polymerization(shrinkage and weight loss), structural relaxation(shrinkage only).

(c) Heating to 1100°C, shrinkage and little weight loss are due to the concurrence of structural relaxation(structure approaches its equilibrium configuration), continued condensation and viscous sintering.

One of the interesting phenomena during the densification of the silica gels is the formation and vanishing of structural defects. Threefold silica rings and fourfold silica rings are the most prominent defects in gel-derived silica which are Raman active and were originally proposed by Galeener[Kro84][Bri86]. These defects are considered extrinsic to the network structure since they are a consequence of incomplete condensation during the densification. The presence of the strained threefold rings are confirmed using NMR[Bri88c]. Results of differential scanning calorimetry also showed that threefold rings are a product of a significantly endothermic reaction involving surface silanol groups.

The concentration of the threefold rings reach a maximum and drop drastically due to the structural relaxation at viscous sintering temperatures (>900°C)[Bri88b]. Therefore only porous silica gels have high concentration of threefold rings and most of the threefold rings are present in surface sites which have direct access to water. These thermally induced defects are metastable and susceptible to opening up the strained bonds by adsorption of water from the surrounding atmosphere[Bri88b]. Elimination of the threefold rings can be achieved by adsorbing water or undergoing further viscous sintering. Tallant et al. have also identified the existence of these defects in other high surface area silica materials including leached glasses and Cab-O-Sil[Bri86][Tal86]. Wallace and Vasconcelos have shown the variations of structural (skeletal) density of the silica gels with increasing densification temperature[Vas89a][Wal91]. The skeletal density of a silica gel also increases to unexpected maximum values of 2.3-2.4 g/cm^3(at ~ 900°C) before it reaches a normal density of a pure silica glass, 2.2 g/cm^3, when the gel is fully densified (at ~1150°C). There is a similarity of the variations of skeletal density and concentration of threefold rings with temperature. Thus, the formation of the strained threefold rings may be one of the contributions to the increase of the skeletal density of the silica gels.

In differential thermal analysis(DTA), there is an exotherm before the glass transition when an acid-catalyzed silica gel is first heated. If the sintered gel is cooled and reheated, only an endotherm appears[Bri90]. This indicates that a structural relaxation (exothermic reaction toward a more thermodynamically stable structure) releases the excess free energy of an "frozen in" open structure, and is the other contribution to an increase in the structural density of the gel[Bri85a][Bri85b][Bri85c].

Water adsorption on the pore surface of as-received silica gels with a large surface area can induce dilation of the substrate. It is indicated by Scherer that the hydrophilic porous glass can absorb water as a polymer absorbs a solvent, resulting in much greater dilation, i.e. swelling[Sch86]. West et al. conducted an experiment which showed that a silica gel preheated to 600 °C and dehydrated in vacuum at 180°C appears to dilate the structure ~ 350 ppm after 24 hours[Wes90b]. They also use INDO theory to calculate the change in structure, i.e. dilation, of a fourfold ring after adsorption of a water molecule. The results show that there is an anisotropic expansion of the ring which indicates a possible mechanism for the observed dilatometric behavior of porous Type VI sol-gel silica[Wes90a][Wes90b].

The above discussions are important in the interpretations of the relaxation of the laser densified region of a porous silica gel, when low bulk density of the silica gels and low laser energy are used in the laser densification[Slo90]. As the bulk density of the gels is much smaller than 2.0g/cm^3, part of the laser energy is consumed and forms the threefold silica rings, which are highly strained species and will open up by adsorbing water from the atmosphere. This reaction, as well as the reaction of water adsorption to the fourfold rings, may cause some degree of the swelling. Thus, relaxation of the laser densified region is observed[Slo90]. In order to prevent the formation of defects, which are environmentally unstable, Chia et al. have shown that it is preferable to use nearly full densified gels (with much less surface area) as substrates for further heat treatments to make optical devices[Chi90].

There are several models that describe the densification of a gel system[Hen90a] [Bri90]. Frenkel's model describes the initial stage of sintering, during which there is considerable neck growth but little densification. Scherer's cylindrical model describes the intermediate stage of sintering. As the cylindrical model densified, the cylinders become shorter and thicker. When the relative density reaches ~0.94, neighboring cylinders touch, at that point the unit cell contains an isolated pore, so the remainder of the densification is described by the Mackenzie and Shuttleworth's model(MS model). The closed pores of the silica gels is modelled as isoland spherical voids in the MS model which applies ideally to the final stage of sintering[Bri90]. Frenkel also proposed the theory of viscous sintering, which holds that the energy dissipated in viscous flow is equal to the energy gained by the decrease in surface area during densification[Sat85]. However, to predict the the evolution of the surface area, more realistic models are required which take into account the pore size distribution which is more complicated[Bri90].

Vasconcelos et al. developed several topological models of the sintering applied to silica gel monoliths. In topological terms, the densification process can be divided into three stages according to the genus, which is defined as the maximum number of non-self reentrant closed curves that may be constructed on the surface without dividing it into two separate parts[Vas89a][Vas89b]

First Stage weld necks grow while the genus remains constant.

Second stage the genus decreases to zero as the pores become isolated

Third stage the genus remains constant at zero while the number of pores
goes to zero

Hench et al. showed that nitrogen adsorption isotherm data can be used to obtain both metric and topological parameters. Topological models provide a means for monitoring the changes in metric parameters such as volume fraction of pores, average pore diameter as well as connective features of the structure such as genus, and the coordination number of pores[Hen90a] In conclusion, there are corresponding models suitable for analyses of silica gels with specific structures(i e a narrow pore size distribution) in the early, middle, or final stage of sintering

Comparisons of glasses from sintering of gels around T_g with the glasses melted at high temperature from batch materials or from gels are discussed by Brinker et al. The major difference is the thermal history which leads to the differences in free energy, phase transformation rate, and crystallization behavior[Bri90] Mackenzie and Scherer et al summarized that the properties of gel silica glass are similar to those of commercial silica glasses after the gels been heated to T_g[Mac82][Sch86] Detailed comparisons of properties of gel-derived pure silica glasses with commercial silica glasses from melt are discussed by Hench et al [Hen88] Dense gel-silica glasses possess merits of low OH impurity, low total cation impurity, high UV transmission low thermal expansion coefficient, and low bubbles and inclusions.

The advantages of producing materials through the sol gel processing, compared with those from melt, are described as follows[Mac82][Mac84][He86][Hen88][Hen89]

(a) Better purity and homogeneity from raw materials.

(b) Processing in molecular manipulation to produce unique homogeneous structures of different colloidal oxides

(c) Capability of controlling the surfaces and interfaces of materials during the earliest stages of production

(d) Lower temperature of preparation

(e) New noncrystalline solids outside the range of normal glass formation

(f) Capability of preparing objects with near net shapes.

Other advantages are that sol gel processing can produce exceptionally homogeneous materials from melted gels. Also, homogeneous glasses can be prepared in the alkaline-earth silicate systems from gels which are impossible to prepare through the melt[Bri90]

In conclusion the driving force for the densification of the silica gel in each processing step is the reduction of solid/liquid or solid/vapor interfacial energy due to the high surface area of the gel. Prior to the consolidation toward dense glasses, the defects of the silica gels form and vanish upon further densification near T_g. The resulting fully densified glasses have the same structures of the melted silica glasses but with higher optical quality and a much lower processing temperature. Further, specially treated wet gels(like those soaked in NH_4OH solution) or partially densified silica gels with tailored structures(like those containing modifying ions) have been applied in various of optical applications

2.1.3 Optical Applications of Sol-Gel Glasses

Optical applications of alkoxide-derived silica include thin films, coatings, optical fibers, and monoliths(Type V full density and Type VI porous gel-silica glasses). Sol-gel process provides excellent materials for optical devices. The advantages include extremely low loss of Type V gel silica glasses, index-matching with fiber optics, and homogeneous pore texture, etc

Sol-gel thin films, normally < 1 μm in thickness are formed by dipping or spinning Porous films have been developed by Brinker and coworkers with tailored features. Optical fibers are drawn directly from the viscous sols at room temperature[Bri90] Hench et al. demonstrated that Type V gel silica glasses made through sol-gel processing have equal or superior physical properties to Type I-IV optical silicas through traditional methods[Hen88] High performance of type V gel-silicas include short UV cutoff low optical absorption throughout the spectrum, high homogeneity, very few defects, low strain birefringence, and low coefficient of thermal expansion. Further, optical elements with diameter 75 and 100 mm or larger are also produced for both Type V and Type VI silicas Factors in size scale up are the drying rate, defects in the as-cast gel silica monoliths, and the removal of chemisorbed water[Hen89]

GRIN(Gradient refractive index) glasses used in photocopiers and FAX machines can be made through sol-gel process taking advantage of the high diffusivity of ions in the liquid phase at the gel point. A multicomponent monolithic gel is prepared by adding one or more index-modifying ions Interdiffusion, leaching and ion-exchange are used to create a GRIN gel Drying and sintering produce a GRIN glass[Yam90][Che90][Yam91]. Compared with MCVD(modified chemical vapor deposition) methods used to manufacture optical fibers[Tak86], the sol-gel process is envisioned to be less expensive and better suited for optical glasses that do not require ultralow optical losses[Bri90][Kon90]

There are many potential applications of Type VI porous gel silica reviewed by Hench et al and King[Hen90b][Kin91] Type VI silica gels can be prepared in any form by near net shape casting, i.e. without any elaborate polishing and grinding, to make lenses used in bulk optics or with a fine embossed surface to make Fresnel lens[Hen89] Type VI porous monoliths can also be a host for many dopants with nonlinear optical properties, specific absorption features(wavelength filters), or dopants like organic dye molecules for laser materials, and inorganic ions for a new solid state glass[Dan90][Whi90]. Doping with organic dye molecules leads to tunable visible solid state lasers, an alternative to solution dye lasers. The addition of optically active compounds in Type VI silica provides a medium for wide range of new devices, called gel silica hybrid optical devices. There are numerous optical applications such as holographic elements, dye lasers, filters, scintillation detectors, wavelength shifters, solar concentrators, transpiration cooled windows, Faraday effect glasses and laser written waveguides[Hen90b][Kin91]. Prasad showed that the sol-gel processed inorganic and organically modified composites have successfully performed as a nonlinear optical element[Pra90].

Hench et al. reviewed the processing of Type VI gel-silica optics and their applications. One of the approaches to making optical channel waveguide is using CO_2 laser heating to enhance the densification of the porous Type VI gel-silica up to full density which creates a surface gradient index distribution in a confined region, where the guiding of the optical ray is allowed[Ram88][Sha89][Sha90][Hen90b]. This study is based on the fact that in gel-silica glasses, the refractive index is a function of densification temperature of Type VI pure gel-silica substrates. The higher the densification temperature and the longer the holding time, the greater the bulk density and the refractive index. Full densification occurs around 1150°C where the refractive index reaches 1.465[Hen90b].

Channel optical waveguides have been fabricated in glass by using Argon or CO_2 laser since 1974[Pav74][Che76][Yam85]. GRIN micro-optical devices, i.e. microlenses, can be created by focusing CO_2 laser and heating the surface of the gel-silica substrate or the porous silicate glass in a confined region ≤ 1 mm in diameter[Chi92a][Vei90][Vei91]. Locally heating the gel silica monoliths using a CO_2 laser is quite promising because of the lure of direct writing optical elements on the surface of Type VI substrates. For micro-optical or integrated optical applications, the formation of geometrical structures is an important feature[Sch90]. For example, laser written optical devices that can be fabricated on Type VI gel-silica substrates are negative microlenses, GRIN microlenses, and geodesic microlenses or their arrays[Chi92b]. The GRIN depth of the lens is approximately 150 μm, the index change is ~0.09 depending on the laser processing parameters and the initial bulk densities of the Type VI gel-silica glasses. Other laser heating applications are discussed by Zelinski et al. They show that heating sol-gel coatings with a laser to densify selected regions is a relatively unexplored area that offers potential for applications in many fields[Fab90][Zel91].

One of the greatest advantages of laser assisted densification is introducing the GRIN region in a Type VI C gel-silica substrate within seconds compared to hours for GRIN gel from soaking and ~ months for GRIN glass from conventional ion-exchange methods[Chi90][Bri90]. The other attractive feature is that laser densification of Type VI gel-silica glass converts the laser irradiated area to Type V full density silica with an absorption loss that is extremely low (~ 0) at wavelengths ranging from 180 to 3500 nm. The resulting full densification of the silica gels matches the refractive index of silica based optical fibers, providing low loss for coupling[Hen88][Kin91].

2.2 Heat Treatment on Glass by Using a CO_2 Laser

Laser damage of glasses was investigated as early as 1963[Cul64] [Dav68]. In the 1970s, studies were carried out on laser drilling, laser welding of special materials, scribing of silicon wafers, grooving of components, trimming, cutting, and laser processing of integrated circuits. From the late 1970's to the early 1980's, high power CO_2 laser and YAG lasers were developed. This led to progress in research in thermal treatments of materials. The CO_2 laser is used for cutting, welding, structuring, and surface treatment[Ber90]. To date, CO_2 laser processing has entered into the production and practical stage[Lei91].

Lasers are high technology tools for locally modifying the surface properties, for example, hardness or refractive index of the material. The 1/e penetration depth of the CO_2 laser in the silica glass is estimated to be 1.5μm. Therefore, laser processing is more effective for treatment of thin surface layers[Mor90]. The surface of the material absorbs the IR ray and induces direct lattice phonon excitation, the heat is generated within the irradiated region as a result of the excitation. There are two types of laser processing in materials, direct heating and indirect heating, according to different mechanisms. In direct heating, the target is the sample which absorbs the laser energy efficiently and the energy is subsequently transformed into heat. In indirect heating, the laser heats the support material, such as a coating, which is intimately attached with the sample. The transformed heat within the support material is conducted into the sample to achieve the densification. Regardless of the type of laser processing, both the heating rate and cooling rate are extremely fast, up to an order of $\sim 10^6$ °K/sec depending on the input power density and the properties of the materials.

Laser processing offers potential for development of a fully adaptive processing technology. Early work of laser direct writing was reported in 1982. To date direct laser writing is one of the most likely technologies to achieve the next-generation circuit and device fabrication[Liu89]. Direct CO_2 laser writing provides a fast and clean processing method, as compared to other techniques, and is suitable for computer-aided automation. For example, the laser/robot first used to weld sheet metal in 1974[Bel90], can be expanded in the fabrication of optical devices in the future. Liu indicated the process considerations in laser direct writing are (1) resolution(beam spot size), (2) writing speed, (3) resistivity(impurity), (4) morphology(nonuniform heating), and (5) adhesion (interfaces)[Liu89]. Bergmann et al. indicated that there are several factors that apply to laser surface treatments[Ber90]Mor90]

(a) a contact-free local treatment,

(b) a high degree of automation.

(c) a good reproducibility of the process,

(d) a feasible alternative or addition to existing techniques.

The direct laser writing on type VI silica gels can induce an increase in surface-refractive index[Chi92b]. Three dimensional freedom of the fabrication, extremely accurate positioning (micron-sized accuracy) and any pattern of optical devices on the glass substrates can be achieved, i.e. geodesic lens, planar GRIN lens, channel waveguides and arrays. The depth, size, configuration can also be accurately controlled.

Other alternatives to create a surface refractive index change is to initiate a photo-induced surface reaction, doping, thermal deposition, or chemical vapor deposition[Sop78][Pau84] [Sla89][Chu89] by irradiating the silica substrate under certain atmospheres where the un-irradiated substrate remains the same because of its chemical stability.

2.3 Microlenses

2.3.1 Review of Optical Information Processing

Optical methods for information processing have been studied since 1953[Mag89]. After the laser was invented around 1960, many applications of laser technology in optical communications (long-haul systems) and optical signal processing (local area networks) become practical and progress occurred rapidly[Mil69]. Development of the semiconductor laser in 1964, and the proposal of Kao and Hockham in 1967 to use glass fibers for guidance operating at, for example, 1300 nm or 1550 nm were of special importance[Gar89]. The invention of the transistor and integrated circuits played the same role in the 50's and 60's in the massive development of electronic systems.

Chen indicated that optical data transmission systems offer the potential of operating at extremely high data rates with low powers[Che87]. Data rate, sometimes referred to as bit rate, is the number of bits processed in a given period of time. Each bit contains information which can be formatted to represent intelligence[Gra88] The frequency of the optical carrier is on the order of 10^5 GHz, as compared to electronic signal processing with fundamental speed limitation at ~ 1 GHz for silicon integrated circuits[Che87] This is one of the attractive features of using optical signal processing

Garrett discussed that optical signal processing covers a wide variety of operations on both analog and digital signals, often operating on two-dimentional inputs, or in guided wave optical technology[Gar89] Typical of these two-dimensional processing techniques is in the applications of image processing, pattern recognition, and robotic vision. A theme that has emerged in the last few years is the data rate "transparent link"(optical data or signal processing connected with fiber communication), where electronics systems cannot really compete. Optical switching in particular allows the transparent link concept to be enlarged to "transparent networks"

More complicated applications of optical information processing are optical logic and optical computing It is realized that optics offers the possibility of highly parallel image processing. The degree of parallelism is reflected in the resolvable points, which, with good lenses, may be of the order of a million[Gar89] Feitelson reviewed that the advantages of using optical computing are speed, low cost, compact size, direct image processing, immunity to electromagnetic interference(EMI) and massive parallelism and connectivity[Fei88]

The advent of the inexpensive, reliable laser source and high performance fiber-optic material were the driving forces for the improvements in optical information processing which involved wide applications For applications involving transparent links, optical computing, integrated optics or other optical micro-imaging systems, individual devices, like microlenses, still require extensive development, both in the materials and in the fabrication technology, to be used widely

2.3.2 Review of Microlenses

Micro-optical components, like microlenses, are developed to fulfill the needs of manipulating an optical beam in various optical applications. Major functions of microlenses are imaging, focusing or transmitting the optical information. Microlenses are categorized into two types according to their inherent features, which are diffractive microlenses and refractive microlenses

Diffractive microlenses have been developed in the past several years. The intensity of the focused optical ray is enhanced by the coherent effect[Hec74] The action of diffractive microlenses is based on near field diffraction at a Fresnel zone plate A intensified focused spot, produced by mutual coherence of the laser, with 91% diffraction efficiency has been made[Jah90]

The importance of using diffractive microlenses for collimating is that one and two-dimensional laser arrays have typically large beam divergence up to a few tens of degrees[Din87]

Applications of diffractive microlenses and arrays include improving the coupling efficiency into fibers for optical communication system, along with multiple imaging and illumination of arrays of optical or opto-electronic devices in digital optics[Str91]

The present techniques used in fabricating diffractive microlenses are UV lithography [Tat84], electron beam lithography[Shi87], laser beam lithography[Har90], integrated circuit techniques[Leg88] and thin film deposition[Jah90]

The advantages of diffractive microlenses are the capabilities of mass production, high reproducibility, ease of fabrication, use at IR range[Swa85], and varieties of design The disadvantages of fabricating diffractive microlenses are sophisticated and sensitive processing steps required, and their restricted use with monochromatic sources.

Refractive microlenses have the capability of focusing light either due to a gradient index effect [Oik81][Oik82][Oik82][Iga82a][Oik84][Vei91] or a geometric effect[Coh74]

[Bor88][Pop88]. According to their functions, refractive microlenses are divided into GRIN fiber lens, GRIN rod lens, shaped lenses, aspherical microlenses, GRIN sphere lens[Koi86], GRIN objective lens , GRIN planar microlens and geodesic microlenses.

In earlier days, a gas lens was proposed to transmit the optical ray for a long distance with low loss[Ber64a][Ber64b][Bec64a][Bec64b]. Losses by scattering and absorption in solid transmission were considered too large to be used in laser communications. The focusing or defocusing capability of a gas lens is attained by the radial index gradient created from the temperature distribution inside a CO_2 gas tube. However, a gas lens has a large instrumental setup, a long focal length, a large size of focused spot and is unable to be bent to a small curvature which greatly limited applications.

Later on, a practical solid-state lenslike medium was prepared by using ion-exchange on a glass medium and is named as SELFOC®[Uch70]. The SELFOC® optical glass fiber with a diameter of ~0.3 mm can be used as a needle scope, fiber scope, fly's eye lens, or multiplex transmission line in a copy machine, for medical application, barcode scanning, or optical communication, optical signal processing[Uch69][Uch70][Mat80][Kaw80][Car91]. Detailed optical properties of GRIN fiber lens arrays, as a function of fiber length, were discussed by Lama[Lam82]. The use of a Gradient-index (GRIN) fiber array made it possible to make the copy machine in compact size and obtained uniform resolution over the entire image area. The disadvantages of GRIN fiber arrays are that there is no variable magnification and they limited in the use of slit exposure[Kaw80].

GRIN rod lenses have been used as optical focusing and coupling elements in optical communication or in electro-optic systems such as copy machines[Mat80][Kaw80][Ree84], facsimile machines[Toy83][Shi87], diode laser arrays[Lia88][Lia89], optical disk pickup systems[Miy80][Dai84], and optical fiber communication systems[Tom80][Sar80][Iga82a][Acc90]. The techniques used in fabricating GRIN rod lens are ion exchange[Pea69][Kin90a], two-step copolymerization [Ohi74], sol gel process[Che90]

[Kon90][Yam86][Sht90b][Yam90][Yam91]. The ion exchange technique has problems of chromatic aberration [Nis80] and the aberrations due to deviations from a parabolic-index distribution.[Yam80] Efforts have been made to reduce or characterize the aberration of the GRIN rod lenses but the problems are as yet unsolved[May80][Gre80][Yam82].

Atkinson et al. designed a GRIN camera objective lens with a focal length of 50mm and pluralities of the lens for correcting the lens aberrations, for example, astigmatism. The GRIN photographic objective design performs comparably to a standard homogeneous system but reduces the required number of elements from six to two. This study indicated that materials with a refractive index of 1.8 and Δn of 0.12 were useful in fabricating designs of this type of the objective lens[Atk82]. GRIN elements have also been shown useful in the design of a wide-angle photographic objective. Atkinson et al. designed a three-element with two axial gradients of a wide angle photographic objective which has a similar imaging performance to a six element homogeneous wide angle design[Atk84]. Other similar GRIN elements designs had been used in a lens system for disc format cameras[Cal86b], binocular objectives[Cal86a][Kin88], and a compact disk systems [Nis86]. Planar GRIN microlens arrays can be made by diffusion[Oik82][Iga82b][Mis84][Oik84], ion-exchange[Ham90a], laser densification[Vei90] [Vei91][Chi92a][Chi92b] or deep electromigration through a mask[Oik81][Oik82]. Diffusion or electromigration may create a large refractive index change(~0.27) and a deep diffusion depth(~few millimeters). However, long processing times cause inevitable problems in achieving reliability and reproducibility. Cluster formation inside the glass after a period of time makes it difficult to maintain stability.

In contrast, laser densification of the porous glass provides an efficient and high production rate for the fabrication of the planar GRIN microlenses. From feedback data of the processing, like temperature, refractive index, and the radius of curvature, this fabrication method has become more accurate and reproducible[Vei90]. Exposure time for the CO_2 laser to make a microlens is very short, ~ 1 second, which prevents contamination or process-sensitive problems. Another advantages of laser densification is the possibility of obtaining aspherical elements[Ver90], negative microlens, multimode channel waveguide and waveguide microlens[Chi92b]

Hemispherical microlenses and arrays can be made through many techniques like coating, mass transport, IC processing, ion-exchange, photolytic technique, ion or laser beam radiation in InP, GaP, plastic or glass[Coh74][Wad81][Pop88][Bor88][Liu88][Liu89][Oik90][Fra91][Bar91]. High quality microlenses and arrays have been made by using a photolytic method[Bor88]. The difficults of using any mass transport method is the spreading of the profile of the hemispherical lens during the heat treatment.

The idea of a geodesic lens was introduced by Rinehart in 1948, and the theory was developed extensively by Kunz in 1954[Mer83]. A geodesic lens with a depressed curvature on the surface of the substrate is one of the possible elements used as a waveguide lens[Rig73][Che78][Mer83][Ham90b]. Sochacki described a uniform mathematics of perfectly imaging geodesic lenses[Soc86]. Ishikawa et al., also analyzed the focusing characteristics of waveguide lenses(including geodesic microlens) using the beam propagation method[Ish90]. Shimano et al., discussed the design for geodesic lenses where the curvature of the lens shape is restricted within an upper limit to prevent the light leaking from the waveguide[Shi90a]. Up to date, fabrication of geodesic lenses involves ultrasonic grinding on a glass substrate with a polyurethane waveguide. However, the depth of the lens can not be accurately controlled by using this method[Che77][Ham90b]. Laser heating can produce a precise and controllable depressed region in a glass substrate which is much better than the present technique which uses local polishing[Chi92b]

Gradient index elements are more powerful than the use of aspheric surfaces since the GRIN lens can be used to correct chromatic as well as monochromatic aberrations [Atk82]. Monochromatically, the functions of a GRIN lens are similar to the aspherical lens. Polychromatically, a GRIN lens offer significant benefits over aspheres[Car91]. Forer discussed that the use of gradient-index elements in an optical design provides additional degrees of freedom for the correction of aberrations The performance of a many-element homogeneous system can be matched with a system consisting of a reduced number of gradient-index components High performance has been achieved with a three element system using two axial gradients of an eyepiece design[For83] Tomlinson found that GRIN microlenses have superiorities over conventional bulk optical elements. For example, a GRIN rod lenses have significantly smaller aberrations than equivalent single element homogeneous lenses[Tom80]

Table 2 1 lists an extensive categorization of materials, fabrication methods, physical dimensions and the corresponding optical properties of micro-optical lenses. Techniques used in fabricating refractive microlenses are ion exchange in glass [Oik82][Cou82][Sam90][Kin9b0][Hau90], photolytic method on photosensitive glass[Bor88], copolymerization in polymer substrate[Koi88], mass transport in InP substrate[Lia88][Lia89], deep UV hardening on quartz wafers[Pop88], thin film deposition on glass fiber[Coh74], laser densification in porous glass substrate[Chi92a][Vei91], ion beam etching on a n-InP substrate[Wad81], deep electromigration in glass substrate[Oik81][Oik82][Oik82][Iga82b]

In all such substrate-defined micro-optical components the optical characteristics of the substrate material are important to the quality of the components to be formed. Future applications of high quality imaging micro-optics will need broad band coverage such as over the visible band of wavelengths[Car91] According to these requirements, pure silica is the most preferrable candidate for the substrate material which is substantially free of organic or inorganic impurities, with wide band transmission, and index matching with fiber optics Requirements of the fabrication of microlenses are accuracy reliability, reproducibility, mass-producibility, smaller focused spot, applicable focal length, larger numerical aperture [Yam83][Asa86] and excellent performance in imaging Acceptable performance and operating conditions are the primary factors for choice of the individual device for a particular optical application.

Table 2.1 Materials, fabrication methods, and properties of different types of optical microlenses

[illegible]	[illegible]	[illegible]	[illegible] Thickness(mm)	[illegible] (mm)	[illegible]	[illegible]	[illegible]	[illegible]	[illegible]	[illegible] Efficiency(%)	[illegible]
[illegible]	Ion-Exchange	a-c	1000	0.06-2	~1.6	0.025-0.1	~0.44	1.1-1.8	0.21-0.32	[illegible]	[illegible]
[illegible] Glass	[illegible] Interfacial-Gel Copolymerization	a-c	[illegible]	[illegible]	[illegible]	[illegible]	[illegible]	[illegible]	[illegible]	[illegible]	[illegible]
[illegible] Glass	[illegible] Ion-Exchange Ion-Diffusion	[illegible]	[illegible]	[illegible]	[illegible]	[illegible]	[illegible]	[illegible]	[illegible]	[illegible]	[illegible]
[illegible] InP GaP Glass	[illegible] Ion Beam Etching Mass Transport Casting IC Processing Photolytic Technique	[illegible]	[illegible]	[illegible]	[illegible]	0	[illegible]	[illegible]	[illegible]	[illegible]	[illegible]
[illegible] or Type VI Gel-Silica Glass	Ion-Exchange Diffusion Deep Electro-Migration Laser Densification	d-e	0.1-0.8	0.1-1.0	1.3-1.57	0.01-0.37	0.2-30	0.2-30	0.01-0.6	40%-87%	[illegible]
[illegible] or Type VI Gel-Silica Glass	[illegible] Laser Densification	[illegible] g G	[illegible]	[illegible]	[illegible]	[illegible]	[illegible]	–	[illegible]	[illegible] or 80%-95%	[illegible]
[illegible] Silicon InP	[illegible] Lithography	f	–	[illegible]	–	[illegible]	[illegible]	1	[illegible]	30%-[illegible]	[illegible]

All the optical properties are measured by using different laser sources at wavelengths from 0.53μm to 10.6μm

a-GRIN fiber microlens
b-GRIN rod microlens
c-GRIN shaped microlenses(convex, concave, sphere, etc.)
d-shaped microlenses(LS-hemispherical lens, GL-concave lens)
e-GRIN planar microlens
f-diffractive microlens
g-aspherical lens

n-refractive index
Δn-change in refractive index
F-F number(FL/Diameter)
FL-focal length
G- geodesic lens
R-refractive microlens
NA-numerical aperture

In summary, glass is the preferred material for the fabrication of the microlenses Refractive microlenses are more useful than diffractive microlenses because of their broadband features, better performance and more mature processing techniques With aforementioned comparisons, geodesic microlenses and GRIN optical microlenses are the more powerful among the refractive microlenses. However, current techniques in fabricating geodesic microlenses and GRIN microlenses involve sophisticated and sensitive processing steps and have problems such as unexpected lens size and lens profile[Pop88][Lia88], and index inhomogeneity, etc [Oik84]

2.3.3 Ray Theory of Planar Gradient Index Microlenses

When a optical ray is incident on a medium with a different refractive index it is reflected and refracted Figure 2 2 illustrates the light ray trajectory , a deflective dashed line, in a GRIN medium. The refractive index profile shown in the right side of the figure is exaggerated to depict the refractive mechanism at the boundaries with a changing refractive index of the GRIN medium. The ray trajectory is forced to deflect toward the region with higher refractive index because the light is preferably traversed in a route with the smallest optical path length[Hec74]

The behavior of a ray propagating through a GRIN medium can be described by using ray theory[Góm86][Mis88][Zhu88][Dor90] Optical parameters like focal length (FL) and the numerical aperture (NA) of a planar GRIN microlens can be derived using the ray theory The following descriptions are derivations of these optical parameters from the ray theory of a GRIN planar microlens developed by Iga, et al [Iga84]

The geometry of the planar microlens is shown in Figure 2.3 It is assumed that the substrate is thick and the ray is focused Inside the substrate The ray is deflected within the GRIN region I and emerges in the medium with uniform index region II The three dimensional distribution of the refractive index of this microlens is formulated as

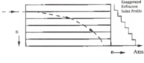

Figure 2 2 The light ray trajectory in a GRIN medium, After[Iga84]

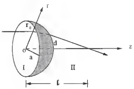

Figure 2.3 Ray trajectory in a three dimension DI medium, a planar microlens. Region I is an index distributed region and II a uniform one, after [Iga84]

$$n^2 (r,z) = n^2 (0,0)[R(r)+Z(z)] \tag{2 4}$$

$$R(r) = 1 \ (gr)^2 \tag{2.5}$$

$$Z(z) = v_{20}(gz)^2 \tag{2 6}$$

where n is the refractive index, r is the radial distance of the DI region I, and z is the distance along the direction of the depth of the medium g is a focusing constant representing gradient index. v_{20} is the parameter of the index distribution with higher order The ray equation is simplified in this case and described as follows

$$\int_{r_0}^{r} \{\sqrt{[R(r')-R(r_0)]}\}^{1} dr' = \int_{0}^{z} \{\sqrt{[Z(z')+R(r_0)]}\}^{1} dz' \tag{2 7}$$

$$\frac{dr_1}{dz}_{z=z1} = - \frac{[\sqrt{[Z(z_1)+R(r_0)]}]}{\{\sqrt{[R(r_1) \ R(r_0)]}\}} \tag{2.8}$$

The optical ray is incident to the planar microlens at $(r_0,0)$ and parallel to the z axis. l is defined as the focusing length When r_0 is close to 0 l is equal to l_0 which is the focal length f. The focusing length l at the output position (r_1,z_1) of the DI region I can be expressed as

$$l = r_1 + z_1 * \frac{\sqrt{[Z(z_1)+R(r_0)]}}{\sqrt{[R(r_1) \ R(r_0)]}} \tag{2 9}$$

where r and z satisfy the following conditions

$$\int_{r_0}^{r_1}[\sqrt{[R(r)-R(r_0)]}]^{-1}dr = \int_{0}^{z_1}[\sqrt{[Z(z)+R(r_0)]}]^{-1}dz \qquad (2.10)$$

$$n_2^2 = n^2(0)[R(r_1)+Z(z_1)] \qquad (2.11)$$

For a paraxial ray, r_0 is approximately equal to 0. The focusing length l_0 can be obtained by substituting equations (2.4.2) and (2.4.3) into equation (2.4.6)

$$l_0 = d + \sqrt{1-2\Delta}\cot[\frac{gd \cdot \sin^{-1}\sqrt{(2\Delta)}}{\sqrt{(2\Delta)}}]/g \qquad (2.12)$$

where $\Delta = [n(0)-n_2]/n(0)$ and d is the depth of the DI region I at r=0. The numerical aperture (NA) is defined as

$$NA = 0.2n_2\sqrt{2\Delta} \qquad (2.13)$$

The predicted data of the l_0 and NA from these formulae are in good agreement with the experimental data[Iga84].

2.3.4 Geometry of Waveguide Geodesic Microlenses

A geodesic lens is situated in the plane of a waveguide and is used for redirecting and focusing the lightwave confined along the waveguide. A typical geodesic lens is illustrated in Figure 2.4. The optical ray is conducted along the waveguide(with ~1% higher refractive index than of the substrate) on the surface of the substrate and then focused by a geodesic lens. The optical ray is transmitted along the depressed region and emerges in the other side of the waveguide toward the focal point.

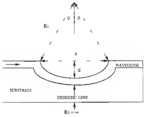

Figure 2 4 Cross section view of a typical geodesic lens.

The focal length of the geodesic lens is evaluated by assuming that the thickness of the waveguide is negligible. In Figure 2 4, a is the diameter of the depressed region, d is the depth of the depression. Considering only the surface shape, the focal length of the geodesic lens can be determined using the formula below[Mer83][Ham90b]

$$\text{Focal Length} = \frac{R\text{Sin}\theta}{2(1-\text{Cos}\theta)} - \frac{a}{4(1-\text{Cos}\theta)} \qquad (2\ 15)$$

where R is the radius of the curvature of the spherical surface and 2θ is the vertex angle subtended by the arc of the depression

The geodesic lens has spherical aberration caused by the spherical depression. Asphericity in the depression of a geodesic lenses is proposed to reduce the spherical aberrations[Ham90b] Modifications of the focal length of a geodesic lens due to the asphericity is discussed by Mergerian et al [Mer83].

2.3.5 Applications of Microlenses

Microlenses can be used in (a)Integrated Optics, (b)Micro-optics and (c)Stacked Planar Optics Some examples of the applications of microlenses in these fields are described schematically as follows

(a)Integrated Optics

An integrated microlens is located in the plane of waveguide and used for redirecting and focusing the lightwave confined along the waveguide The manipulation of the optical ray is achieved by the geometry, diffraction, or GRIN effect of these lenses Integrated optical microlenses include (a)shaped bump lens, (b)Luneburg lens, (c)geodesic lens, (d)grating lens(Fresnel lens), (e)embedded shape lens and (f)recessed shape lens as shown in Figure 2.5[Fei88][Car91] Numerous techniques for lens fabrication have been

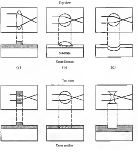

Figure 2.5 Integrated optical microlenses, after [Fei88] and [Car91]

(a) Flat bump with microlens
(b) Luneburg microlens
(c) Geodesic microlens
(d) Grating microlens
(e) Embedded shaped microlens
(f) Recessed shaped microlens

developed, three of which are the geodesic, Luneburg, and diffraction lens techniques[Hut87].

One application of the integrated lens in a radio-frequency(RF) spectrum analyzer is shown in Figure 2.6[Hut87]. This device consists of a hybrid package that includes a butt-coupled laser diode, a waveguide on substrate, two waveguide lenses, a surface acoustic wave transducer array, and a butt-coupled linear photodiode array. A light beam is spatially modulated by the input RF signal, using acousto-optic or electro-optic techniques. The modulated beam is then collimated and focused by the waveguide lenses on a detector array[Fei88]. Other related applications include acousto-optic correlator, signal sampling, analog-to-digital conversion and dual channel acousto-optic processor[Hut87].

(b)Micro-optics

In micro-optics, the major functions of the microlenses are focusing, imaging, or transmitting optical rays. For instance, microlenses are used to improve the coupling efficiency or focusing ability, potentially used in opto-electronics and in optical computing systems[Jah89][Jah90], or providing the interconnections of a VLSI(Very Large Scale Integrated Circuit) system. The optical ray is incident on the lens perpendicularly and is focused in the other side of the lens. Six types of the micro-optical lens used in micro-optics are depicted in Figure 2.7. They are (a)GRIN fiber microlens, (b)GRIN rod microlens, (c)GRIN geometric microlens, (d)geometric microlens, (e)GRIN planar microlens, and (f)diffractive microlens. The microlenses are distinguished by the optical functions of the lenses, i.e. the focusing ability of the lens is achieved by either diffraction, refraction or surface curvature.

Feitelson discussed the feasibility of creating a digital optical computer[Fei88]. Cylindrical lenses and lens arrays are important elements in an optical computer to provide the multiple imaging which is widely applied to matrix vector multiplication, optical interconnection, space variant parallel processing, etc.[Ham90b]. One example of a

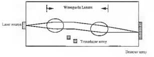

Figure 2.6 A radio-frequency spectrum analyzer, after [Hut87]

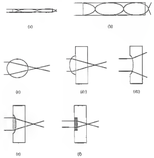

Figure 2.7 Micro-optical lenses.

(a)GRIN fiber lens
(b)GRIN rod lens
(c)GRIN shaped lens(convex, concave, sphere,etc.)
(d1)Hemispherical lens
(d2)Concave lens
(e)GRIN planar lens
(f)Diffractive lens

microlens array used in an optical computer is illustrated in Figure 2.8. It shows a simpler way to implement a discrete space variant linear transform with a lens array. The input f is at the left-hand side. A set of N^2 detectors is at the right-hand side. An array of N^2 lenses creates N^2 distinct images of the input on each detector. A mask is placed between the lens array and the detector array modifying the light distribution falling on the detectors. At the moment only prototypes of the basic elements of an optical computer exists. The quest for materials and technologies is far from over[Fei88]. Development of a high speed digital optical processor will depend on small devices interconnected by micro-optic systems, i.e.small array size of the lenslets. Thus,the micro-optic system will be achieved only through nontraditional manufacturing techniques[Jew90].

(c)Stacked Planar Optics

Besides one single microlens, a two-dimensional planar microlens array can be used in laser output collimation for a two dimensional diode laser array (opto-electronics). The features of this planar microlens array are demonstrated in Figure 2.9. A two-dimensional planar microlens array is designated on the planar surface of the substrate. A GRIN region located under the surface can focus the optical ray.

Another application of the microlens array is stacking of the planar microlens arrays which provides an interconnection between fibers, as illustrated in Figure 2.10, discussed by Iga et, al[Iga82b]. This design is used to overcome difficulties like optical alignment and fabrication. Two-dimensional arrayed optical components, such as microlenses, filters, mirrors, and detectors, can be stacked together to construct functional optical components[Iga84].

A negative microlens arrays is proposed to be stacked together with the focusing microlenses array, the same as in Figure 2.10. to provide more possibilities for manipulating the optical beam[Chi92b]. For example, this stacked compound microlenses can be used to reduce lens aberrations like chromatic, spherical, astigmatism, curvature of

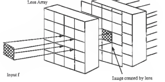

Figure 2.8 Microlens array used in the optical computer, after [Fei88] and [Ham90]

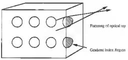

Figure 2.9 A planar GRIN microlens array

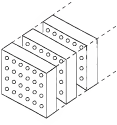

Figure 2.10 Stacking of planar optical devices, after [Iga84]

field coma and distortion[Rud78] The use of compound microlenses is also capable of preventing chromatic aberration when a tunable laser, with selective wavelengths, is used as a light source. Another capability of this compound microlenses or microlens arrays is that it allows adjustment of the focal length of the microlens arrays, i.e functioned like a 'zoom' microlenses.

2.3.6 Summary

As discussed in section 2.1, Type VI gel silica glass has a unique homogeneous pore texture, the porosity of the gel silica glass decreases during furnace densification The physical, mechanical, and optical properties of gel silica glass improve upon densification. The final product is a Type V full density gel silica glass which is structurally like a commercial pure silica glass and has superior thermal and optical properties The difference in the densification between Type VI and Type V gel silica glasses can be enhanced by introducing a laser to locally densify the Type VI porous gel-silica glasses. Thus, the created index change between the irradiated region and the silica substrate gives rise to the developments of devices used in optical transmission system. Basically,the laser processing time is much faster than the conventional routes to obtain a microlens

From the discussions in previous section, microlenses have large varieties of applications in integrated-optics, micro-optics, and stack-planar-optics Current fabrication methods listed in Table 2.1 have disadvantages such as

(a)A period for hours are required for obtaining a GRIN gel from soaking or a GRIN glass from conventional ion-exchange methods.

(b)A strain-induced index change in a diffused microlens caused by the diffusant size

(c)The photolithograph technique based on melting of the lens material is very difficult to control the the spreading.

And most of the techniques involve tedious, sophisticated, and process sensitive steps. In contrast, the advantages of introducing laser densification to produce microlenses include

(a) a fast and clean process,

(b) a contact free local treatment,

(c) a high degree of automation and a good reproducibility of the process,

(d) a feasible alternative or addition to existing techniques.

Further, the optical properties of the laser densified region of the gel-silica glasses are improved instead of degrading the modified region by the diffusants. It is also possible to obtain a full density region by laser heating which exhibits high optical transmittance from UV to NIR. All these merits show the necessary routes of producing optical devices by using laser heating on the gel-silica substrates.

2.4 Review of FTIR

The first infrared(IR) spectrum of sunlight was taken by Sir William Herschel about a century and three quarters ago[Cra76]. The first infrared spectrum of substance is obtained from the measurements of distilled water which also taken by Sir William Herschel. However, the structure of the molecule was little understood at that time. The development of molecular structures and observation of the infrared molecular spectra began at the end of 19th century.

The molecular energy consists partly of[Col90]

(a) translational energy

(b) rotational energy

(c) vibrational energy

(d) electronic energy

Electronic energy transitions normally give rise to absorption or emission in the ultraviolet and visible regions of the electromagnetic spectrum from 0.01 to 0.78 μm. Molecular vibrations give rise to absorption bands throughout most of the infrared region of the spectrum from 0.78 to 50 μm(near and middle infrared). Pure rotation gives rise to absorption in the far infrared or the microwave region from 0.005 to 100 cm.

It is known that the vibration energy levels of a molecule are quantized from the quantum viewpoint. One of the selection rules for infrared spectroscopy is that the incident photon has the right energy to increase the vibrational quantum number by one which has a frequency equal to the classical vibrational frequency of the molecule[Col90]. As most of the molecules at normal temperature exist in the ground state, the fundamental transitions of the molecules dominate the infrared absorption spectrum. The other selection rule is that in order to absorb infrared radiation, a molecular vibration must cause a change in the dipole moment of the molecule. Thus, the intensity of an infrared absorption band either depends on the population of the energy levels or is proportional to the square of the change in dipole moment.

Table 2.2 describes the assignments of the absorption bands of the silica glasses in IR spectra. Hair discussed that the strong absorption band observed at ~ 3750 cm^{-1} in the IR absorption band of silica is attributed to the fundamental stretching vibration of a hydroxyl group attached to a silicon atom on the surface of the silica which is referred to as "free hydroxyl groups" or "isolated silanol groups". The strong, broad adsorption band that appears to peak about 3500 cm^{-1} is attributed to molecular water that is physically adsorbed upon the surface. The broad peak at 3400 cm^{-1} is assigned to the vibrations of molecular water[Hai67].

Bertoluzza et al. reported a series of infrared spectra from 200 to 4000 cm^{-1} on silica gels[Ber82]. IR spectra of the gel-silica samples densified at increasing temperatures up to 800°C were compared. The band at 960 cm^{-1}, a typical Si-OH stretching mode, drops in intensity with increasing temperature which indicates the involvement of the

Table 2.2 Assignments of molecular vibration modes of the silica glass

IR Absorption Bands (1/cm)	Assignments	References
800	TO band, network Si-O-Si symmetric bond stretching vibrations	[Dur86][Kir88]
960	Stretching vibration of external Si O⁻ groups	[Dur86]
1076-1088	TO band mode of Si-O-Si adjacent O atoms execute the motion of asymmetric bond stretching vibration in phase with each other	[Ber82][Kir88]
1160	LO band, mode of Si-O-Si, adjacent O atoms execute the motion of asymmetric bond stretching vibration 180°out of phase with each other	[Kir88]
1200	TO band, mode of Si-O-Si, adjacent O atoms execute the motion of asymmetric bond stretching vibration 180°out of phase with each other	[Kir88]
1256	LO band, mode of Si-O-Si, adjacent O atoms execute the motion of asymmetric bond stretching vibration in phase with each other	[Kir88]
3200	Si-OH hydrogen bonded groups	[Ber82]
3400	Vibrations of molecular water	[Has67]
3500	Physically adsorbed molecular water	[Has67]
3700	Fundamental stretching vibration of isolated silanol groups	[Has67][Ber82]

polycondensation process The vibrational bands at ~3200 and 3420 cm^{-1} were attributed to adsorbed water and/or to silanol OH hydrogen bonded groups, while those in the range of 3650-3680 cm^{-1} can be attributed to silanol (SiOH) unassociated groups These spectra give evidence for the dehydration and polycondensation of the gel-silica samples at progressively higher temperatures. They also reveal a progressive transformation of the gel structure toward the structure of fused quartz The structural transformation is practically complete at 800°C although densification is not completed until 1100-1150°C[Wan88] [Vas89a]

Lucovsky et al reported that a strong infrared absorption at ~1075cm^{-1} of a silicon dioxide film is due to a stretching vibration in which the oxygen atom motion is in the plane of the Si-O-Si bond and in a direction parallel to a line joining the two silicon atoms [Luc87] The ~1080 cm^{-1} band in the infrared spectra of silica gels is associated with the TO mode of Si-O-Si asymmetric bond stretching vibrations(AS)[Ber82] The absorption band at 960 cm^{-1} in silica gels is assigned to the stretching vibration of external Si-O⁻ groups[Dur86] The weak absorption band at 800 cm^{-1} has been assigned to a network Si-O-Si symmetric bond stretching vibration(SS)

Kirk studied the LO-TO modes in the infrared absorption spectrum of amorphous silica[Kir88] LO and TO modes are illustrated in Figure 2.11 (a) and (b), respectively He observed that the TO band and its high frequency shoulder are due to an asymmetrical stretch(AS) motion in which the O atom moves back and forth along a line parallel to the axis through the two Si atoms. AS motion is illustrated In Figure 2 12(a) The AS motion actually gives rise to two vibrational modes.(1) an AS_1 mode(TO band centered at ~1076 cm^{-1}) in which adjacent O atoms execute the AS motion in phase with each other, and (2) an AS_2 mode(TO band centered at 1200cm^{-1}) in which adjacent O atoms execute the AS motion 180°C out of phase with each other A symmetrical stretching(SS) of the O atom along a line bisecting the axis formed by the two Si atoms characterizes the vibrational mode of the middle TO band centered at ~810cm^{-1} SS motion is illustrated in Figure

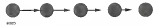

(a) Longitudinal-optic mode

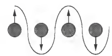

(b) Transverse-optic mode

Figure 2.11 Schematics of longitudinal-optic and transverse-optic lattice vibration modes of a monoatomic chain of atoms

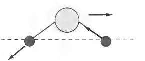

(a)Asymmetric stretching(AS) vibration of amorphous silica

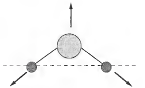

(b)Symmetric stretching(SS) vibration of amorphous silica

Figure 2.12 Schematics of local vibrational motions of asymmetrical stretching and symmetrical stretching of the oxygen atoms with respect to the silicon atom in amorphous silica, after Kirk[Kir88].

2.12(b). LO modes are not observed in normal incidence infrared absorption spectra since they do not interact with light due to the Berreman effect[Kir88]. The LO AS_1 and LO AS_2 modes are located at 1256 and 1160cm^{-1}, respectively.

Duran et al. studied the structural evolution of gel silica glasses prepared at different R values(H_2O/TEOS molar ratio). They showed that the IR absorption band at 960 cm^{-1} (NBO) drops progressively with densification temperature and almost disappears at 800°C [Dur86]. In contrast, the band at 800 cm^{-1}, a symmetric network stretching vibration, intensifies with increasing temperatures. The combination of both aspects allows one to infer that a polycondensation process occurs with the formation of Si-O-Si bonds as a result of thermal treatment. Also, the asymmetric Si-O stretching band shifts to higher wavenumbers (1085→1105 cm^{-1}) during densification which involves a strengthening of the network and can be interpreted as sintering produced by interparticle bonding formation (when $R < 20$).

Anisotropic expansion of a 4-fold silica ring with adsorption of a water molecule, predicted by an INDO calculation, also indicates a longer Si-O bond length for a porous gel silica glass with a high concentration of silanol groups[Wes90a]. Silanols-rich gels are hydrophilic and easily adsorb water from the ambient atmosphere. This may also contribute to the shift in the asymmetric Si-O stretching band of porous silica gels to a higher frequency as the concentration of the silanol groups decreases during sintering; in other words, the less the amount of water adsorbed on a porous gel, the less is the dilation of the network(stronger silica network or shorter Si-O bond length).

It has been suggested by Devine et al. that evaluating the shift of the dominant IR absorption bands at ~ 440, 800, 1070 cm^{-1} of an undensified silica may be used to determine thin film densities with thicknesses < 100 nm[Dev88]. The shifts of dominant peaks are related to the Si-O-Si bond angle as well. Densification can be categorized as elastic and plastic densification when the amorphous silica and α–quartz are densified by using hydrostatic pressure[Dev88][Wal91]. All α–quartz data indicate a elastic densification involving a variation in Si-O Si bond angle which is reversible and can relieve the strain on release of the pressure. Both bond angle variation and structural reorganization occur in the plastic densification of amorphous silica, and the reorganization permits a partial relaxation of the angular variations Plastic densification is irreversible (bond breakage to form smaller rings), does not change on release of the pressure and is stable with time at room temperature However, compressed amorphous silica with density of 3 0 g/c c appears unstable against annealing at high temperature ~ 950°C

Viscoelastic compaction is another mechanism for a amorphous silica under pressure densification The viscoelastic compaction includes a elastic component (allowing a reversible change) and a plastic component(causing a permanent deformation when the pressure exceeds the critical point) Same viscoelastic compaction mechanisms occurred in a laser irradiated amorphous silica examined by Devine et al [Fot86][Wal91]. The permanent deformation is due to ring collapse forming smaller rings and not due to laser damage induced defects

Walrafen et al. reviewed that there exists an angle and bond length correlation in structure modifications of amorphous silica[Wal86][Wal91] The structure modifications occur by applying a compressive or a tensile stress on the glass substrate. A decrease in the mean equilibrium bond angle(intratetrahedra bridging oxygen) will produce a corresponding increase in both the mean equilibrium Si-O bond length and the mean equilibrium dihedra(or tilt) angle between the adjoining silica tetrahedra.

It is concluded that the shift in the absorption spectra of the gel-silica glasses densified at different temperatures indicates that IR spectra are density-sensitive. Thus, the density sensitive shifts can be used to identify the structural changes The structural variations of the glasses by laser irradiation seem similar to the glasses under stress or pressure. Viscoelastic compaction mechanisms occurred in a laser irradiated amorphous silica as well as in a glass under stress or pressure.

CHAPTER 3
PROCESSING AND PROPERTIES OF GEL-SILICA GLASSES

3.1 Introduction

3.1.1 Goals of Sol-Gel Processing

The sol gel process includes mixing casting, gelation aging drying, stabilization, dehydration and densification The gel silica glasses made through the sol-gel process at increasing densification temperature include dry gel, Type VI partially densified gel-silica glass, and Type V full dense gel silica glass

The product of the sol-gel processing described in this study is a partially densified gel-silica glass. The partially densified gel-silica glass, termed Type VI gel silica glass, has a unique homogeneous pore texture. The gel-silica glasses have small pore radii(~12Å), large pore volumes(≤0 40 >0 c c./g), and a high concentration of silanols on the pore surface. The pore volume of the partially densified gel silica glass decreases as the densification temperature increases. Simultaneously, the bulk density of the partially densified gel-silica glass increases upon furnace densification until it reaches a maximum, 2.2 g/c c The fully densified gel-silica glass is termed a Type V fully dense gel silica glass

These partially densified gel-silica glasses are to be used in this study as substrates for further CO_2 laser densification. The thermal effect induced by CO_2 laser heating enhances the densification of the Type VI partially densified gel silica substrate. However, a previous study showed that there was a structural relaxation of the laser densified region on a partially densified gel-silica substrate with bulk density equal to ~1 56 g/c c [Slo90]

Cracking of the laser densified region was also observed when the bulk density of the gel silica substrate is low.

In order to avoid these problems, one goal of the sol-gel processing in this study is to make a Type VI gel silica substrate with high bulk density above 1.80 g/c.c. The strength of the partially densified gel-silica glass is higher as the pore volume decreases upon densification. Thus, a more stable laser irradiated region is expected on the partially densified gel-silica glass with high bulk density of >1.80 g/c.c.

The requirements of Type VI gel-silica glasses for laser densification of optical components are surface flatness, homogeneity, transparency, and sufficiently high bulk density to prevent subsequent relaxation after laser heating. Surface flatness and homogeneity are necessary for the fabrication of arrays of optical components on the surface of the gel silica glass, and for the ease of analyses, such as surface profiles, focal length, etc. Characterization of optical properties of the laser densified spots would be impossible if any bulk inhomogeneity or foaming is present. Each processing step of the gel-derived glasses must be carefully accomplished to fulfill these requirements.

Chemical stabilization is used to make a Type VI porous gel-silica substrate with higher bulk density >1.8 g/c.c. This is due to the fact that gel silica glass foams easily when the densification temperature is above 900°C if only thermal stabilization is used. Trapped water expands within the closed pores which causes the foaming. Chemical stabilization with gaseous chlorine compounds is the most effective means of removal of hydroxyl groups of the gel-silica glass prior to consolidation of pores[Bri90]. Therefore, in this study, gel silica glasses densified are with chemically stabilized prior to densification to >1.80 g/c.c.

The advantages and motivation of using sol gel glasses for optical components have been discussed in Chapter 2. Low impurities, homogeneity, excellent transmission from UV to NIR etc., are the most significant properties of the monolithic Type V gel silica glasses that have been achieved to meet the requirements in optical applications. Detailed discussions of the properties of a Type V gel-silica glass were reported by Hench et al[Hen88][Hen90a][Hen90b]. A goal of this study is to achieve equivalent high quality properties in laser densified regions on Type VI gel silica substrates. The laser densified regions can be utilized as optical components, i.e. microlenses or microlens arrays. The laser-enhanced densification region has a higher bulk density and a higher refractive index than the substrate. Thus, the irradiated region can be used to manipulate optical rays, such as focusing or magnifying, within a substrate of lower refractive index.

3.1.2 Properties of Furnace Densified Gel-Silica Glass

Hench et al. discussed that there are relatively few papers describing the thermal, mechanical, and optical properties of gel-derived monoliths. This is because of the difficulty of producing large stable structures[Hen90a]. Consequently, it is necessary to determine the physical properties as well as structural characteristics of the substrates developed in this study.

Four characterization techniques for monolithic gel-silica glasses with increasing densification temperature are demonstrated herein. Characterization methods include physical(bulk density and pore texture), thermal(thermal expansion and contraction), mechanical(microhardness), and optical properties(UV/VIS/NIR transmission spectra, Micro-FTIR reflectance spectra, and the refractive index) of the gel-silica glasses densified at different temperatures. For comparison, bulk density, refractive index, and UV/VIS/NIR spectrum, values of a Type V fully dense gel silica glass are obtained from Hench et al.[Hen88][Hen90a][Hen90b]

3.2 Preparation of Type VI Gel-Silica Glasses

A schematic illustration of the gel-silica glass processing sequence with scaled characteristic structures for each processing step is shown in Figure 3.1[Hen90a]. To ensure the reproducibility from batch to batch, it is important to control processing parameters such as the pH of the sol, gelation time,time and temperatures of the aging, drying, stabilization, dehydration and densification process.

The sol was a homogeneous mixture of tetramethylorthosilicate(TMOS), deionized (DI) water and was catalyzed by using nitric acid. The amount of water and acid is controlled in order to obtain a complete hydrolysis. The average pH of the sol is approximately 1 before casting. The sol was cast into a plastic mold and tightly sealed to avoid evaporation.

A high ratio of diameter to thickness of the mold is preferred for the surface optical applications due to the ease of achieving surface flatness and diminution of the effect of surface meniscus. Low surface roughness , high chemical resistance, and high thermal stability of the mold are also required.

Gelation of the sol proceeded at room temperature for 65 hours. The surface flatness of the wet gel is ensured during the gelation by maintaining horizontal storage and avoiding any vibration. The gels are then aged in sealed containers for the time and temperatures shown in Figure 3.2.

The aged gel was removed from the mold and immersed into a container filled with DI water. Drying of the silica gel is one of the crucial steps to obtain the monolithity of the gel. Large capillary stresses occur and lead to catastrophic fracture if the capillary pressure in the gel network is not well controlled. Pressure control can be obtained by reducing the diameter of the gas outlet on the container during drying.

The drying schedule is illustrated in Figure 3.3. The final step of >100°C in the drying schedule is used to eliminate the pore liquor within the pores of the gel and increase

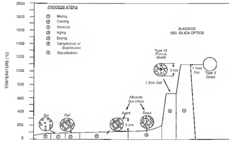

Figure 3.1 Gel-Silica Glass(pore radius = 1 2 nm) Process Sequence with scaled structural characteristics

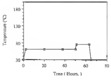

Figure 3.2 Schematic of the aging schedule for a pure gel-silica monolith

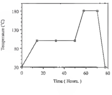

Figure 3.3 Schematic of drying schedule for a pure gel-silica monolith

the strength of the gel. The product of the drying process is called a xerogel. The dried xerogel has a very large surface area (>400 m^2/g) and a very high concentration of silanols on the pore surface which may result in thermal and environmental instabilities of the dry gel.

A stabilization treatment is required to overcome the the chemical instabilities of the dry gel. The stability of the dry gels can be improved by using either thermal stabilization or chemical stabilization. Thermal stabilization involves heating the xerogel in a tube furnace in dry air which reduces the porosity and increases the bulk density of the dry gel. Dry air, at constant pressure, is flowed through the tube to carry out the gaseous products during thermal stabilization i.e. water molecules and organics, etc.

However, it is difficult to obtain complete dehydration by using thermal stabilization alone. Bloating or foaming usually occurs when the residual water expands after pore closure occurs during densification. Thermal stabilization can be used to increase the strength of the gel prior to chemical stabilization and densification up to 1150°C. A dry gel directly undergoing chemical stabilization is susceptible to cracking without prior thermal stabilization.

A typical schedule of the thermal stabilization treatment is shown in Figure 3.4. The heating rate ≤ 10°C/hour starting from 600°C is used, depending on sample thickness. The heating rate can be higher for a thinner sample. The highest temperature of stabilization ranged from 700°C to 900°C depending on the physical dimension of the sample. The stabilization temperature should be high enough to achieve sufficient strength for subsequent chemical stabilization, and concurrently the pore connectivity must be preserved to allow chemical dehydration to occur. Determination of an appropriate stabilization schedule is the second crucial step to obtain a monolithic gel-silica glass for further dehydration and densification.

Chemical stabilization is the most effective means of removal of hydroxyl groups prior to consolidation[Bri90]. The most effective chemicals used in surface dehydration of

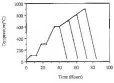

Figure 3.4 Schematic of thermal stabilization schedule for pure gel-silica optical substrates.

gel silica glass are $ClSi(CH_3)_3$, $SiCl_4$, Cl_2, and CCl_4 which react with the surface hydroxyl groups to form HCl and desorb from the the gel body over a temperature range of 400°C - 800°C when the pores are still fully connected[Sny66][Hen90b]

A typical dehydration and densification schedule used in this work is shown in Figure 3.5. The chemical stabilization occurs with a CCl_4 atmosphere carried by a steady He flow at 550°C, followed by a steady dry air flow during partial densification. Generally, the period of chemical dehydration is from 6 to 48 hours depends on the porosity and dimension of the gel silica monoliths. Flow rate, heating rate, dehydration time, previous thermal stabilization temperature and the position of the sample in the tube furnace are important variables that must be controlled to sustain the monolithicity of the silica gel. This is the third crucial step to obtain a monolithic gel-silica glass for further laser treatment.

Different bulk densities of the gel-silica samples produced using the schedules described above ranged from ~1.10 g/cm^3 to 2.20 g/cm^3. These densities were achieved by different thermal treatments (from 180 °C to 1150 °C). The samples are termed as dry gel (~1.10 g/cm^3), stabilized gel-silica glass by thermal stabilization(> 1.17 g/cm^3,<2.0 g/cm^3), near fully densified gel-silica glass by thermal and chemical stabilization(~2.0 g/cm^3) and fully densified gel-silica glass(2.2 g/cm^3)

3.3 Physical Properties

3.3.1 Bulk Density and Pore Texture Analysis

The bulk density of the gel-silica glass is calculated by using the equation below:

$$\text{Bulk density} = \frac{\text{weight of the material}}{\text{volume occupied by solid and voids}} \qquad (3.1)$$

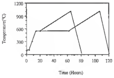

Figure 3.5 Typical chemical stabilization and densification schedule for gel-silica glass optical substrates

The weight of each gel-silica glass is measured after dehydration in a vacuum oven heated at 150°C. The volume of the gel silica sample is obtained by using a mercury pycnometer. In this measurement, without external pressure, the mercury will not intrude into the micropores of the gel-silica glasses because of the high surface tension of the mercury. Thus, the volume occupied by the solid and voids can be measured.

Pore texture of the gel silica glasses is obtained by using nitrogen gas adsorption analysis on a Quantachrome Autosorb 6. The pore texture includes surface area, pore radius, and pore volume of the gel silica glasses. Nitrogen gas adsorption analysis is usually employed for structures with pore radii smaller than 1000 Å[Vas89a]. The pore texture is determined from the "adsorption isotherm", a relationship between the quantity of the adsorbate(nitrogen gas) and the relative ratio of the adsobate equilibrium pressure(P) to the adsorbate saturated equilibrium pressure(P_0)[Lau91]

BET theory was developed by Brunauer, Emmett, and Teller in 1938[Bru38][Vas89a]. The BET theory assumes that the uppermost molecules in adsorbed stacks are in dynamic equilibrium with the vapor. The BET equation is formed as followed[Low79]

$$\frac{1}{W(P_0/P-1)} = (\frac{1}{W_m C} + \frac{(C-1)P}{W_m C P_0} \qquad (3.2)$$

where

W: weight of vapor adsorbed

W_m: weight of vapor in a complete monolayer

P: adsorbate equilibrium pressure

P_0: adsorbate saturated equilibrium pressure

C: a BET constant

The surface area of the material is determined from a plot of $W(P_0/P-1)$ versus P_0/P, it is usually a straight line. The slopes s and the intercept i of a BET plot are

$$s=\frac{C-1}{W_mC} \tag{3.3}$$

$$i=\frac{1}{W_mC} \tag{3.4}$$

W_m and C are solved from equations (3.3) and (3.4).

$$W_m=\frac{1}{s+i} \tag{3.5}$$

$$C=\frac{s}{i}+1 \tag{3.6}$$

The total surface area can be calculated from the following equation

$$S_t=\frac{W_mNA}{M} \tag{3.7}$$

where

S_t Total surface area

N Avogadro's number

A. cross-sectional area

M : molecular weight of an adsorbate molecule

Since the pore texture is assumed to be a cylindrical geometry, the total surface area S_t is equal to[Low79]

$$S_t = 2V/r \tag{3.8}$$

Where V is the total pore volume, r is the average pore radius.

3.3.2 Results and Discussions

Figure 3.6 shows the relationship of the pore volume and the bulk density of the gel silica glasses with increasing densification temperature. Bulk density of the gel silica glasses increases as the densification temperature increases, and the pore volume decreases at increasing densification temperature. From equation (3.1), it is known that the bulk density increases as the volume occupied by voids decreases. That means the bulk density of the porous gel silica glass is increased at the expense of reducing pore volume during densification.

Figure 3.7 shows the variation of the pore radius and surface area of the gel silica glass with increasing densification temperature. Surface area decreases as the densification temperature increases. Note that the pore radius exhibits very little change during the densification. The surface area of gel silica glasses drops drastically above 900°C. Since the pore texture is assumed to have a cylindrical geometry, the surface area is proportional to the pore volume at a constant pore size according to equation (3.8). The surface area decreases as the densification temperature increases as a result of the reducing pore volume.

The driving force in densification is the reduction of solid/liquid or solid/vapor interfacial energy due to the very high initial surface area of the silica gels (~800 m^2/g). Below 150°C, shrinkage of the silica gel is caused by the desorption of water and alcohol. Between 150°C and ~525°C, shrinkage is attributed primarily to polymerization of surface silanols and structural relaxation[Wal91]. Above 900°C, the shrinkage is due to the concurrence of structural relaxation, continued condensation of silanols and viscous

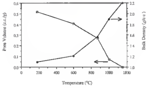

Figure 3.6 Pore volumes and bulk densities of gel silica glasses at increasing densification temperature.

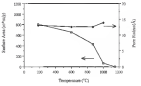

Figure 3 7 Surface area and pore radii of gel silica glasses at increasing densification temperature sintering[Elm83][Sch86][Bri90] The variation in physical properties of the gel-silica glasses during densification are correlated with these mechanisms

3.3.3 Conclusions

The bulk density of the gel-silica glass increases at the expense of reducing pore volume The surface area of the gel silica glasses drop drastically above 900°C when viscous sintering occurs. In addition, Figure 3 6 and Figure 3 7 show that there is still appreciable pore volume with invariant pore radius after thermal stabilization above 800°C which permits dehydration to be completed. The relationships between physical properties as a function of densification temperature are consistent with the previous work[Hen88][Wan88][Vas89a][Vas89b]

3.4 Thermal Property

3.4.1 Dilatometer Analysis

Dilatometric behavior of gel silica glasses in an ambient atmosphere were measured using a Theta Industries Research II Electronic Dilatometer This dilatometer equipped with a tube furnace records the linear dimensional change of the test sample at a given heating rate and cooling rate. The highest temperature of the furnace can be raised up to 700°C. The samples are polished in a rectangular shape with length of 10 mm and ~3 mm in thickness A sample from the NBS(National Bureau of Standards, now the National Institute of Standards and Technology) of fused silica is used as a standard for all the measurements

The thermal schedule for the dilatometer analysis is 3°C/min. for heating(up to 700°C) and cooling(down to room temperature) Arrows indicate the direction of the dimensional change of the samples upon heating and subsequent cooling. Curve 1(sample termed S1) shown in Figure 3.8 is the thermal behavior of a full density gel silica glass provided by Zhu[Zhu89]. Curves 2 and 3 are the thermal hysteresis loops of the gel-silica glass stabilized at 900°C (S2) and at 700°C(S3), respectively. Corresponding bulk densities of samples used to obtain curves 2 and 3 are 1.58 and 1.34 g/c.c., respectively.

Full density gel-silica glass exhibits linear thermal expansion and shrinkage upon heating and cooling as shown in Figure 3.8. There is no hysteresis loop of the Type V gel silica glass in curve 1. It behaves the same as a commercial pure silica glass.

Sample S2 shrinks immediately at the beginning of the heating, there is no significant expansion around 100°C and slightly expands during cooling below ~320°C.

Sample S3 expands up to ~100°C and shrinks afterwards upon heating, a significant expansion is observed below ~320°C during cooling. The resulting linear dimensional change of S3 is larger than S2, i.e. the discrepancy of the loop of S3 is larger than that of S2.

There are many mechanisms responsible for the structural changes of porous gel silica glass that occur during the dilatometry measurements. The correlated mechanisms of the thermal behavior of porous gel-silica glasses are discussed by Brinker et al. Zhu, Wallace and others[Elm83][Sch86][Zhu89][Bri90][Wal91].

Results from the above studies can be summarized as follows. The shrinkage of the Type VI porous gel silica glass upon heating and cooling can be attributed to

(1)Below 150°C, shrinkage of S2 and S3 is caused by the desorption of water and alcohol from the pores.

(2)Between 150°C and 700°C upon heating, shrinkage is attributed primarily to the polymerization of silanols to form siloxane bonds. Simultaneously, there are high concentrations of threefold rings formed on the internal pore surface[Wal91]. This type of polymerization may not result in permanent

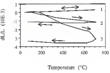

Figure 3.8 Dilatometric behavior of gel silica glasses exposed to ambient atmosphere.

shrinkage if the gel-silica sample is re-exposed to the ambient atmosphere after reheating especially if water vapor is present.

(3)Pore elimination which results in permanent shrinkage.

(4)Structural relaxation

The expansion of the Type VI gel silica glass upon heating and cooling can be attributed to

(1)The expansion at low temperature is due to the anharmonic lattice vibrations.

(2)The rehydrolysis of the threefold rings occurs, by adsorption of water molecules onto the strained threefold rings on the internal pore surface (physisorption). It is followed by rehydroxylation via a dissociative bond-breaking reaction(chemisorption), as discussed by Wallace[Wal91].

(3)As the average pore radius of S2 and S3 is small ~12.5Å, water adsorption and absorption on other silanol groups(i.e. inside the skeleton of the gel) depends on the rate of transportation of water molecules into the pore network of the porous gel-silica glass.

(4)Structural relaxation

Thus, there are three types of the thermal behavior of the porous gel-silica glass during heating and cooling in the dilatometer study. They are:

(i)expansion,

(ii)permanent shrinkage,

(iii)temporary shrinkage

The magnitude of the expansion of the stabilized gels during cooling(<320°C) decreases as the densification temperature increases[Wal91]. The densification temperature of sample S2 is larger than of sample S3. Therefore, the stiffness of the matrix of S2(densified at 900°C) is larger than S3(700°C). Thus, the thermal stability of the gel-silica glass is improved at increasing densification temperature.

The temporary shrinkage will recover by expansion upon cooling (or after a period of time) through re-adsorption water molecules from the ambient atmosphere If dry air flow is used during cooling no expansion is observed due to the lack of water molecules [Zhu89]

The discrepancy in the hysteresis loops of Curves 2 and 3 in Figure 3.8 indicates the existence of permanent shrinkage which results in the thermally stabilized gel silica glasses S2 and S3, e.g. The initial length of the test sample is longer than the final length. The porosity of S3 is larger than that of S2 (Figure 3.6) so the resulting permanent shrinkage of sample S3(densified at 700°C) is larger than that of sample S2(900°C) Permanent shrinkage is not observed in sample S1 due to the lack of porosity

In conclusion, gel-silica glass as heated to 700°C - 900°C are still not chemically or thermally stable due to the existence of the hysteresis loop in the dilatometer study As long as there is an open porosity in the gel silica glass there will be a certain amount of permanent shrinkage after reheating The magnitude of the expansion of the thermally stabilized gel-silica samples during cooling decreases as the densification temperature increases. So the term "stabilized" gels does not mean they are necessarily fully thermally stabilized. They can be continually shrunk during reheating until they are fully densified.

However, this thermal instability of the Type VI porous gel silica glass supports the concept of enhancing densification by using laser heating on the porous gel-silica substrate Permanent shrinkage is the expected result from laser heating.

3.5 Mechanical Properties

3.5.1 Load/size Effect(ISE) in Microhardness

Indentation methods are widely utilized for the microhardness characterization of materials. Microhardness of a material is dependent on many variables, such as load/size effect(ISE), test environment, geometries of indenter(Brinell, Knoop, or Vickers), crystal plane tested and crystallographic orientation of a single crystal, etc [Li91a][Li91b].

The indentation load/size effect(ISE) is the effect of the applied indentation load and the indentation size on the calculated microhardness of a material. Most experimental results reveal that the measured microhardness appears to increase if lower indentation test loads are used, i e most materials exhibit an ISE effect

In Figure 3.9, after [Li91a][Li91b], a relationship between the calculated microhardness(H) and the dimension of the impression(d) of a material is illustrated. The value of H is increased as the impression d decreases. This behavior is due to the fact that the impression d decreases as the applied load decreases, as shown in equation(3 9) Above the ISE boundary($H=H_0$, $d>d_0$,$P>P_c$), the measured microhardness H_0 is indentation size(or load) independent, where the parameters are

P: the applied load,
P_c: the critical indentation load,
d: the indentation size,
d_0: a characteristic indentation size.

However, the sample surface exhibits a crack failure when the applied load is too large. Thus, a proper test load must be found between the ISE load($P \sim P_c$) and the crack-induced load($P \gg P_c$) in order to obtain a true value of microhardness

The load dependence of microhardness was initially addressed in terms of the classical Meyer's law[Li91a][Li91b]

$$P = Ad^n \tag{3 9}$$

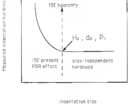

Figure 3 9 Schematic of ISE effect in solids, illustrating the ISE boundary, after [Li91]

In equation (3.9) P is the indentation test load and d is the resulting dimension of the impression. A and n are coefficient and exponent, respectively, and are related. However, A values are observed to have a serious dimensionality problem, i.e. a lack of any physical meaning[Li91a][Li91b]. This creates substantial uncertainty as to the meaning of both A values and n-values obtained experimentally.

The peculiar dimensionality of the classical Meyer's law was addressed by applying the concepts of a load-independent "true" microhardness, a critical indentation load and a characteristic indentation size. Li and Bradt have recently introduced a normalized Meyer's law to address this problem[Li91a][Li91b]. The resulting normalized Meyer's law is

$$P = \frac{2P_c}{n}\left(\frac{d}{d_0}\right)^n \qquad (3.10)$$

In equation (3.10) P_c is the critical indentation load, d_0 is a characteristic indentation size, and n is the same exponent as in the classical Meyer's law. This normalized form of Meyer's Law solves the dimensionality problem of the A value in a self-consistent manner, as discussed by Li and Bradt[Li91b]. It also suggests that the extent of the ISE can be quantitatively described for different materials by the physically related terms, P_c and d_0. Furthermore, Li and Bradt have also proposed a proportional specimen resistance(PSR) model to interpret ISE. The PSR is expressed as[Li91b]

$$PSR = a_1 d \qquad (3.11)$$

where the a_1 coefficient represents the contribution of the PSR to the ISE. Li and Bradt show that the a_1-value depends on.

(i) the elastic properties of the test material

(ii) the interfacial friction between the indenter facets and the test specimen

The a_1-value was shown to agree with the Young's modulus of various test specimens was confirmed by Li and Bradt[Li91b] In order to explain ISE more completely, a relationship between P and d was also developed by Li and Bradt. Their resulting relation is shown as follows

$$P=a_1d+a_2d=PSR+a_2d=PSR+(\frac{P_c}{d_0*d_0})d^2 \tag{3 12}$$

From equation (3 12), the term a_2d can be used to represent the effective indentation test load. The a_2-value is directly related to the test specimen's load independent hardness, but is dependent on (i) the test material and (ii) the crystallographic reference for single crystals. a_2 is equal to $(P_c/(d_0*d_0))$ where P_c and d_0 naturally evolve from the self-consistent approach to the development of the normalized form of Meyer's Law, as discussed by Li and Bradt[Li91b]

By combining equations (3 10), (3 11), and (3 12), the test load/indentation size dependence of a microhardness measurement can be quantitatively expressed by the relationship

$$H=C[(\frac{a_1}{d})+(\frac{P_c}{d_0*d_0})] \tag{3 13}$$

where C is a constant depending on the geometry of the indenter The equation (3 13) describes the ISE, since the first term $(\frac{a_1}{d})$ represents an indentation test-load-dependent region relating to the PSR. The second term $(\frac{P_c}{d_0*d_0})$ represents an indentation test-load-independent region where the hardness is a constant. The contribution of PSR to the ISE increases with decreasing indentation test load when $d<d_0$ or $P<P_c$ When the load is

above $P_c(d>d_0)$, the contribution of the PSR to the ISE can be neglected, and the hardness represents the load independent "true" hardness$(=P_c/(d_0*d_0))$.

3.5.2 Microhardness Analysis

In the microhardness study pursued herein a semi-automatic LECO DM-400F Hardness Tester was used to obtain the Vickers hardness number(VHN) of the gel-derived silica glasses with different densification temperatures. The VHN is determined by the following equation[Vas89a]

$$\mathrm{VHN} = \frac{1.854P}{L^2} \tag{3.14}$$

where P is the applied load(kg), L is the average length of the diagonals of the indentation(mm). Good quality indentations require a good focus on the sample and the test sample must be maintained horizontal during the measurement.

As discussed above, the VHN remains a constant at $P>P_c$. The value of P_c must be determined in advance. P_c can be evaluated from the plot illustrating the relationship between the VHN and the applied load(from 10 g to 200 g). In Figure 3.10, VHN of the gel-silica samples increases as the indentation load ≤ 50 g. A load of ≥300 g induced cracks on the gel-silica sample easily which made it hard to obtain a "qualified" indentation. Therefore, it is found from the above results that P_c is ~ 50 g. A load of 100 g is used in this study to avoid ISE and no crack was observed around the indentation during testing.

Figure 3.11 shows the increasing VHN of gel-silica glasses with increasing densification temperature from 180°C, 600°C, 875°C, 900°C, to 1000°C. Figure 3.12 illustrates a relationship between the VHN and the bulk density of the gel-silica glasses. The bulk densities of each gel-silica sample are 1.02, 1.26, 1.46, 1.59, 1.82, 2.2 g/c.c.,

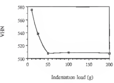

Figure 3.10 A relationship between the measured microhardness of a partially densified gel-silica glass with increasing indentation load.

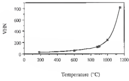

Figure 3.11 Vickers hardness number of gel-silica glasses at increasing densification temperature.

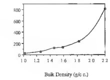

Figure 3 12 Vickers hardness number of gel silica glasses at increasing bulk density respectively VHN of the gel-silica sample increases as the densification temperature and the bulk density increase Especially above 900°C, the VHN of the gel-silica glass increases drastically These relationships are consistent with results reported by Vasconcelos[Vas89a].

The low VHN below ~900°C of the gel silica glasses may be attributed to the large amount of open porosity When the sintering temperature is above 900°C, viscous flow occurs which enhances the densification intensively The VHN reaches a maximum value of 812±18 of a fully dense gel-silica glass(provided by GelTech Inc.)

In conclusion, the VHN of a gel silica glass is increasing with increasing bulk density or densification temperature When the sintering temperature is above 900°C, VHN increases considerably when viscous flow occurs Thus microhardness is a feasible method to investigate variations of surface properties of gel silica monoliths at various levels of densification. However the independent load P_c should be determined before VHN measurements are made.

The large change in VHN associated with viscous sintering of a porous gel silica glass supports the concept of using local laser heating on the surface of the gel-silica glass to create an extensive change in local density and VHN The difference of VHN and density between the irradiated and un-irradiated region on the surface of the porous gel silica glass can then be used to produce an optical device. This is because an optical device requires changes in the refractive index Therefore if it is assumed that the VHN change or the bulk density change is proportional to the refractive index change, changes in VHN will also result in gradients in refractive index within the substrate.

3.6 Optical Properties

3.6.1 UV/VIS/NIR Spectroscopy

UV/VIS/NIR spectra from 180 to 3200 nm were measured using a Perkin-Elmer Lambda-9 UV-VIS-NIR Spectrophotometer. The O-H stretching vibration of the surface silanol groups with their overtones are often observed in this range[Wal91].

Figure 3.13 shows two UV/VIS/NIR spectra of a Type VI porous gel silica glass(a) and a fully dense gel silica glass(b). The objective of this figure is to contrast the difference of transmission(%) between these two gel silica glasses, one is porous, the other is fully dense. The absorption bands in spectrum(a) is due to the O-H stretching vibrations, its overtones and combination[Wal91][Per91]. Absorption bands in the spectra are listed as follows

(1)Absorption at 2.82 μm is attributed to the O-H stretching vibration of surface silanol groups hydrogen bonded to water molecules[Wal91]

(2)Absorption at 2.732 μm is attributed to the O-H stretching vibration of adjacent, vicinal silanol groups hydrogen bonded to each other[Wal91]

(3)Absorption at 2.657 μm is attributed to the O-H stretching vibration of isolated surface silanol groups, the peak at 1.365 μm is its overtone[Wal91]

(4)Absorption at 2.20 μm is attributed to the combination of stretching vibrations for silanols with a contribution from the bulk matrix[Per91]

(5)Absorption at 1.90 μm is attributed to the combination of stretching and deformation vibrations for water[Per91]

(6)Absorption at 1.46 μm is attributed to O-H stretching vibration in water molecules hydrogen bonded to surface silanol groups[Wal91]

Other overtone and combination vibrational peaks of partially densified silica are discussed in detailed by Hench et al[Hen90a]. These absorption bands in spectrum (a) of the partially densified silica gel can be eliminated by further dehydration and densification

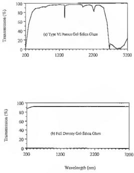

Figure 3.13 UV/VIS/NIR transmissions of (a) a Type VI porous gel silica glass and (b) a Type V full density gel-silica glass.

as shown in spectrum(b) Spectrum(b) of a fully dense gel-silica glass exhibit high transmission from 200 to 3500 nm[Hen88](as 160-4200 nm discussed in [Hen90a]). Due to this excellent optical property, gel-silica glasses are very suitable to be used as a substrate to make a wave-guiding device which requires low optical loss and wide band transmission

3.6.2 FTIR Reflectance Spectroscopy

Reflection methods provide a valuable means of examining materials that are too opaque for transmission experiments[Hai67] Hair discussed that the spectrum of reflected light is as unique to a material under investigation as its transmission spectrum[Hai67] The penetration depth of IR is on the order of a wavelength of the radiation and depends upon the refractive indices of both phases and the angle of incidence. So intensities from internal reflection(or Attenuated Total Reflection), a reflection from the penetrating IR beam, may be counted in the specular reflectance spectrum. However the varying angle of incidence and phase change of the reflected light must be considered in structural interpretations of the wavelength intensity dependence.

The intensity of reflectivity also depends on the surface roughness of the test sample. However, Sanders and Hench et al found that grinding a glass surface(with low soda content) with a SiC paper(600 grit) resulted in a very reproducible surface in the IR reflection study[San74] The spectra (i e. peak positions)is not changed due to sample roughness[Won88]

Surface FTIR reflectivity spectra show high intensity in the molecular absorption region Heaney et al. studied the reflectance of fused silica from 10 to 10000 cm^{-1}[Hea83] There are two dominant peaks at ~1100 cm^{-1} and ~800 cm^{-1} in the reflectance spectra of a 1.5 mm thick Suprasil W where there is zero transmission These two peaks can be assigned to asymmetric(AS) and symmetric(SS) Si-O-Si bond stretching vibrations [Ber82]

Almeida discussed the reflectance spectroscopy of vitreous silica at 20°-off normal incidence The results showed that the band between ~1200-1260 cm^{-1} is associated with the LO mode of the Si-O-Si asymmetric bond stretching vibration[Alm90] The ~1120 cm^{-1} band in the infrared reflectivity spectra(oblique incidence) of vitreous silica[Gal83] can be associated with the TO mode of the Si-O-Si asymmetric bond stretching vibration(AS) The peak at 940 cm^{-1} is assigned to a stretching vibration of an external Si-O^{-} group(NBO)[Alm90]

It is concluded that the dominant peaks in the reflectance spectra of amorphous silica are due to the AS and SS(1122cm^{-1}, 782cm^{-1}) absorption vibrations. In an absorption spectrum, the AS and SS absorption vibrations are shifted to different frequencies as 1080cm^{-1} and 810cm^{-1}, respectively This indicates a structural difference exists between the surface and the interior of the silica glass.

In section 2 4, review of FTIR, the shift in AS and SS absorption vibrations of silica gels densified at different temperatures indicates that IR spectra are density sensitive. The shift in AS peak is related to the degree of densification of the silica gels Thus, the density-sensitive shifts can be used to identify the structural changes and evaluate the change in bulk density of the silica gels

3.6.3 FTIR Reflectance Microspectra Analysis

Micro-IR spectra of gel-silica glasses were obtained by using a Nicolet 20SXB FTIR microspectroscope at normal incidence with resolution of 0 5 cm^{-1} The instrument is equipped with an optical microscope and a computer data station. This technique records infrared spectra on areas of a sample by using an infrared transmitting optical microscope. Currently, the diffraction limit of infrared radiation(10-20 μm) is the limiting condition for obtaining absolute spectra from a given area of a material[Mes88] In this study, the investigated region was reduced to a diameter of 100 μm by using a pinhole which is beyond the diffraction limit. IR radiation (not polarized) was focused on the sample at zero incident angle, i.e. at normal incidence. Specularly reflected energy was detected.

Figure 3.14 illustrates the reflectance, using micro-FTIR, of four gel-silica glasses, 180°C(G1), 800°C(G2), 1000°C(G3), and 1150°C(G4) from 700 to 1500 cm^{-1}. The reflectances shown on the figure of each sample are based the same scale from 0 to 100%. The peak maximum positions are also indicated on the figure.

(1)The peak at ~ 1120 cm^{-1} is assigned as a AS_1 TO mode[Ber82][Luc87][Kir88]

(2)The shoulder at ~ 1200 cm^{-1}, attributed to an asymmetric Si-O-Si stretching vibration, is assigned as a AS_2 TO mode[Kir88]

(3)The peak at ~ 940 cm^{-1} is attributed to a stretching vibration of external Si-O groups, a typical Si-OH stretching mode[Ber82][Dur86]

(4)The peak at ~ 810 cm^{-1} is assigned as a SS TO mode by Kirk[Kir88].

As the incident angle in the reflectance spectrum is zero, only the TO vibrational mode can be observed due to the Berreman effect. This is because the electromagnetic waves are transverse and the IR radiation can be absorbed by TO phonons and not by the LO phonons[Kir88].

The peak maximum position(PMP) of G1(180°C) at ~1084 cm^{-1} has the lowest intensity comparatively. It is intensified at increasing densification temperature. There is also a major shift in the AS_1 TO mode from 1084 cm^{-1} of a dry gel to a higher freqnency of 1122 cm^{-1} for a fully dense gel-silica glass. The resulting shift in the peak maximum position of the gel-silica glasses is equal to 38 cm^{-1} from dried density to full density.

The other minor shift of SS TO mode found in Figure 3.14 is 787 cm^{-1} for a dry gel. The SS TO mode moves to a lower frequency of 782 cm^{-1} for a fully dense gel. However, there is an increase in intensity of this mode at increasing densification temperature.

The assigned AS_1 TO stretching mode at ~1122 cm^{-1} of a full density gel-silica glass in Figure 3.14(at normal incidence) is close to the reflectance vibrations at ~1122-

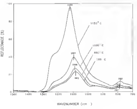

Figure 3 14 Normal reflectance micro-spectra of four gel-silica glasses at increasing densification temperatures.

1125 cm^{-1} of vitreous silica (at oblique incidence, near normal or 20-70° off-normal)[Sim53][San74][Gal83][Alm90] This means that once the gel silica glasses are fully densified, they become structurally like a commercial fused silica glass.

The intensification in the AS_1 TO mode with densification is consistent with the findings of Sanders et al They showed that as the %Li_2O increases(or SiO_2% decreases) in lithia-silica glasses, the AS_1 reflectance decreases. The increase in %Li_2O resulted in a more open glass structure. Since the AS_1 TO mode is a network vibration mode its intensity should increase with increasing SiO_2 content. They concluded that infrared reflectances are proportional to the concentrations of the vibrational species causing them [San74]

In this study, as the thermal densification consolidated the silica network there is an increase in the concentration of the vibrational species Consequently, the intensity of the AS_1 TO mode increased as the density of the gel silica glass increased

A shift in the AS_1 TO (~38 cm^{-1}) mode reveals the extent of the molecular structural change and is indicative of consolidation of the amorphous structure. As the densification temperature increases there is a larger intratetrahedral bond angle, a stronger Si-O bond strength, and a shorter bond length.

The longer bond length of a dry gel may be attributed to the high surface area and the high concentration of silanols on the pore surface. Water adsorbed on the pore surface resulted in structural dilation[Sch86][Wes90a][Wes90b] The longer bond length of a dry gel resulting in a smaller bond angle may be attributed to less repulsive forces between oxygens at the corners of silica tetrahedra. This conclusion is an agreement with Walrafen that a decrease in the mean equilibrium bond angle(intratetrahedral bridging oxygen) also corresponds to an increase in the mean equilibrium Si-O bond length[Wal86]

The peak at ~940 cm^{-1} in a dry gel is due to the vibration of Si-O groups, a typical Si-OH stretching vibration This indicates a high concentration of silanol groups in dry gels which decrease in intensity and disappear when the gel-derived glass undergoes a polycondensation process during densification

In agreement with the literature the peak at ~800 cm^{-1} is assigned to a SS TO vibration and is attributed to the formation of Si-O-Si bonds as a result of thermal densification[Dur86][Kir88] It is known that as the densification temperature of the gel-silica glasses increases, consolidation occurs and the formation of the Si-O-Si bonds are increased. Thus the SS TO mode of the gel-silica glass is intensified as the densification temperature increases.

3.6.4 Refractive Index Analysis at 0.633 μm

Refractive indices of porous gel-silica glass are difficult to obtain due to the absorption of liquid or water vapor into the pores. The radius of the pore of the porous gel silica glass is ~12Å which is so small that it enhances adsorbtion due to capillary forces Therefore, it is impossible to use a commercial refractometer for index measurements of porous gel-silica monoliths because the test sample must contact index matching liquids.

A useful technique is developed herein to obtain the refractive index of porous silica gel silica monoliths by measuring the normal reflectivity of the gel-silica sample without any liquid contact. The refractive index, n , of the silica glass can be calculated from the normal reflectance, $R_S(\%)$, at the wavelength of 6328Å by using the formula listed as followed

$$R_S = \frac{I_s - I_b}{I_r - I_b} * R_r \tag{3 15}$$

$$n = \frac{1+\sqrt{R_s}}{1-\sqrt{R_s}} \tag{3 16}$$

where R_s and R_r(~20 1%)are the normal reflectivities of the gel-silica sample and the reference material I_s, I_r, and I_b are the measured intensities of the gel-silica sample, reference material, and the background, respectively A reflectometer a microscope equipped with an optical source, is used to obtain the normal reflectivities of the gel-silica glasses A SiC crystal is used as a reference material due to its high reflectivity. The refractive index is calculated according to equations (3 15) and (3 16) Gel silica glasses are dried and heated to 150°C in a vacuum oven immediately before the reflectivity measurements

Gel-silica samples measured in this study are densified at 180°C, 615°C, 900°C, and 1150°C. The corresponding bulk densities are 1 06(A1, 1 06/2 2=48% densified), 1 20(A2, 54%), 1 45(A3, 66%) and 2 2(G4 100%), respectively Results are shown in Table 3 1 The difference in refractive index is Δn. For instance, Δn = n-1.24 is obtained based on the n value of the dry gel(n=1.24) Table 3 1 shows that the refractive index increases as the bulk density of the gel-silica glass increases

This approach of obtaining the refractive index of the porous materials is clean, reliable, and easy to use It is found that the refractive index is ~linearly proportional to the degree of densification which will be discussed in the following section. The data of the refractive index of the fully dense gel silica glass is consistent with Hench et al[Hen88]

Figure 3 15 illustrates a linear relationship between the refractive index and the bulk density of the gel silica glasses The densification temperature of each gel-silica sample is also indicated in the figure The linear relationship of refractive index of the gel silica glass with the bulk density is consistent with Hench et al shown in Figure 3 16[Hen90a] In Figure 3 16 the results showed that the refractive indices of the crystalline silica phases, quartz, cristobalite, tridymite and the gel-silica glasses are proportional to the corresponding densities of these materials. Within the experimental error, the results can be predicted by Lorenz-Lorenz equation[Kin76]

Table 3.1 Degree of densification and corresponding refractive indices and index change at 632.8 nm of gel-silica glasses.

Densification(%)	Refractive Index	Δn
48	1.24	0
54	1.27	0.03
66	1.31	0.07
100	1.46	0.22

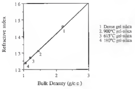

Figure 3.15 A relationship between the refractive indices at 632.8 nm and the bulk densities of the gel-silica glasses. Densification temperatures are indicated.

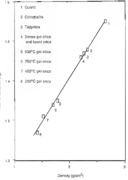

Figure 3 16 Indices of refraction versus densities of gel silica glasses and crystallines phases after [Hen90]

In this study, the refractive index of the gel-silica glasses increases as the polycondensation proceeds during the thermal densification. This behavior, an index change proportional to density change, is consistent with Fiori et al. They showed that the density and the refractive index of amorphous silica polymorphs obey an essentially linear relationship, when the increase in refractive index of the amorphous silica is increased by applying a compressive pressure[Fio86]

In addition, in Figure 3.15 and 3.16, the results showed that the silica gel optics can be heated to specific temperatures to obtain a required combination of density and the refractive index[Hen90a]. This result also support the concept of enhancing densification of Type VI gel silica glass using laser heating. According to the above discussion, the irradiated area will yield a higher refractive index than the un-irradiated area. Thus, the laser heated region can be used as an optical device that is based on a refractive index gradient.

3.6.5 Refractive Index at 3.57 μm

The corresponding refractive index change at 3.57 μm is analyzed by using a Kramers-Kronig transformation described in Appendix I. A refractive index spectrum can be obtained from a reflectance spectrum at normal incidence if the reflectance is measured over a sufficiently large frequency range. The choice of the wavenumber(or wavelength) to obtain the specific refractive index should avoid high absorption bands like the Si-O-Si stretching vibration at ~1100 cm^{-1} or the O-H stretching vibration at ~3750 cm^{-1}. The selected wavenumber is at 3.57 μm for the refractive index study in the infrared range.

Figure 3.17(a) shows a typical normal reflectance micro-spectrum of a fully dense gel silica glass with resolution of 0.5 cm^{-1}. A refractive index spectrum is shown in Figure 3.17(b) and a corresponding absorbance spectrum in (c) which is transformed from (a). The strong absorption peaks in spectra (a) and (c) are mainly attributed to Si-O-Si

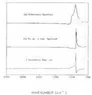

Figure 3.17 A typical normal infrared reflectance micro-spectrum(a), a transformed refractive index spectrum(b) and a transformed absorbance spectrum(c) of a Type V gel silica glass

stretching vibrations. The transformation of the spectrum is executed by using Kramers-Kronig methods in a LabCal software. The method is described in Appendix I. The resulting absorbance spectrum(c) is equivalent to the absorbance measurement of a 0.01 mm thick sample of the material[Lab90]

Figure 3.18 shows the refractive indices(line 1) at 3.57 μm of silica gels densified at increasing temperatures, 180°C(G1), 800°C(G2), 1000°C (G3), and 1150°C(G4) provided by GELTECH Inc. The bulk densities of each gel silica sample are 1.08 (1.08/2.20=49%, degree of densification), 1.19(54%), 1.40(64%) and 2.2 g/c.c.(100%), respectively. The refractive index of the gel silica glass increases linearly with increasing degree of densification(%)

The refractive indices of gel-silica glasses at 0.633 μm is given in Table 3.1 and also shown as line 2 in Figure 3.18. The refractive indices at 3.57 μm is larger than the refractive indices at 0.633 μm, although both are proportional to the degree of densification of the gel silica glasses. The difference in n between the two wavenumbers is due to the dispersion of silica. The data indicate that dispersion decreases as densification is greater. This study shows that the refractive index as well as the reflectivity of the gel silica glass increases as the densification temperature increases. The index change must be attributed primarily to the consolidation of the gel-derived glasses at an elevated densification temperature.

Consequently, the reflectance spectrum of the gel-silica glasses are not only sensitive to a density change but also sensitive to the refractive index change. The index change at 3.57 μm can be obtained by transforming the reflectance spectrum using Kramers-Kronig methods.

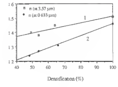

Figure 3.18. Refractive indices at 3.57 μm(line 1) and at 0.633 μm(line 2) of gel silica glasses at increasing degrees of densification

3.6.6 Composite Diagram of the PMP and the Refractive Index

This composite diagram is to illustrate a relationship between the refractive index at 0.633 μm and the peak maximum position(PMP) of the gel-silica glasses. This diagram can be used to predict the refractive index by using the FTIR microspectroscopy which is more feasible.

The left side of Figure 3.19 shows the PMP of the AS_1 TO mode of the gel-silica glasses, G1, G2, G3, and G4 as a function of the bulk density (provided by GELTECH Inc.). The peak maximum positions(PMP) of gel-silica glasses G1-G4 are obtained from the IR reflectance spectra in Figure 3.14. The right side of Figure 3.19 is the refractive index at 0.633 μm of the gel-silica glasses(prepared by author except the fully dense gel silica glass) calculated from the normal reflectivity in equations (3.15) and (3.16). The bulk densities of each silica gel-silica glass for the refractive index study are 1.06(A1, densified at 180°C), 1.20(A2, 615°C), 1.45(A3, 900°C), and 2.20 g/c.c (G4, 1150°C).

Figure 3.19 shows that the maximum change in PMP is 38 cm^{-1}. The maximum change in the refractive index is 0.22. Thus, there is a linear relationship between the bulk density and the change in optical properties even though these pure gel silica glasses are prepared at different densification temperatures.

From Figure 3.19, it is shown that the IR spectrum is density-sensitive, the change in the peak maximum position is large as a function of the bulk density of the gel-silica glasses, and the corresponding refractive index of the gel-silica glasses at 0.633 μm can be evaluated. Conversely, if the bulk density of the gel-derived glass is known, both the peak maximum position and the refractive index of the material can be estimated.

For example, the refractive index of a gel-silica sample with bulk density 1.91 g/c.c. can be determined. Estimated from Figure 3.19, the corresponding PMP is 1112.5

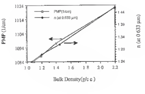

Figure 3 19 Peak maximum position(PMP at left side) of gel silica glass substrates with different bulk densities densified at different temperatures: G1(180°C), G2(800°C), G3(1000°C) G4(1150°C) and refractive index n at 632 8 nm (right side) of A1(180°C), A2(615°C), A3(900°C), and G4(1150°C)

cm^{-1} and the corresponding n is 1 405 at 0 633 μm. The measured PMP 1108 cm^{-1} of this gel-silica sample is close to the estimated PMP 1112.5 cm^{-1}

This linear relationship can be used to evaluate n in the visible range for the Type VI pure gel-silica glasses if the bulk density, or the peak maximum position is known These values can be obtained easily and accurately using a mercury pycnometer and FTIR micro-spectroscopy

3.7 Conclusions

In this study gel silica glass substrates are densified at 1000°C with chemical stabilization Each processing step of the gel derived glasses was carefully optimized to achieve reproducibility of the optical substrates. Crucial processing steps include drying, thermal stabilization, and chemical stabilization. These gel-silica glasses with high bulk density above 1 80 g/c.c were used for further laser densification.

Characterization of various properties of the gel silica glass during densification are demonstrated. Mechanisms of the physical, thermal, mechanical and optical properties of the gel-silica glasses are discussed. The drastic property change of the gel silica glass at 900°C support the concept of laser enhanced densification The optical results demonstrate a high optical transmission of a Type V fully dense gel-silica glass over a wide range of wavelengths.

FTIR microspectroscopy provides a mean of structural investigation of the gel-silica glass This technique is demonstrated to be sensitive to density of the gel-silica glasses due to the shift in the AS_1 TO mode. The consolidation of the gel-silica network was followed by observing the changes in the AS_1 TO mode in a normal incidence reflectance spectrum. As the densification temperature increased from 150 to 1150°C, it was observed that this band changed in intensity as a result of increasing concentrations of the vibrational species(AS of Si-O-Si). The wavenumber of the AS peak shifted towards higher frequencies as a result of polycondensation and densification of the silica network.

Refractive indices of the gel-silica glasses in the visible range can be calculated from normal reflectivity using equation (3.16). The refractive indices of the gel-silica glasses at 3.57 μm can be obtained from a normal reflectance spectrum using a Kramers Kronig method. Conversely, the linear relationships in Figures 3.15 and 3.19 can be used to evaluate n in the visible range for the Type VI pure gel-silica glasses if the bulk density or the peak maximum position is known.

The relationships between structural characteristics of the porous gel-glass matrices, such as bulk density, and optical properties, especially index of refractive index, make it possible to develop optical devices by use of localized densification with a CO_2 laser.

CHAPTER 4
LASER DENSIFICATION OF GEL-SILICA GLASS

4.1 Introduction

Microlenses discussed in this chapter are used as optical elements in optical communication and data processing systems[Shi87]. They may also provide optical interconnections in a very large scale integrated circuit (VLSI) system[Iga82]. Techniques used to fabricate microlenses include dopant diffusion, photolytic, mass transport, mesa etching, UV lithography, electron beam lithography and thin film deposition[Shi87][Bor88][Oik82][Lin89][Jah90][Shi87][Tat84]. Most of these techniques involve tedious and process sensitive steps. The diameters of the resultant microlenses range from few micrometers to a few millimeters depending on the fabrication techniques and applications.

We describe a fabrication process for microlenses using laser densification with a CO_2 laser (maximum power ~ 25 W) on porous gel-silica glass substrates. The porous substrates are termed Type VI gel-silica glasses [Hen88]. During the furnace densification of the gel-silica glass, the bulk density is increased and the optical properties are improved. In this study, laser heating is introduced to enhance the densification of the partially densified gel-silica glass, also reported by Ramaswamy et al.[Ram88] and King et al [Sha89][Kin90c][Kin92]. King and Shaw have established upper and lower thresholds for the laser densification on Type VI gel-silica glasses.

Laser densification is a direct technique that simultaneously improves the optical performance of the laser irradiated area and produces the focusing lens in the substrate. Laser densification is useful because bulk density, mechanical strength, optical transmittance are improved as the densification temperature increases, as discussed in Chapter 3.

Advantages of using gel-silica glass as a substrate is the compatibility with fiber optic material as discussed and a wide range of high optical transmission for a fully densified silica gel-silica glass is achieved with good optical transmission from 200 nm to 3500 nm [Hen88]. In addition, the temperatures induced by laser heating in the irradiated region have been calculated using computer generated models discussed in Chapter 7 [Chi90]. The calculations make it possible to design laser densified refractive index profiles in a gel-silica substrate.

In this work, optically transparent and densified spots in the range of 1 mm diameter have been made on the partially densified gel silica substrates by using a CO_2 laser and the necessary densification conditions established. Corresponding surface profiles and the physical appearance of the laser densified spots on the surface of the gel-silica substrate are shown and processing conditions are described.

The irradiated area on the gel silica substrates is more dense than the substrate based on the measurements of the Vickers hardness number(VHN) and the peak maximum position in macro-FTIR spectra on the surface and the cross section of laser densified spots. Profiles of the VHN and the peak maximum position of the laser densified spot are shown.

The environmental stability of these densified regions is investigated by monitoring the profile of VHN on one spot as a function of time, since a previous study [Ram88] [Slo90] indicated that laser densified gel-silica may relax with time, thereby eliminating index of refraction gradients induced by the CO_2 laser beam.

It is known that a strong and broad absorption at ~3500 cm^{-1} of the porous gel-silica glass is observed in the FTIR absorption spectrum. Large amounts of physical water are adsorbed on the porous silica surface. Two approaches are required to prevent the water effect on the laser densified region and increase the efficiency of laser densification. The first approach is pumping out the physically adsorbed water of the gel-silica sample by heating the gels in a vacuum oven up to 150°C. The second approach is to control the humidity during laser densification. All laser densified spots in this study are made using these control steps. The goal of this work is to fabricate a stable laser densified region which is equivalent to full density silica.

4.2 Methods of Laser Densification and Characterization

4.2.1 Method of Laser Densification

Type VI porous gel silica glasses were prepared by using a process described in Chapter 3. Type VI porous monolithic gel-silica glasses were obtained after dehydration and partial densification to over 1000°C. These porous substrates are to be further densified by using the CO_2 laser heating. Figure 4.1 illustrated the process sequence of sample treatment prior to the laser densification. Each gel silica sample is characterized by measuring the bulk density, called the starting density. Then the sample is heated in a vacuum oven at 150°C for about two hours to eliminate the physically adsorbed water and mounted on a holder inside the sealed glass box filled with nitrogen at a humidity of ~ 18% RH.

The microlenses are made on partially densified gel silica substrates by using a CO_2 laser in a pure TEM_{00} mode. The laser exposure time and power are approximately 1 second and 16W depending on the starting density of the gel silica samples. Figure 4.2 shows the instrumental arrangement for the laser densification process. The CO_2 laser beam is focused by using two ZnSe lenses, the focal length of the lenses are 6.35 and 2.54 cm, respectively.

A computer-controlled plotter is used to permit lateral (in both x and y directions) positioning of the gel silica samples. The approach to enhance the densification of the gel silica surface is to translate the gel silica sample in front of the focused laser beam continuously to obtain a track(using a fixed y but a moving x value), or in a stationary

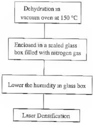
Dehydration in
vacuum oven at 150 °C
Enclosed in a sealed glass
box filled with nitrogen gas
Lower the humidity in glass box
Laser Densification

Figure 4 1 Process sequence of treatment of gel-silica sample prior to laser densification.

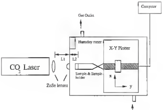

Figure 4 2 Instrumental arrangement of laser densification on gel-silica glasses mode to obtain a microlens, or in consecutive steps to obtain a microlens array(using fixed x and y).

Variables in the laser densification process are laser power setting(mA), exposure time(seconds), and positions in x and in y directions(mm). There are two distance variables in the y direction. One is the distance (L1) from the first ZnSe lens (the one attached to the CO_2 laser) to the second ZnSe lens (the one attached to the sealed glass box), the other variable is the distance (L2) from the second ZnSe lens to the gel-silica sample. The silica gel glass is in a closed glass box purged with N_2 gas to minimize and control humidity.

The power of the CO_2 laser (maximum power ~ 25W) ranges from 1.5W to 20W and is controlled by selective laser power settings (12 mA and above) and pulse width (0.01 second and above). Figure 4.3 shows the resultant laser energy obtained by varying the pulse widths and the power settings. The beam profile of the CO_2 laser is obtained by measuring the laser power across the beam at a distance far away from the source(~ 0.6 m). A slit (width ~ 1 mm) is attached on the window of the detector. The shape of the beam is gaussian like, as illustrated in Figure 4.4.

4.2.2 Methods of Characterization

The characterization of the laser densified spots includes surface profile, VHN, and micro-IR spectra. Surface profiles of the irradiated spots are measured by using a Dektak surface profile measuring system. The limit of the depth of the measurement using the system is 500 μm.

The laser irradiated spots on the gel-silica glass are characterized using a microhardness tester (LECO Corporation). A load of 100g is used in this study. This load yields load independent microhardness values, as shown in Chapter 3. One advantage of using microhardness characterization is that a profile of the VHN can be obtained because

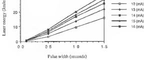

Figure 4.3 Corresponding CO_2 laser energy at varied pulse widths and power settings.

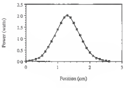

Figure 4.4 Energy profile of the CO_2 laser used in this study

of the size of the indentation is small enough(~20 μm in diameter). The diameter of the laser densified spot is > 1000 μm. The profile of VHN on the irradiated spot is obtained by making a track of indentations across the densified spot. Stability of the spots is determined by monitoring the VHN profile as a function of time under ambient conditions of humidity.

Laser irradiated spots are also characterized by using a FTIR spectroscope equipped with a microscope described in section 3.6.3. Micro-IR spectroscopy is a fast and nondestructive technique. This technique allows an immediate investigation of the structural changes of the laser densified spot. The micro-IR investigated region is 100 μm(in diameter) along the diameter of the laser irradiated spot(~1400 μm). A series of the IR spectra across the laser densified spot are obtained. Peak maximum positions (cm^{-1}) of the laser irradiated spots are determined from the IR spectra. A profile of the peak maximum position(PMP) is plotted which describes the relationship between the peak maximum position, which is proportional to density and index of refraction, see Chapter 3, with the investigated position across the laser irradiated spot.

4.3 Results

4.3.1 Bulk Density Effects on Laser Densification

To create optically transparent microlenses on the gel-silica glasses, specific combinations of laser power, exposure time and focal length L2 are required. A composite diagram (Figure 4.5) illustrates the densification conditions, and corresponding surface profiles of the transparent spots on the gel-silica glasses. A three dimensional diagram in the lower part of Figure 4.5 shows the laser densification conditions(within the envelopes) required to make optically transparent spots on the gel-silica glass with increasing starting densities (a)=1.50±0.10 g/c.c., (b)=1.70±0.10 g/c.c. and (c)=1.90±0.10 g/c.c. The three

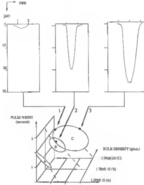

Figure 4.5 Laser densification conditions of the gel samples with different starting densities. Corresponding surface profiles of points 1, 2, and 3 are also shown above.

axes represent the exposure time(seconds), the power setting (mA) and the starting densities of the gel-silica glasses, respectively Within the process control envelopes A B and C are the densification conditions (exposure times and power settings) of the CO_2 laser required to make optically transparent spots on the silica gel-silica glasses There is no further densification of the substrates at the laser densification conditions below each dashed line and envelope. Above the ABC regions and the dashed lines, only cracked or foamed spots can be produced on a silica gel-silica glass substrate

Within envelope A are the restricted set of laser conditions for densifying the silica gel-silica glass with a bulk density ~1 50±0 10 g/cm^3 In envelope B, higher power settings and longer exposure times are required to create transparent densified spots on the silica gel-silica glass with higher bulk density(~1 70±0 10 g/cm^3) In conditions A and B, constant laser focal lengths L1 and L2 were used

The size of the envelope C is larger due to use of varied focal lengths L2 (shown in Table 4 1) Within envelope C are the densification conditions to make transparent spots on a silica gel with bulk density of 1 90±0 10 g/cm^3 The three dark points on envelope C are the densification conditions for the corresponding surface profiles. Table 4 1 lists the densification conditions of these three points(1, 2, and 3)

Optically transparent and densified spots ~1 mm in diameter have been made on the partially densified gel-silica substrates by using a CO_2 laser and the necessary laser densification conditions established. Comparing the laser processing conditions of envelopes A and B, pulses with substantially greater power are required to produce optically transparent spots on a silica gel with a higher starting density, and processing conditions are quite restricted in both A and B regions.

This result is consistent with the discussions in section 3 4 that the gel-silica sample S3(densified at 700°C) has a higher amount of permanent shrinkage than S2(densified at 900 °C) in the same thermal analysis Sample S2(900 °C) needs a higher thermal energy to further enhance the densification and to result in a larger permanent shrinkage. That means

Table 4.1 Laser densification conditions of the three points within envelope C of Figure 4.5

Point	1	2	3
Power(mA)	12	12	16
Pulse(sec)	1.5	1.0	1.5
L1(cm)	12.70	12.70	12.70
L2(cm)	10.16	8.89	12.70

the minimum laser energy required to densify sample S2(900 °C) is larger than sample S3(700°C) The gel-silica sample S2(900 °C) requires a higher laser energy to create the same amount of the permanent shrinkage

In envelope C, use of a variable focal length L2 enlarges the possibilities of CO_2 laser processing to make optically transparent spots on gel-silica substrates There are more choices of exposure times and power settings to produce microlenses or other optical elements. Thus, the processing conditions described by envelope C will be used to make micro-optical lenses arrays

4.3.2 Surface Investigation of Heat Affected Zone(HAZ)

Characterization of the surface of the laser irradiated spots include dimensions and physical appearance at various laser densification conditions, VHN profiles at various bulk densities and laser densification conditions and profiles of the peak maximum positions(PMP) of the TO AS_1 vibration mode of the laser densified spot described in section 3 6.3

Pictures of the physical appearance of the laser irradiated spots are obtained using a Nomarski microscope which is sensitive to the change in surface refractive index Therefore, the irradiated region can be easily distinguished from the unirradiated glass substrate The VHN profile is obtained from a track of indentations along the diameter of the laser irradiated spot. The maximum VHN of the gel-silica glass is 812±18 which is the VHN of a fully densified gel silica glass obtained in section 3.5.2. The peak maximum position of the TO AS_1 vibration mode can be regarded as an indication of the degree of the densification, as discussed in Chapter 3 The maximum value of the peak maximum position of the gel silica glass is 1122 cm^{-1}, which is the PMP of a fully densified gel-silica glass obtained in section 3 6 3

It is found that the diameter of the laser irradiated spots on the gel silica sample increases (i.e higher heat affected area) as the pulse width increases(i e larger incident laser energy). The results are shown in Figure 4 6. The diameters of the spot on a dry gel(bulk density=1 07 g/c.c) are larger than on a partially densified gel silica glass(bulk density=1 47 g/c.c.) at the same power setting. The laser processing parameters are indicated beside the figure. These results show that the laser energy required to make a densified spot on a partially densified gel-silica glass is larger than required for a dry gel

Figure 4 7 shows a typical appearance of a laser irradiated spot on a dry gel The laser processing variables, L1 L2, power setting I(mA) pulse width τ (sec), bulk density of the sample and dimension of this spot are shown on the figure. Cracks are usually observed on the surface due to the weak strength of the substrate, no matter how the laser densification conditions are arranged. No optically transparent spot can be produced on a dry gel Thus, use of gel silica samples with a higher starting density produces a better irradiated result, i.e. excellent optical transparency This is partially due to the higher strength of the substrate, discussed in Chapter 3 Figure 4 8 illustrates the physical appearance of the laser irradiated spots, (a), (b), and (c) on the gel silica samples with starting densities of 1 60 g/c c and 1 87 g/c c , indicated on the figure The diameter of the irradiated spots (a), (b), and (c) are 1 1, 1 1, and 2.4 mm, respectively Optically transparent spots can be made using the laser densification conditions shown on the right-hand side of Figure (a) and (b). If excess laser energy or a shorter focal length L2 are used, a foamed spot (c) was produced due to the trapped water(product of condensation) expanding within the closed pores when the spot is overheated

Figure 4 9 demonstrates the VHN profile on the surface of the the laser irradiated spot on a gel silica sample A4, with an initial bulk density~ 1 60 g/c.c The surface VHN profile is obtained by making a track of indentations along the diameter of the laser irradiated spot. The center of the the laser irradiated spot shows a maximum VHN (~265) and decreases gradually towards the periphery of the spot(VHN ~125). The change in

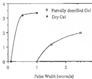

L1=10.16 cm

L2=6.35 cm

pulse width=variable

Power setting=12 mA

Figure 4.6 Comparisons of laser densified spot sizes of a dry gel and a partially densified gel at different pulse widths.

Bulk Density= 1.09 g/c c

L1= 10.16 cm

L2= 6.35 cm

Power Setting= 14 mA

Pulse Width= 1.0 sec

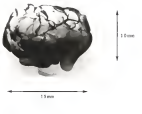

Figure 4.7 Appearance of a laser densified spot on a dry gel.

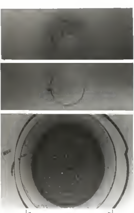

(a)
Too Little Laser Energy
Bulk Density= 1.60 g/c.c.
L1= 7.62 cm
L2= 12.70 cm
Power Setting= 12 mA
Pulse Width= 1.0 sec

(b)
Effective Laser Energy
Bulk Density= 1.87 g/c.c.
L1= 7.62 cm
L2= 17.15 cm
Power Setting= 16 mA
Pulse Width= 1.5 sec

(c)
Too Much Laser Energy
Bulk Density= 1.87 g/c.c.
L1= 7.62 cm
L2= 12.70 cm
Power Setting= 16 mA
Pulse Width= 1.5 sec

Figure 4.8 Appearance of laser densified spots on gel samples with different starting densities

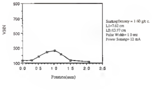

Figure 4.9 Surface VHN profile of a laser densified spot on a gel sample, laser densification conditions are also indicated.

VHN from center to the periphery of the spot is ~140. The temperature induced by laser heating is high enough to enhance the densification of the substrate. However, the VHN of a Type V full density gel-silica glass is 812±18(=VHN_m) which is much higher than the resulting 265 on sample A4. In addition, the change in VHN from center to the periphery of the spot is not high enough to produce an environmentally stable material. Therefore, the sample A4 with starting density ~ 1.60 g/c.c. is not qualified to be a substrate for an useful optical device. Results also show that the distance between two irradiated spots on this sample can not be less than 2 mm, otherwise severe cracking occurs. These results suggest that the strength of the gel-silica glass with bulk density equal to 1.60 g/c.c. is not high enough to be useful.

Although an optically transparent spot is made using the proper laser densification conditions on sample A4(bulk density~ 1.60 g/c.c.), the change in VHN is not high enough. As the spot will be used as a lens to focus optical ray, a large index change or the change in VHN between the laser irradiated region and the substrate is necessary.

The advantage of using higher bulk density substrates, like 1.80 g/c.c., sample A5, is shown in Figure 4.10. Under proper laser densification conditions, the maximum VHN~789 of the VHN profile of the laser irradiated spot is close to VHN_m. The substrate VHN is equal to 230; therefore, the change in VHN is ~559. In addition, the distance between the two irradiated spots(~ 1 mm in diameter) on this sample can be lower than 2 mm, almost next to each other, due to higher strength of the gel-silica sample. The above results show that the gel-silica sample A5 with bulk density equal to 1.80 g/c.c. has sufficient strength and large enough change in VHN to qualify as a substrate for laser densified optical components.

A higher laser energy input is used to enhance the densification of the gel silica glass to full density. The resulting VHN profile of the laser irradiated spot on a gel-silica sample with starting density = 1.81 g/c.c., sample A6, is shown in Figure 4.11. The laser irradiated spot is produced under stronger laser densification conditions than sample A5,

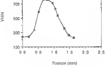

Starting density= 1 80 g/c.c.
L1= 12 70 cm
L2= 11 43 cm
Pulse Width= 1.0 sec
power Setting = 14 mA

Figure 4 10 Surface VHN profile of a laser densified spot on a gel silica sample(A5) laser densification conditions are also indicated

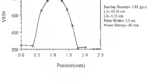

Figure 4 11 Surface VHN profile of a laser densified spot on a gel silica sample(A6), laser densification conditions are also indicated.

e.g. 16 mA for 1.5 sec vs 14 mA for 1.0 sec. The maximum VHN=802 of the densified spot on sample A6 is within the experimental error of the VHN$_m$ (812±18) of a fully densified gel silica glass (see Chapter 3). The substrate VHN is ~ 229. Thus, the change in VHN is ~573. An optically transparent full density region is achieved on sample A6 using laser densification. The diameter of the full density region(FDR), i.e. region with VHN within the experimental error of VHN$_m$, on the surface of the laser irradiated spot is ~ 300 μm.

The VHN profile shown in Figure 4.11 indicates a gradient property change that follows the intensity profile of the incident laser (Fig. 4.4). The shift of VHN from 229 towards 802 means that the laser irradiated spot is decreased in porosity from the periphery to the center(fully densified region). Because the spot has achieved full density in the center and a smooth gradient in density the laser irradiated spot on A6 can be used as a optical lens.

Further demonstration that a fully densified region can be achieved by laser heating on a Type VI gel silica glass is shown in Figure 4.12, a PMP profile. Micro IR spectra of the laser irradiated spot on gel-silica sample A7, bulk density=1.91 g/c.c., are obtained along the diameter of the laser irradiated spot shown in the upper part of Figure 4.12. The diameter of each area analyzed is 100 μm, from region 1 to region 10. IR spectra are shown in Chapter 6. Peak maximum positions(PMP) of the TO AS$_1$ vibrational mode are determined from these micro IR spectra. The profile of the peak maximum position of the laser irradiated spot is illustrated in the lower part of Figure 4.12. The laser densification conditions of this laser irradiated spot are listed on the figure. It is known from section 3.6.3 that the PMP indicates the degree of densification of the gel-silica samples. For a dry gel, the PMP is equal to 1084 cm^{-1}. For a Type V full density gel-silica glass, the PMP is shifted to a higher wavenumber of 1122 cm^{-1}.

In this study, the PMP at the center of the laser irradiated spot(=1122 cm^{-1}) is the same as that of a full density gel silica glass, and the PMP decreased from the center to the

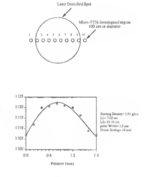

Figure 4.12 Schematic of micro FTIR investigations of a laser densified spot(upper) and the corresponding PMP profile(lower) with indicated laser densification conditions of this spot

periphery(~1107 cm^{-1}) The estimated diameter of the fully densified region is ~ 300 μm (regions with PMP ~1122 cm^{-1}) This diameter is consistent with the result estimated from the VHN profile of sample A6 (Fig 4 11) The shift in PMP from 1107 to 1122 cm^{-1} means that there is a change in intratetrahedral bond angle which becomes larger, and the Si-O bond length, which becomes shorter, for the investigated regions from 1 to 10 The average bond angle and bond length in the center of the laser irradiated spot are close to the values of a full density gel silica glass(~144° ~1 62Å) PMP profile in the micro-FTIR reflectance measurement also indicates a gradient property change of the laser densified spot which follows the intensity profile of the incident laser beam

In conclusion, gel-silica samples with higher bulk densities > 1 80 g/c c can be used successfully as a substrate for generating density gradients. Gel-silica samples with lower starting densities, ~1 10(a dry gel) or 1 60 g/c.c (sample A4) usually crack or result in insufficient density change to be useful The reasons could be:

(i) high concentration of silanol groups,

(ii) high surface area of the gel-silica substrates resulting in low strength of the substrate and inefficient laser densification.

Samples A5 and A6 with higher starting density (≥ 1 80 g/c c.) have enough change in VHN and PMP after laser irradiation to be useful optical devices. The maximum VHN of the laser irradiated spot close to VHN$_{si}$ has been successfully produced on sample A6. The diameter of the heat affected zone is ~1 4 mm. The diameter of the fully densified region on the surface of the laser irradiated spot is ~ 300 μm as estimated from the VHN profile of sample A6 and the profile of the peak maximum position of sample A7 This is the desired result for successful laser densification of Type VI gel silica glass

Both the VHN profile and the profile of the peak maximum position indicates property changes which follow the profile of the laser intensity. The center of the laser irradiated spot shows full densification(VHN=802 and PMP=1122 cm^{-1}) which means the center of the laser densified spot is structurally similar to a commercial vitreous silica [Alm90].

4.3.3 Cross Section Investigation of Heat Affected Zone

The cross section of the laser densified spot is also investigated which includes appearance, VHN profile along the depth, and PMP profile along depth. The cross section of a gel silica sample is polished to the position near the center of the irradiated spot as shown in Figure 4.13(a), the surface of the laser irradiated spot remains unpolished. The diameter of the laser irradiated spot is evaluated to be ~1.4 mm. Pictures of the cross section of the laser irradiated spots are taken using a Nomarski microscope (equipped with a camera) which is sensitive to the surface refractive index change. The cross section of the laser irradiated region is a hemispherical shape, as shown in Figure 4.13 (b). The laser densification conditions and the bulk density(=1.91 g/c.c.) of the gel silica sample, A7, are listed on the figure. Figure 4.13 (b) and (c) are the pictures of the cross section of the spot (a), where (c) has twice of the magnification of (b). The depth of the heat affected zone is ~ 135 μm measured using a microscope.

The VHN of the cross section of the laser densified region is measured along the depth shown in Figure 4.14. The depth of the heat affected zone is estimated from this figure to be < 200 μm which is similar to the value measured using a microscope shown in Figure 4.13(c). The depth of the fully densified region is evaluated to be ~ 10 μm. The VHN value at the surface (≈802) in Figure 4.14 is obtained from the surface VHN profile discussed in the previous section which is within the range of VHN_{gs}(812±18).

This study indicates that a depth gradient in VHN occurs due to heat conduction into the substrate. The heat is generated by absorption of the CO_2 laser energy (absorption depth ~ 10 μm described in Chapter 7). This VHN profile follows the temperature profile induced by the laser heating.

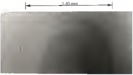

(a)

Top View

Bulk Density= 1.91 g/c.c.
L1= 7.62 cm
L2= 16.51 cm
Power Setting= 16 mA
Pulse Width= 1.5 sec

(b)
Cross section of (a)

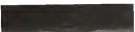

(c)
Cross section of (a)

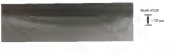

Figure 4.13 Appearance of surface(a) and cross sections(b) and (c) of a laser densified spots on a gel silica sample.

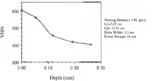

Figure 4.14 Cross section VHN profile of a laser densified spot on a gel-silica sample. Laser densification conditions of this spot are also indicated.

Further confirmation of the gradient property change along the depth of the laser irradiated spot is obtained using FTIR micro-spectroscopy. Macro-spectra of a laser irradiated spot on a gel silica sample A7, bulk density=1.91 g/c.c., are obtained along the depth of laser irradiated spot as shown in the upper part of Figure 4.15, from region 1 to region 4. The diameter of each investigated region is 100 µm. Peak maximum positions(PMP) of the TO AS_1 vibrational mode are determined from these micro IR-spectra, as described in section 3.6.3. The PMP profile along the depth of the laser irradiated spot is illustrated in the lower part of Figure 4.15. The laser densification conditions of this laser irradiated spot are listed on the figure also. The diameter of the heat affected zone is estimated to be less than 200 µm.

The PMP in region 1 (~1118 cm^{-1}) is close to the wave number of a Type V gel silica glass (~1122 cm^{-1}). The discrepancy (~4 cm^{-1}) is due to the depth of the heat affected zone (~150 µm) being close to the diameter of investigated region 100 µm. Region 1 covers most of the heat affected zone including a small part of the fully densified region(<10% in depth). Therefore, the PMP of region 1 is 1118 cm^{-1} instead of 1122 cm^{-1}.

The PMP profile also indicates a gradient property change which follows the energy profile of the temperature profile induced by laser heating. The densification of the laser irradiated spot decreases at increasing depth. The shift in PMP from the surface into the substrate indicates that there is a structural change in intratetrahedral bond angles (they become smaller) and Si-O bond lengths (which become longer) within the investigated region.

As shown in section 3.5.2 the VHN of a gel silica glass increases as the densification temperature increases using furnace heating. The above results show that there is also a VHN change of the laser irradiated spot using laser heating which is consistent with the results of section 3.5.2. It is demonstrated that a fully densified region can be created on a partially densified substrate (with diameter ~300 µm and depth ~10 µm)

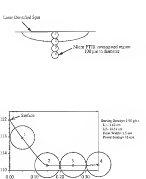

Figure 4.15 Schematic of micro-FTIR investigations on the cross section of a laser densified spot(upper) and the corresponding PMP profile(lower) with indicated laser densification conditions of this spot.

without cracking and foaming. Further confirmation of the dimension of the heat affected zone and the fully densified region are obtained from the study of the PMP profile on the surface and cross section of the laser irradiated spot. The results show that the fully densified region successfully produced by laser heating is structurally similar to that of the commercial vitreous silica. The depth of the laser densification zone depends on the incident laser energy and the thermal history of the gel silica sample.

In summary, these studies show that there is a gradient in properties (VHN change and PMP shift) on the surface (VHN from 229 to 802, PMP from 1107 to 1122 cm^{-1}) and along the depth (VHN from 425 to 802, PMP from 1111 to 1118 cm^{-1}) of the laser irradiated spot. It is also demonstrated that the measurements of VHN and micro-IR spectroscopy can be used to determine the degree of densification of the laser irradiated spot.

4.3.4 Stability after Laser Densification

Stability of the laser densified regions is investigated by monitoring the profile of VHN on one spot as a function of time. A previous study [Slo90] indicated that laser densified gel-silica may relax with time, thereby eliminating index of refraction gradients induced by the CO_2 laser beam. Instability of the laser irradiated spot was concluded in their studies by observing that the depth of the surface profile of a laser irradiated track decreased with time. Incorporation of water within the densified region might have contributed to this structural relaxation.

Based on the studies in Chapter 3, two approaches were chosen to prevent the water effect on a laser densified region and increase the efficiency of the laser densification. The first approach was pumping out the physically adsorbed water of the gel silica sample by heating the gels in a vacuum oven up to 150°C. The second approach was to control the humidity during laser densification. In addition, gel silica samples with higher starting density were used for the stability study, based upon the dilatometry results discussed in Chapter 3.

To monitor the stability, a laser irradiated spot was produced on a gel-silica sample with bulk density = 1.81 g/c.c. The laser densification conditions of the irradiated spot are listed on the top of Figure 4.16. Three tracks of microhardness indentations across the same laser irradiated spot were made at different times. They are used to determine if the VHN profile is changed with time. The diameter of the indentation is ~ 20 μm in length or width which is much smaller than the diameter of the laser densified spot (1.4 mm).

In the right corner of Figure 4.16 are shown the three tracks of indentations on the spot in different orientations. The densified spot was exposed to ambient atmosphere after the laser irradiation. Track 1 was made 3 months after the spot was irradiated. Tracks 2 and 3 were made after 3.5 and 4 months, respectively. The VHN values for the three tracks show very little change in the profile with time. The maximum VHN value ~802 at the center of the laser irradiated spot is also close to VHN_m of the fully densified gel-silica glass(812±18). There is no time dependent deterioration observed on this densified spot, although it was under long term humid conditions. Thus, the laser irradiated spots on the partially densified gel-silica glass(bulk density=1.81 g/c.c., 82% dense) exhibited the environmental stability required for optics. This result shows that the approach of eliminating water before laser densification combined with the use of low-humidity environment and higher starting density gel-silica substrates are necessary to attain a stable laser irradiated spot.

The other proof of stability of the laser irradiated spot is that the PMP at the center of the laser irradiated spot on sample A7 was maintained at 1122 cm^{-1} after four months of humid exposure. Thus, once the laser irradiated spot is densified to full density, the laser irradiated spot will exhibit environmental stability.

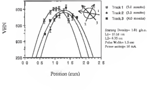

Figure 4 16 Stability of surface VHN profile of a laser densified spot on a gel sample measured at different times after the laser densification(Tracks 1, 2, and 3), laser densification conditions of this spot are also indicated.

4.3.5 Comments on Previous Work[Slo90]

Reasons for the instabilities of the laser irradiated spot by Slocumb's work are summarized [Slo90]. The gel-silica sample they used was 71% dense (starting density=1.56 g/c.c.). By using Figure 3.14, the estimated refractive index was 1.33. This sample has a preference of forming high concentration of threefold rings according to Vasconcelos et al. and Wallace [Vas89a][Wal91]. These rings are susceptible to be eliminated by incorporating water molecules which results in some swelling of the bulk known from the study in section 3.4. Therefore, after laser densification of low density gel-silica, the concentration of the threefold rings increases which tend to be eliminated after exposure to ambient atmosphere. When the threefold rings incorporate water molecules some swelling, i.e.relaxation, occurs.

The resulting n change by laser densification in Slocumb's work is 0.06, i.e. the final n is 1.39 which is still far away from the n value (=1.46) of a full density gel silica glass. Therefore, a fully densified region was not achieved and relaxation occurred in this case. The insufficient index change may attributed to use of low incident laser energy, a long 1.2, and a humid environment during laser densification (resulting in inefficient laser densification). In Chapter 3, it was shown that if the starting density of the gel-silica sample is not high enough(i.e.< 1.8 g/c.c.), the resulting maximum VHN can not reach VHN_m and relaxation can also happen in this case. So unless a fully densified region is achieved by the laser heating, there is a risk of relaxation after exposure to the ambient atmosphere.

Therefore, the conditions required to achieve a stable laser densification are: (i) use of a gel-silica substrate with higher starting density (>1.8 g/c.c.), (ii) proper laser densification conditions to achieve full densification, (iii) desorption of adsorbed water in gel-silica sample prior to irradiation, and (iv) a low humid environment during irradiation. All four conditions must be satisfied to maximize the efficiency of the laser densification. The stability of the laser irradiated spot can be assured when these conditions are met.

4.3.6 Mechanisms of the Instability

The mechanisms of the instability of laser densified gel-silica glass are summarized as follows. The relaxation at room temperature of the laser irradiated spot on a partially densified gel-silica sample can result from:

(a)Rehydrolysis of the threefold rings on the pore surface. A very large concentration of threefold rings on the pore surface form upon densification. The strained rings reopen after incorporating moisture by adsorption of water molecules. The adsorption is followed by rehydroxylation via a dissociative bond breaking reaction [Wal91]

(b)Rehydrolysis within the skeleton Gel-silica samples sintered at low temperatures have a high OH content and therefore a low viscosity [Bri90] The low viscosity of the gel stabilized at lower temperatures make structural relaxation possible at room temperature.

(c)Structural relaxation(extremely slow) and relief of strained bonds induced by laser heating This mechanism is significant when the viscosity of the gel-silica sample is low due to incorporation of water in the structure.

Mechanism (a) and (b) occur by adsorbing water from the ambient atmosphere. Mechanism (c) shows an extremely slow rate of recovery of the residual stress if the gels are sintered at temperatures near the glass transition region(~1200°C)[Bri90] If the gels are incompletely sintered, a low temperatures structural relaxation can be more rapid.

Thus, a higher starting density (1.80-2.00 g/c.c.) of the gel-silica sample is preferred to be used for an optical substrate not only for the environmental stability but also for the achievement of a fully densified region Use of a lower starting density gel-silica substrate will have a preference for forming threefold rings by laser heating and will relax after exposure to the ambient atmosphere.

4.4 Mechanisms of Laser Induced Densification

In section 3.4, expansion, permanent and temporary shrinkage by furnace heating was observed in the dilatometry analysis for partially densified gel-silica glasses. Gel silica glasses sintered at 700 °C had a significant amount of shrinkage, including both permanent and temporary shrinkage. The mechanisms of temporary shrinkage and subsequent relaxation of the gel silica sample during furnace heating and cooling is similar to the unstability observed for laser irradiated spots. Consequently, the mechanisms of laser densification of the gel-silica samples must be similar to the mechanisms of shrinkage and expansion during furnace heating and cooling. The absorbed laser energy is transferred into heat which results in densification the porous gel silica network. The phonons from the laser-induced heat are consumed by the following densification mechanisms[Elm83] [Sch86] [Zhu89][Bri90][Wal91]

(a) Shrinkage due to the desorption of water, alcohol, and removal of organics.

(b) Structural relaxation via loss of excess free volume.

(c) Formation of threefold rings by condensation of adjacent surface SiOH groups. They are close enough to react which result in an increase in the structural density to a maximum value at 900°C followed by a decrease in the structural density due to structural relaxation.

(d)Decrease in the NBO/BO ratio via the formation of bridging Si-O-Si bonds, in the matrix(skeleton condensation) and on the pore surface (by pore collapse or sintering across the pores as shown in Figure 4.17)

For stable laser densification of the gel silica samples, the shrinkage in the surface layer may be attributed to mechanisms (a), (b), and (d), i.e. irreversible condensation

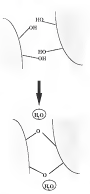

Figure 4 17 Schematic of permanent shrinkage mechanism condensation of neighboring silanol groups on pore surface resulting in pore closure and densification reactions and structural relaxation. Thus, the efficiency of laser densification can be improved by

(1)using a gel silica sample with high bulk density,

(2)pre-desorbing physical water from the gel-silica sample and

(3)providing a dry environment for laser densification

Mechanisms (b) and (d) are associated with the laser densification on a gel-silica sample with bulk density > 1 80 g/c.c Unstable laser densification results when shrinkage of the porous gel silica glass is dominated by mechanism(e), e.g , the laser densified region may relax within hours or days

According to the mechanisms of laser densification discussed above, the laser induced densified regions in Type VI gel-silica substrates can be categorized as Regions I, II and III. Figure 4 16 illustrates the structural evolution of a laser irradiated spot on a Type VI gel-silica substrate. The upper part of the figure is the magnified structure of the cross section before laser densification the lower part are the three types of the laser densified regions. In fact, the structural features of the laser irradiated spot vary gradually according to the property changes illustrated in Figure 4 14 and Figure 4 15 The property gradient of the laser densified region is changed from the center to the periphery of the spot. Therefore there is no sharp edge between those regions Scales of the structures and the dimension of the laser irradiated spot are also shown on the figure. Characteristics of the three regions are summarized as

(I) Elastic densification(reversible) i e open up of the threefold rings on the pore surface which is thermodynamically favorable and not kinetically limited for a gel-silica glass with large surface area.

(II) Viscoelastic densification (a mixture of reversible and irreversible), i e. relief of the residual stress, but the rate of the recovery is extremely low if the viscosity of the partially densified gel silica substrate is high. It is thermodynamically favorable but is kinetically limited.

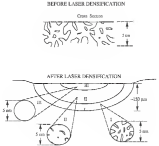

Figure 4 18 Structure characteristics before and after laser densification of a Type VI gel-silica glass.

(III)Plastic densification region(irreversible) which is sintered to full density
through skeleton condensation and pore collapse during viscous sintering

The dimension of the thickness of each region depends on the starting density of the gel-silica samples and the laser densification conditions For example if the bulk density is 1.60 g/c.c. or the input laser energy is not high enough, the fully densified region can't be achieved, so only region I and II is formed. In this case, the dimension of region I is significant which will result in a subsequent relaxation Recovery of region II is also possible due to the low viscosity of the gel-silica substrate.

If 2.2>bulk density≥1.8 g/c.c., the skeleton density is close to that of the melted glass which is concluded from the measurements of the He pycnometry [Vas89a][Bri90][Wal91] Thus, the recovery of region II is extremely difficult due to the high viscosity Region III can be produced in this case through sintering by complete pore closures. Therefore, the resulting shrinkage is permanent Elimination and prevention of water adsorption before and during laser densification makes it possible to obtain a fully densified region III which is environmentally stable

4.5 Conclusions

Fully densified regions can be produced on gel-silica glasses directly, using a CO_2 laser without masks, diffusion, or other intermediate processing steps The laser densification conditions have been established to produce various diameters of optically transparent spots The gradient property change of the laser densified spot yields its capability of manipulating optical rays. Microlenses with different diameters can be fabricated by controlling the variables in the laser densification conditions. Microlenses ~1 mm diameter can be used to focus the optical rays parallel or perpendicular to the sample surface Arrays of 3×3 microlenses have been made using conditions within envelope C of Figure 4.5 discussed in this Chapter

It is demonstrated that the technique of micro-IR spectroscopy allows an immediate investigation of the structural change of the laser densified spot. The shift in the PMP of the asymmetric stretching vibrations of Si-O-Si indicates a gradient structural change from the periphery(1107 cm^{-1}) to the center(~1122 cm^{-1}) of the laser densified spot.

The evaluated diameter and the depth of the fully densified region is ~300 μm, by ~10 μm, respectively. The diameter and depth of the heat affected zone can be produced up to ~1400 and 140 μm, respectively. Laser irradiated spots on gel-silica samples with bulk density > 1.8 g/c.c. show environmental stability and the capability of attaining a fully densified (2.2 g/c.c.) region. This is the best result for laser densification on Type VI porous gel-silica glass that can be possibly achieved.

The stability of the laser irradiated spot can be assured by

(i)using a gel-silica sample with higher starting density(>1.8 g/c.c.) as a substrate for laser densification,

(ii)proper laser densification conditions to enhance the densification to full density,

(iii)predesorption of adsorbed water in the gel-silica substrate, and

(iv)providing a low humidity environment during laser densification.

Conditions (iii) and (iv) are required to prevent the effect of water on the laser densified region and increase the efficiency of laser densification.

Mechanisms of laser densification on Type VI gel-silica glasses are proposed, including: (I) Elastic densification(reversible), (II) Viscoelastic densification(reversible, and irreversible), and (III) Plastic densification(irreversible). They are consistent with the experimental results of gradient property changes and the observed phenomena of relaxation after laser densification.

CHAPTER 5
APPLICATIONS IN OPTICS

5.1 Introduction

The objective of this chapter is to demonstrate qualitatively the optical applications of laser densified Type VI and Type V gel-silica glasses. A slight surface depression of the gel silica substrate is formed after the laser irradiation due to shrinkage of the Type VI porous substrate or vaporization of the Type V gel-silica substrate if the induced temperature by laser irradiation is high enough.

A surface depression can be used to defocus an optical ray and function as a negative microlens. Previous studies in Chapter 4 shows that a full density region(FDR) can be produced using CO_2 laser heating on a porous gel-silica substrate, and the laser densified region exhibits a gradient property change and has a higher density than the substrate. This GRIN(gradient index of refraction) region can be used to manipulate optical rays such as focusing, imaging or directing. Optical devices that can be made through laser densification include geodesic lens, planar GRIN lens, negative lens and multimode waveguides[Sio90]. The advantages of laser densification and the previous work of laser densified channel waveguides are discussed.

Three types of microlenses can be made on Type VI gel silica substrates(shown in Figure 5.1 (a)) and Type V gel-silica substrates(or commercial silica glasses shown in Figure 5.1 (d)) by using laser densification. The types include

(a)MI microlens or microlens arrays(Figure 5.1 (b)) which are geodesic lenses or compound lenses on the surface of porous gel-silica glass.

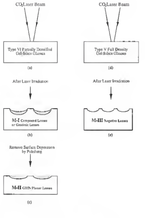
CO$_2$ Laser Beam
CO$_2$ Laser Beam
Type VI Partially Densified Gel-Silica Glasses
(a)
Type V Full Density Gel-Silica Glasses
(d)
After Laser Irradiation
After Laser Irradiation
M-I Compound Lenses or Geodesic Lenses
(b)
M-III Negative Lenses
(e)
Remove Surface Depressions by Polishing
M-II GRIN Planar Lenses
(c)

Figure 5.1 Three types of microlenses, M I, M II and M III, produced by laser irradiation on gel silica glasses

(b)M-II planar GRIN microlenses or microlens arrays(Figure 5.1 (c)) on the surface of porous gel-silica glass after removing the slight depression on the irradiated surface.

(c)M-III microlenses or microlens arrays(Figure 5.1 (e)) which are negative lenses on the surface of fully densified gel silica substrate.

The above microlenses can be applied in integrated optics shown in Figure 2.5 or in micro-optics shown in Figure 2.7. A M-I microlens, termed as a compound lens, is due to the combination of a depressed region(which diverges light) and a GRIN region(which converges light) is illustrated in Figure 5.2. However, it is observed that the surface depression of the laser irradiated spot dominates the optical behavior of a M-I microlens. The light is diverged by a M-I compound lens if the optical ray is incident perpendicularly on the surface of the glass substrate as shown in Figure 5.2. The deflection of optical rays(solid lines) is narrower because of the GRIN region which will act to converge the optical ray. Dashed lines represent the deflected optical rays if the GRIN region is not present.

A M-I microlens can also be used as a geodesic lens if the light is propagating parallel to the surface of the gel-silica substrate. A geodesic lens, as described in section 2.3.4, is used for redirecting and focusing a lightwave confined along the surface. The manipulation of optical rays using a M-I geodesic lens can be achieved by the geometry or the GRIN effect of the lens. Since the laser densified region shows a gradient change in refractive index, the focusing capability of a M-I geodesic lens is mainly attributed to the GRIN effect.

M-II microlenses or microlens arrays are produced by removing the surface depression of the laser irradiated regions. A M-II microlens can be used to focus the incident light either perpendicular or parallel to the surface of the gel-silica substrate. The focusing capability of a M-II microlens is also attributed to the GRIN effect. Theoretical predictions of the focal length and the nominal numerical aperture of a hemispherical GRIN

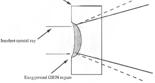

Figure 5.2 Diverged optical rays by a M-I compound lens. The optical rays(dashed lines) are deflected in a wider angle if a GRIN region does not exist.

planar microlens are described in this chapter The calculated focal length was compared with the measured focal length.

A M III negative microlens is formed on a full density gel-silica substrate(or on a commercial silica glass) Only a surface depression exists(i.e no GRIN region is present) for the M-III microlens In general, a M III microlens can be used for defocusing or imaging However, a focusing phenomenon due to the diffraction effect has also been observed with a negative microlens[Hec74] Virtual images formed by the arrays of M-III negative microlenses have also been demonstrated.

5.2 Advantages of Laser Densification

Various fabrication methods of GRIN or convex microlenses have been described in section 2 3 include coating, diffusion, mass transport, and ion-exchange techniques The disadvantages of these methods include

(a)A strain induced index change in a diffused microlens caused by the size of diffusant

(b)In the photolithograph technique based on melting of the lens material, it is very difficult to control the spreading Thus, the melting process results in a uncontrollable lens size and the isolation of the close packed lenses[Pop88]

(c)Hours are required for obtaining a GRIN gel from soaking-and-drying method or a GRIN glass from conventional ion-exchange methods.

The above techniques also involve tedious, sophisticated and process sensitive steps. The advantages of direct laser-writing optical elements on Type VI(porous) or Type V(full density) gel-silica substrates are summarized as follows[Ber90][Mor90][Chi92b]

(a)Producing GRIN optical devices which have significantly smaller aberrations than equivalent single-element homogeneous lenses[Tom80] (b)Producing various types of optical elements, some of which cannot be made easily by any other means.

(c)Attaining full density optical elements which exhibit high optical transmittance from UV to NIR wavelengths(broad band coverage),

(d)A much faster and environmentally cleaner process,

(e)A single step contact free treatment,

(f)A high degree of automation and good reproducibility,

(g)A feasible alternative or addition to existing techniques

(h)Control of GRIN profiles,

(i)Wider range of Δn than other chemical based methods for making GRIN optics

In summary, the fabrication time of laser densification is the laser exposure time which is only ~1-2 seconds. Thus, this method is much faster than the conventional routes to obtain a GRIN microlens. Laser densification improves the optical properties of the porous gel-silica substrate rather than degrading the modified region by use of diffusants. Further, laser densification has high degree of automation which is feasible using the current techniques.

5.3 Geodesic Microlenses(M-I)

A M-I microlens can be used as a geodesic lens if the light is propagating along the surface of the gel-silica substrate. This is because a M-I microlens has a slight depression as well as a GRIN region beneath the surface shown in Figure 4.13(b).

Half of the porous gel silica sample is removed by polishing, as shown in Figure 4.13(a), in order to observe the focusing phenomenon. The depth and diameter of the geodesic lens produced in this manner are ~ 135 μm and 1.4 mm, respectively. The index change Δn of the GRIN region is determined to be 0.09 at 632.8 nm, as discussed in section 6.3 3 Therefore, the M-I geodesic lens can be used in integrated-optics, acoustic optics, or a focusing element for a two-dimensional diode laser

Figure 5 3 (a) shows the simulated focusing phenomenon of a geodesic microlens A 10x objective lens is used as a beam expander A lightwave is penetrating through a pinhole(adjustable diameter ≥ 1 mm, 3 mm is used) and a slit(3 mm in width, 50 μm in length) Optical rays are incident immediately on the cross section of the gel silica substrate. The incident light is in a rectangular shape formed by the slit. As the geodesic lens is used for focusing the lightwave confined along the surface,the slit, herein, is used to simulate that condition to observe the focusing capability of a geodesic lens produced by laser densification. The length of the slit is much smaller than the depth of the geodesic microlens, but the width of the slit is larger than the diameter of the geodesic microlens. The sample is situated on a three-dimensional micro-positioner in order to allow the rectangular light to project precisely on the geodesic lens

The focusing phenomena of a M I geodesic lens produced by laser densification is shown in Figure 5 3(b) It was observed that as the rectangular shaped lightwave is incident on the geodesic lens, there is a sharp and straight line formed by the geodesic lens and a bright spot on the end of the sample following the straight line as shown in Figure 5.3(b) The optical ray is focused as soon it emerges from the GRIN region. The focal length of this geodesic lens is estimated to be ~0 7 mm which is the radius of the geodesic lens. A rectangular spot(similar to the shape of the slit) is observed in the end of the sample without the geodesic lens. The focusing capability of M I geodesic lens is mainly due to the GRIN effect.

Thus, Figure 5 3(b) demonstrates that the laser densified geodesic lens on a Type VI porous gel-silica sample can be used to focus an optical ray parallel to the surface An incident lightwave in a rectangular shape is focused by the GRIN region of the geodesic lens. This focal length of this geodesic microlens is very short due to the large index change(~0 09) and large GRIN depth(~0 7 mm)

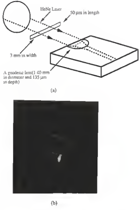

Figure 5 3 Instrumental arrangements(a) for the observation of focusing phenomenon of a M-I geodesic microlens The result is shown in (b)

5.4 Planar GRIN Microlenses and Arrays

Arrays of laser densified spots were made on the surface of a Type VI porous gel-silica sample(bulk density = 2.13 g/c.c.) using a computer-controlled plotter, as shown in Figure 4.2. Since the surface depression formed after laser heating will diverge optical rays, the depression was removed to produce a M-II GRIN planar microlens. The surface depression, ~ 30 μm in depth, was carefully polished because of the thin layer of the GRIN region(≤ 150 μm in depth). Example of a M-II microlens produced after polishing is shown in Figure 5.4.

As discussed previously, M-II microlenses and microlens arrays can be used in micro-optics. Figure 5.5 (a) illustrates use of such an M-II microlens array.

Optical rays are incident perpendicularly on the surface and penetrate through the substrate which contains the array of laser densified spots. The focusing phenomenon of an array of planar lens can be observed only if the surface flatness and the homogeneity of the gel-silica sample are well maintained.

A 10x objective lens is used experimentally as a beam expander during the observation. The expanded HeNe laser beam is incident perpendicular on the surface of the gel-silica substrate with arrays of planar GRIN microlenses shown in Figure 5.5(a). The distance between the GRIN microlenses is 2 mm. The diameter of each GRIN planar microlens in the array is ~ 800 μm. The index change of this GRIN microlens is evaluated to be ~0.02. An arrays of focused spots is observed on a screen behind the gel-silica sample as shown in Figure 5.5(b). In this figure, the black spot is the surface defect on the other unpolished side of the gel-silica sample. The focusing ability of the array of planar microlenses is attributed to the GRIN regions beneath the surface. The focal length of these gel-silica planar GRIN microlenses is ~ 5.26 cm. This focal length is a little longer than desired due to an insufficient index change Δn

Figure 5.4 A M II microlens produced after polishing, the diameter is $\sim 800\ \mu m$.

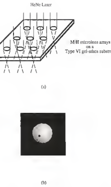

Figure 5 5 Focusing phenomenon of arrays of the M-H GRIN planar microlens on a porous gel silica sample The result is shown in (b)

The magnification formed by a gel-silica GRIN planar microlens is demonstrated in the following manner. The diameter of the M-II microlens is 1 0 mm on the surface of a porous gel silica glass(bulk density=1 40 g/c c.) The rectangular region(1 5 cm • 2 0 cm) in Figure 5 6 is the gel silica substrate The magnification of a character "s" indicated by an arrow is shown in Figure 5 6, about two times larger than the original size. The index change present in the GRIN region of the planar lens contributes to this magnification of the character s

It is demonstrated that a planar gel-silica microlens can be used to focus an optical ray or magnify an image by the GRIN region produced by laser densification. The focal length and the power of the magnification of a microlens depend on the index change and the thickness of the GRIN region The initial density of the substrate and power of the laser pulse control these variables.

5.5 Theoretical Analyses

5.5.1 Theoretical Analyses

The focal length and numerical aperture of a hemispherical planar GRIN microlens are analyzed using ray theory discussed in section 2 3 3[Iga84] Experimental variables in the calculations include the radius(a) of the microlens, GRIN depth(d), and the index change(Δn=the maximum refractive index-the refractive index of the substrate) The focusing length l_0 and the nominal numerical aperture(NA) of a planar GRIN microlens in Figure 2 3 can be obtained using the following equations

$$l_0 = d + \sqrt{1-2\Delta}\cot[\frac{gd \cdot \sin^{-1}\sqrt{(2\Delta)}}{\sqrt{(2\Delta)}}]/g \qquad (2\,9)$$

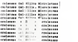

Figure 5.6 Magnification of a character "s" by a gel-silica microlens M-II on a porous gel-silica sample.

$$\mathrm{NA} = 0.2 n_2 \sqrt{2\Delta} \qquad (2.10)$$

Where $\Delta = [n(0)-n_2]/n(0)$, g is a focusing constant(=$[\sqrt{(2\Delta)}]/a$), d is the depth of the DI region I at r=0 shown in Figure 2.3. It is assumed that optical rays are focused inside the substrate medium with infinite length.

The relationships between the index change Δn(a=0.50 mm, d=0.10 mm), the calculated focal length and calculated numerical aperture are shown in Figure 5.7. Focal length decreases as the index change increases. The calculations show that the nominal numerical aperture of the microlens increases as the index change increases and the maximum NA is 0.10. In this study, the index change depends on the initial refractive index of the gel silica substrate. As discussed in Chapter 4, a substrate with density >1.80 g/c.c. has a stable laser densified region and a full density region in the middle of the laser densified spot. From this result, the maximum index change of the gel silica glass that can be produced by laser heating is ≤0.09 on a substrate with density ≥1.80 g/c.c. This index change is estimated using Figure 3.19. Therefore, the minimum calculated focal length produced by laser densification on a gel silica substrate is ~2 cm because of the limited index change ≤0.09. The maximum nominal numerical aperture(~0.10) is also limited by the index change in this study.

The relationships between the radius a(Δn=0.09, d=0.10 mm), GRIN depth d(Δn=0.09, a=0.50 mm) and the calculated focal length are illustrated in Figure 5.8. The corresponding focal length decreases drastically as the radius a of the microlens decreases(or GRIN depth increased). The minimum focal length ~0.25 mm can be achieved by reducing the radius of the microlens to 0.05 mm. The minimum focal length is ~12.5 cm if the GRIN depth is at 0.15 mm(when Δn=0.09 and a=0.50 mm). The GRIN depth d is limited by the low thermal conductivity of the silica glass. Comparatively, the radius of the microlens has a greater influence on the resulting focal length of the microlens.

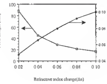

Figure 5.7 Relationships between the index change(Δn) and the calculated focal length and the nominal numerical aperture of lenses

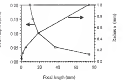

Figure 5.8 Relationships between the radius(=a), GRIN depth(=d), and the calculated focal length of lenses

The calculated ranges of the focal length of laser densified lenses are from 0.25 mm(a=0.05 mm, d=0.10 mm, Δn=0.09) to 88.07 mm(a=0.50 mm, d=0.10 mm, Δn=0.02) at different processing variables. Among these variables GRIN depth d(<200μm) is limited by the thermal conductivity of the pure silica glass. Index change Δn(≤0.09) is limited by the initial refractive index of the gel silica substrate and the required stability of the laser densified region. The only processing variable in the calculations that can be changed to shorten the focal length is to reduce the radius(a) of the GRIN microlens. Radius(a) could be decreased by using a mask to control the size of the laser densified region on the gel silica substrate. The other possible method of improving the GRIN depth is to increase the frequency of the laser pulse with lower energy. A densified region with higher Δn could potentially be achieved by use of dopants such as GeO_2 prior to densification, but this would detract from the simplicity of the process.

5.5.2 Comparisons

The measured focal length of the laser densified gel silica GRIN planar microlens(described in section 5.4) is compared with the calculated focal length using ray theory. The parameters for the equations(2.9) and (2.10) used in the comparison are listed below:

d= 0.150 mm(determined from Figures 4.14 and 4.15)

n_2= ~1.44(determined using Figure 3.19)

$n(0)$= ~1.46

Δ= 0.02/1.46= 0.014

a= 0.40 mm

g= [$\sqrt{(2\Delta)}$/a)= 0.42

The calculated results are.

FL= 38 1 mm

NA= 0 05

The predicted data of the focal length l_0 from equation (2 9) is equal to 38 1 mm. However, the medium is assumed to be infinite along the direction of the optical ray and the focal point is located within the medium. l_0 should be modified by an equation due to the finite thickness of the gel silica sample which is listed below

$$l_0' = \{[l_0 \text{ sample thickness}(=3 \text{ mm})]*[n(o)(=1\ 46)]]\} \qquad (6\ 1)$$

The modified l_0 is 5 14 cm compared to the measured focal length which is ~5 26 cm. Thus, the calculated focal length is in good agreement with the measured focal length

In conclusion, equations (2.9) and (2.10) are useful in predicting the FL and the NA of a planar hemispherical GRIN microlens The calculated focal length is consistent with the experimental result. The calculated focal length decreases drastically at decreasing radius(a) of the microlens, or increasing index change and increasing GRIN depth d. The shortest calculated focal length is 0.25 mm where the experimental variables are radius a=0 05 mm, GRIN depth d=0 10 mm, and index change Δn=0 09 This short focal length of a GRIN planar microlens is more applicable in micro-optics than the ~ 5 cm value obtained experimentally However, the variables have been identified which can lead to producing short focal lengths.

5.6 Negative Microlenses(M-III)

A M III negative microlens can be produced on a Type V full density gel-silica glass or on a commercial pure silica glass by laser irradiation, as shown in chapter 4 The surface depression is formed due to evaporation of the surface during laser heating. No GRIN region is formed beneath the surface since a Type V gel silica glass is already fully densified. The optical ray is incident perpendicularly to the surface of the gel-silica sample and diverges due to the surface depression. However, the optical ray will be 'focused' if observed from a farther distance.

In an experimental analysis of a laser produced M-III negative microlens, a 10x objective lens is also used as a beam expander. The expanded HeNe laser beam is incident perpendicular on the surface of the gel silica substrate with arrays of M-III negative microlenses shown in Figure 5.9(a). Black spots can be observed if the screen is located right behind the gel-silica sample(in Figure 5.2) due to the surface depression. As the screen is moved away from the gel-silica sample(~ 30 cm), arrays of bright spots are observed on the screen, shown in Figure 5.9(b). The bright spots and the outside concentric rings result from the diffraction effect of the lenses. This "focusing ability" of the negative microlens is due to diffraction, not by refraction, which is similar to the phenomenon observed by Maraldi as early as in 1723[Hec74]. It is called a "crude focusing lens" and this 'focal length' is too large to function as a focusing lens. However, this type of negative microlens may be used as a component of a compound microlens for imaging or defocusing.

In a second experiment, images of a lamp source(used for illumination of a microscope) are formed by using arrays of M-III negative microlens. The setup for this observation is illustrated in Figure 5.10(a). The images of the lamp source are shown in Figure 5.10(b). The round and black region(~0.8 mm in diameter) in the picture is the negative microlens due to the surface depression which will diverge the incident lightwave. The observed virtual images are located just above the M-III negative microlens found by changing the focal distance of the microscope.

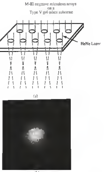

(a)

(b)

Figure 5.9 Focusing phenomenon of M-III negative microlens arrays on a silica substrate. The focusing phenomenon is due to a diffraction effect.

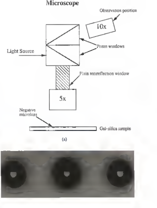

Figure 5.10 Images of a lamp source of a microscope(b) formed by two negative microlenses on a silica substrate observed using a microscope(a)

Thus in conclusion arrays of M-III negative microlens can be used to focus optical rays by a diffraction effect or used as a component of a compound lenses for imaging or defocusing

5.7 Multimode GRIN Channel Waveguide

A multimode waveguide is one of the devices applied in short distance transmission of optical signals at moderate speeds using a LED source[Hec87] Currently, ion-exchange and diffusion techniques are used to fabricate multimode channel waveguides. The disadvantages of the current fabrication methods include

(a)The significant modal dispersion of a step-index multimode fiber(or a waveguide) has virtually eliminated their use in telecommunications systems of any length today[Gra88]

(b)The lithographic technique is restricted to production of rectangular optical waveguides which cause excess transmission loss and coupling loss[Koi88]

The remedy for the loss and dispersion of the step index or rectangular optical waveguide is to fabricate a GRIN waveguide The disadvantages of current methods of forming GRIN waveguide include

(a)There is a strain induced index change in a diffused waveguide caused by the diffusant size

(b)The waveguide made from the ion-exchange process in crystals produce radical differences[Par89]

Multimode channel waveguides can be made by direct laser writing on the partially densified gel-silica glasses. A gel-silica channel waveguide made by laser densification on a gel-silica substrate with density equal to 1 56 g/c.c was previously reported by Slocumb[Slo90] The optical loss of the GRIN gel silica waveguide was reported to be large 5.2 dB in 11 mm along the guiding region However, as discussed earlier, a full density region was not achieved. Consequently, the channel waveguide was still porous and scattered light and therefore was lossy.

Loss mechanisms of the surface planar waveguide which should be considered include

(a)Attenuation caused by surface roughness induced radiation loss, and

(b)In plane scattering caused by refractive index fluctuations from compositional variations and by dimensional fluctuations associated with variations in the depth and/or width of the waveguide[Hal87].

From the discussions in previous section, the fabrication of multimode channel waveguides on a gel-silica substrate by laser densification is feasible. An index change of $\Delta n \sim 0.01$ for a channel waveguide with low loss can be produced using a substrate density of ~2.19 g/c.c. However, the surface of the gel-silica glasses must be maintained at high quality before laser irradiation, i.e. minimal dimensional and density fluctuations must be achieved.

5.8 Conclusions

There are three types of microlenses that can be fabricated on Type VI porous gel silica substrates and Type V full density gel-silica substrates. They are (a)M-I microlenses, a geodesic lens or a combined lens, (b)M-II microlenses, a planar GRIN lens, and (c)M-III microlenses, a negative microlens. These microlenses can be used in the fields of integrated-optics or micro-optics described in section 2.3.5. Advantages of the gel microlenses produced by laser heating are summarized above in section 5.2.

It is demonstrated that a M-I GRIN geodesic lens can be used to focus an optical ray parallel to the surface and the focal length is feasible for use in integrated-optics or acoustic-optics applications. It is also shown that a M-II planar gel silica microlens can be used to focus an optical ray perpendicular to the surface or magnify an image by the GRIN region created by laser densification

Theoretical analysis of the optical properties of the planar GRIN microlenses show that the focal length decreases drastically as the radius(a) of the microlens decreases. The focal length(FL) decreases as Δn or depth(d) of the microlens increases. The minimum focal length can be reduced to 0.25 mm if the radius of the microlens is reduced to 0.05 mm. The calculated FL of 5.14 cm is consistent with the experimental result measured, 5.26 cm. It is also demonstrated that arrays of the M-III negative microlens can be used to defocus an optical ray as a component of a compound microlens.

The above findings indicate the variables to control in order to obtain a low-loss GRIN surface channel waveguide. They are speed of translation of the gel sample in front of the laser beam or vice versa, densification in a dry environment, use of gel samples with density >1.8 g/c.c , high quality surface and laser densification conditions of proper pulse energy. Future work will be directed to establishing the relative importance and limits of these processing variables.

CHAPTER 6
CHARACTERIZATION OF LASER DENSIFIED OPTICS

6.1 Introduction

This chapter is focused on the quantitative analysis of the optical properties of laser densified optical devices produced on a Type VI (porous) or Type V (full density) gel-silica substrates. It is observed that a slight surface depression and a more dense region was formed on a porous gel-silica substrate using laser heating. This region, termed heat affected zone, has a higher density, higher strength, and a higher refractive index with gradient characteristics. The optical ray is deflected within this region due to the refractive index change. Thus, this laser densified region can be used as a focusing component. It is categorized as a M II GRIN planar microlens in Chapter 5 when the surface depression is removed by polishing.

Optical characterization of an M II microlens is shown in this chapter. The characterization measurements include IR reflectance spectra of the surface of the laser densified spot. By using a microscope, the diameter of the investigated region is reduced to 100 μm. A series of IR spectra were obtained across the laser densified spot with a diameter of ~ 1400 μm. The IR spectrum in the middle of the laser densified spot is compared with the spectrum of a Type V full density gel-silica glass. The result shows a similarity between these two spectra.

A series of IR reflectance spectra along the cross section of the laser densified spot at the same depth is also shown. A profile of the peak maximum position along the cross section is obtained.

Refractive index profiles of the laser densified spot at both 0.633 μm and 3.57 μm are obtained. The index profile at 0.633 μm is evaluated from the profile of the peak maximum position using Figure 3.19. The index profile at 3.57 μm is transformed from the reflectivities of the IR reflectance spectra using a Kramers-Kronig transformation discussed in Appendix I. The optical characterization of the GRIN planar microlenses is discussed which includes focal length, coupling efficiency, and the numerical aperture. A profile of the focused spot formed by a GRIN planar microlens is also shown.

In addition, a surface depression was formed on a full density gel silica substrate or a pure silica glass by laser heating. This surface depression is unique in the application of integrated optics because the depth of the depression can be well controlled using laser technology. The surface depression can be used to guide optical rays if coated with a higher refractive index film on a full density silica substrate, such as shown in Figure 2.5 (c). The optical rays are conducted parallel to the surface of the glass substrate.

In micro-optics, the surface depression on a glass surface can be used as a negative microlens for imaging or defocusing, which is termed as a M-III negative microlens discussed in Chapter 5. The optical rays are incident perpendicular to the surface shown in Figure 2.7 (d2). The focal length of the negative microlens with the corresponding laser processing parameters are derived according to the measured diameter and depth of the depression.

6.2 Characterization Methods

6.2.1 Characterization Methods of the M-II Microlenses

A M-II microlens has a more dense region than the porous Type VI gel silica substrate and the surface depression has been removed by polishing. The more dense region can be used to focus an optical ray which is incident perpendicular to the surface, shown in Figure 2.7 (e).

The instrumental arrangement for measuring the focal length of the GRIN planar gel-silica microlens is illustrated in Figure 6.1[Oik82][Shi87]. A HeNe laser is used as an optical source. The laser beam is expanded using a objective lens(10x) to obtain a beam with uniformly distributed intensity. The expanded beam is incident on a diaphragm adjusted to 1 mm in diameter and projected on the hemispherical GRIN microlens. The focal length of the microlens is indicated on the figure. A photo-detector behind the lens is used to determine the position of the focal point at which the highest intensity was detected.

Figure 6.2 illustrates the instrumental setup for the measurement of the coupling efficiency of the microlens[Shi87]. Similarly, an objective lens is used as a beam expander. The diameter of the diaphragm 1 and diaphragm 2 are 1.0 mm and 0.5 mm in diameter, respectively. The detector is located at the focal plane of the microlens. The coupling efficiency is determined as

$$\text{Coupling efficiency} = (\mathbf{I}_1 / \mathbf{I}_0)*100\% \qquad (6.1)$$

$\mathbf{I}_0$ is the incident laser intensity on the microlens. I_1 is the focused intensity by the microlens.

There are two types of numerical aperture(NA), one is the nominal numerical aperture, the other is the measured numerical aperture. Nominal numerical apertures are different if derived from different theories. According to Iga[Iga84], the nominal numerical aperture is

$$\mathrm{NA} = 0.2n_2\sqrt{2\Delta} \qquad (6.2)$$

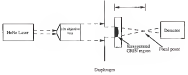

Figure 6.1 Instrumental arrangement for the measurement of the focal length of the GRIN planar gel silica microlens

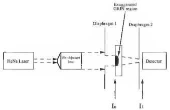

Figure 6.2 Instrumental arrangement for the measurement of the coupling efficiency of the GRIN planar gel silica microlens

Where Δ is equal to $[n_0-n_s]/n_0$, n_0 is the maximum refractive index in the GRIN region n_s is the refractive index of the substrate.

According to Asahara et al [Asa86] the nominal numerical aperture is

$$NA = \sqrt{(n_0-n_s)(n_0+n_s)} \tag{6 3}$$

The measured numerical aperture is equal to[Mis84]

$$NA = a*n_s/f \tag{6 4}$$

where a is the radius of the GRIN lens, f is the focal length of the microlens All these numerical apertures are evaluated and compared in this study

The characterization methods of the IR spectra and the surface depression of the microlenses were discussed in Chapter 3 and Chapter 4, respectively

6.2.2 Characterization Method of the M-III Microlenses

It is demonstrated that a depression is formed on the surface of a Type V gel-silica substrate (or a commercial silica glass) after the laser irradiation shown in Figure 6.3 No enhanced densification was formed under the surface The surface depression is due to the evaporation of the silica induced by laser heating. The sample is a pure silica glass R_1 is the curvature of the surface depression Curvature R_2 is equal to ∞ due to the flatness of the substrate The depth of the depression(d in µm) is obtained by using a Dektak surface profile measuring system. The diameter(D in µm) of the irradiated spot is measured by using a microscope The focal lengths of the negative microlenses(|FL| in mm) are calculated according to the formulae below·

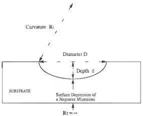

Figure 6 3 Cross section of a negative microlens made by laser heating on the surface of a pure silica glass

$$R1=(d^2+0.25\ D^2)/(2*d) \tag{6.5}$$

$$|FL1|=|R1|/(n-1) \tag{6.6}$$

The focal length is evaluated from the measured diameter and depth of the depression. In this study, the variations of the focal length of the negative microlens with different laser processing parameters are shown

6.3 Characterization Results and Discussion

6.3.1 Surface IR Spectra Analysis

A series of micro-IR spectra across the laser densified spot are obtained using a FTIR spectroscopy equipped with a microscope. Ten areas with diameter of 100 µm along the diameter of the densified spot are investigated shown in Figure 6.4 (a) Each number of the circle indicates the position of the investigated area.

From the periphery to the center of the laser densified spot, five reflectance spectra are illustrated in Figure 6.4 (b) The number (from 1 to 5) of the spectra correspond to the investigated area indicated on Figure 6.4 (a) There are two dominant peaks in the IR specera, the left side is the asymmetric and the right side is the symmetric Si-O-Si streaching vibrational modes. AS_1 and SS indicated on Figure 6.4 (b) represent the asymmetric and symmetric vibrational modes. The peak maximum positions of asymmetric and symmetric modes from spectrum 1 to spectrum 5 are listed in the right corner of the figure The peak maximum position of the asymmetric vibrational mode is shifted to a higher frequency from 1107 to 1122 cm^{-1}, and is intensified (from ~45% to 85%) from spectrum 1 to spectrum 5 The peak maximum position of the symmetric vibrational mode is slightly shifted to a lower frequency and intensified from spectrum 1 to spectrum 5

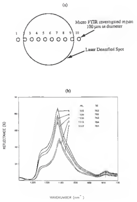

Figure 6.4 Method of obtaining IR reflectance spectra across a laser densified spot using FTIR microspectroscopy(a) and the results(b). The asymmetric and symmetric stretching vibrations of Si-O-Si bonds are indicated.

In section 3 6 3, it is concluded that as the densification temperature increases, there is a shift and an increase in intensity of both the asymmetric and symmetric stretching vibrational modes. The shift in the asymmetric mode to a higher frequency indicates a stronger Si-O-Si bond strength[Dev88][Alm90] An increase in the intensities of the asymmetric and symmetric modes indicates the formation of Si-O-Si through polycondensation as a result of thermal treatment[Dur86] Sanders and Hench et al concluded that infrared reflectances are proportional to the concentrations of the vibrational species causing them[San74] In this study, as the thermal densification proceeded, the silica network consolidated Thus, an increase in the concentration of the vibrational species formation of Si O-Si, intensifies the AS_1 mode

The results shown in Figure 6.4 (b) are in accordance with this conclusion The densification of the laser heated region is gradually enhanced from the periphery to the center, following the intensity distribution of the CO_2 laser beam The peak maximum position of the center area has the highest wavenumber ~ 1122 cm^{-1} and has a lower value of 1107 cm^{-1} at the periphery of the laser densified spot. The gradient densification of the laser densified spot is a result of the gradient temperature distribution induced by laser heating as described in Chapter 7

In Figure 6.5 (b), the reflectance spectrum in the center area of the laser densified spot is compared with the spectrum of a fully densified gel silica glass, shown in Figure 6.5 (a). The peak maximum positions of these two spectra are identical. The asymmetric and symmetric modes of both spectra are located at 1122 and 782 cm^{-1}, respectively That means the structure, i.e average Si-O-Si bond strength and intratetrahedral bond angle, of the center of the laser densified spot is similar to the structure of a Type V full density gel-silica glass or a commercial silica glass

In conclusion, the variations in the IR reflectance spectra on the surface of the laser densified spot indicate a gradually enhanced densification The total shift of the asymmetric vibrational mode is 15 cm^{-1}, the total intensity change is ~40% from the periphery to the

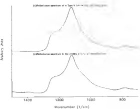

Figure 6 3 Comparisons of the micro-IR spectrum of a Type V full density gel silica glass(a) and the spectrum of the middle of the laser densified spot(b) center of the laser densified spot. Consequently, the periphery of the spot is still porous whereas the center is fully densified and structurally similar to a commercial silica glass. The laser induced heat enhances the densification of the irradiated region which has the same results as furnace heating

6.3.2 IR Spectra Analysis of the Cross Section

A series of micro-IR spectra across the cross section of the laser densified spot at the same depth were obtained The cross section of the gel silica sample was prepared by polishing off half of the laser densified spot shown in Figure 4 13 Thirteen areas with a diameter of 100 µm along the diameter of the densified spot are investigated, as illustrated in Figure 6 6 Each number of the circle indicates the position of the investigated area. The depth of the laser densified region is ~140 µm, as discussed in Chapter 4

From the periphery to the center of the laser densified spot, four reflectance spectra are illustrated in Figure 6.7 The number (from 1 to 7) of the spectra correspond to the number indicated on Figure 6.6. The two dominant peaks in the IR spectra are the asymmetric and symmetric Si-O-Si stretching vibration modes, respectively The peak maximum positions of the asymmetric modes are indicated from spectrum 1 (1103 cm^{-1}) to spectrum 7 (1118 cm^{-1}) The peak maximum positions of the symmetric modes are shown from spectrum 1 (787 cm^{-1}) to spectrum 7 (783 cm^{-1}) The profile of the peak maximum position along the cross section of the densified spot is shown in Figure 6.8.

From the periphery to the center of the laser densified spot, the peak maximum position of the asymmetric vibrational mode is shifted to a higher frequency, as shown in Figure 6 7 and Figure 6 8 The peak maximum position of the symmetric vibration mode is slightly shifted to a lower frequency The mechanisms of the shifting were discussed in the previous section Thus the densification on the cross section of the laser heated region also shows a gradient densification from the periphery to the center of the spot.

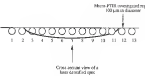

Figure 6.6 Method of obtaining IR reflectance spectra across the cross section of a laser densified spot at the same depth using FTIR microspectroscopy.

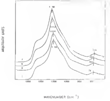

Figure 6.7 Results of the micro-IR spectra along the cross section of the laser densified spot, the peak maximum positions of the asymmetric(left) and symmetric(right) stretching vibration modes are indicated

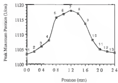

Figure 6.8 The profile of the peak maximum position on the cross section of the laser densified spot at the same depth, corresponding numbers of the investigated area are indicated.

However the peak maximum position in the middle of the laser densified spot has the highest value of 1118 cm^{-1} rather than 1122 cm^{-1} because the diameter of the investigated region is larger than the diameter of the fully densified region on the cross section The diameter of the fully densified region along the cross section is estimated to be ~10 µm from the study of the VHN profile of the cross section in section 4 3 3 Therefore, the highest peak maximum position in the IR spectra does not show as 1122cm $^{-1}$ but instead is an average of 1118 cm^{-1}.

In conclusion the densification of the cross section of the laser densified spot is gradually enhanced from the periphery to the center The total shift of the asymmetric stretching vibration mode is equal to15 cm^{-1}

6.3.3 Index Profiles

A refractive index profile of the laser densified spot at 0 633 µm is obtained using Figure 3 19 Figure 3 19 illustrates the relationships of the peak maximum position refractive index and the corresponding bulk density of the gel-silica glasses densified at different temperatures The refractive index at each position across the laser densified spot is evaluated from the peak maximum positions (shown in Figure 4 12) using Figure 3.19

The resulting surface index profile of a laser densified microlens is shown in Figure 6 9 The maximum refractive index is ~1 46 and is decreased gradually to the periphery of the laser densified spot. The maximum refractive index in the center of the spot is equal to the refractive index of a Type V gel-silica glass The refractive index of the substrate is evaluated to be ~1 37 The index change of the laser densified spot at 0 633 µm is ~ 0 09 The gradient index profile ascertains the GRIN characteristics of the laser densified spot

The index profile is obtained from the reflectivities at 3 57 µm in the IR spectra using a Kramers-Kronig transformation discussed in section 3 6.5 The refractive index at 3 57 µm at each position(from 1 to 10 shown in Figure 6.4 (a)) of the laser densified spot

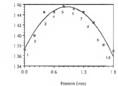

Figure 6 9 The refractive index profile on the surface of the laser densified spot at 0 633 µm, corresponding numbers of the investigated area are indicated.

is transformed from the corresponding reflectivity. The resulting index profile is illustrated in Figure 6.10. The maximum refractive index is ~ 1.69 and is decreased gradually to the periphery of the laser densified spot. The refractive index of the substrate is estimated to be ~ 1.61. Thus, the index change of the laser densified spot at 3.57 µm is ~ 0.08.

Both the index profile(at 0.633 µm and 3.57 µm) shows a gradient index change and is parabolic in shape. Figure 3.19 proved to be useful in evaluating the refractive index at 0.633 µm from a known peak maximum position of the asymmetric Si-O-Si bond stretching vibration in the IR spectrum. The IR spectrum of the laser densified spot can be obtained faster and accurately. The estimated index change induced by CO_2 laser heating at 0.633 µm and at 3.57 µm are 0.09 and 0.08, respectively.

The resulting index change and the change in the peak maximum position of the laser heated region are consistent with the characteristics of the porous gel-silica glass during furnace densification discussed in Chapter 3. Figure 6.11 shows that the mechanical property and the optical properties of the gel silica glasses vary with the bulk densities summarized from Chapter 3. The VHN, refractive index, and the peak maximum positions of the gel silica glasses increase as the bulk density increases during furnace densification. Therefore, the resulting property change of the gel-silica glass induced by laser heating or by furnace heating appear to be the same. Upon heating, the bulk density, mechanical strength and the refractive index of the gel-silica glass increase. The only difference is that the dimension of the heat affected region by using a CO_2 laser is very much smaller.

6.3.4 Optical Properties of M-II Microlenses

The feature of the M-II microlens is the GRIN region under the surface after polishing off the surface depression induced by laser heating. The net shape of the GRIN planar microlens is hemispherical. The GRIN region has a higher refractive index than the

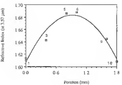

Figure 6.10 The refractive index profile on the surface of the laser densified spot at 3.57 μm, corresponding numbers of the investigated area are indicated.

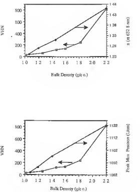

Figure 6 11 Properties of the gel silica glasses with increasing bulk density the substrate discussed in the previous section and can be used to focus an optical ray. The theory of the focusing ability of the GRIN lens is discussed in section 2.3.3.

Optical properties of M-II GRIN planar microlenses are characterized by the focal length, coupling efficiency, and the numerical aperture. The methods of characterization are mentioned in section 6.2. The results of the optical properties of the microlens are shown in Table 6.1.

The measured range of the focal length of the laser densified planar microlenses is 4.32 to 12.70 cm. This focal length is a little large for micro-optics application. The depth of the GRIN region is limited by the extremely low thermal conductivity of the pure silica glass substrate. However, the focal length can be reduced by stacking two planar microlens (shown in Figure 2.10) to increase the depth of the GRIN region[Iga84]. From Figure 5.8, if the depth of the GRIN region is increased from 100 µm to 200 µm the focal length of the microlens can be reduced from 3.00 to 1.52 cm. The measured focal length by stacking two gel-silica planar microlens is 2.49 cm.

The measured range of the coupling efficiency is from 85% to 95%. The coupling efficiency is excellent due to the high transmittance of the gel-silica glasses. The variations of the coupling efficiency from lens to lens depends on the depth of the GRIN region which is affected by the input laser power.

The nominal numerical aperture of the planar microlens depends on the definition used. The measured numerical aperture is obtained according to Misawa et al[Mis84]. The results are shown in Table 6.1. The numerical aperture can be also enlarged by stacking two planar microlens to increase the index change, the depth of the GRIN region or the resulting focal length[Iga84]. The nominal numerical aperture can be increased by increasing the index change as shown in Figure 6.12[Iga84]. The nominal numerical aperture is increased from 0.05 to 0.11 if the index change is increased from 0.02 to 0.10. The measured numerical aperture is increased from 0.02 to 0.03 if the focal length is reduced from 4.32 to 2.49 cm.

Table 6 1 Optical properties of the GRIN planar gel-silica microlenses.

Characterizations	Results	References of method
Focal Length	1 70" 5.00"	[Oik82] [Shi87]
Coupling Efficiency	85% 95%	[Shi87]
Numerical Aperture	~0.096	[Iga84]
	0.006-0 02	[Mis84]
	~0 50	[Asa86]

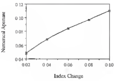

Figure 6 12 The effect of the index change on the nominal numerical aperture.

Optical properties of the M-II microlenses are demonstrated. The focal length is a little large due to the extremely low thermal conductivity of the pure silica substrate. The focal length can be reduced by increasing the index change or the depth of the GRIN region. The coupling efficiency is excellent due to the high transmittance of the gel-silica glass at 0.633 μm. The numerical aperture can also be enlarged by increasing the index change or the depth of the GRIN region.

6.3.5 Profile of the Focused Spot

The profile of the focused spot formed by a GRIN planar gel-silica microlenses is measured using the setup shown in Figure 6.2. Instead of using diaphragm 2, a slit(with width 50 μm) is attached in front of the detector. The profile of the focused spot is obtained by recording the intensity across the focused spot as shown in Figure 6.13. The half width of the intensity profile of the focused spot is estimated to be – 100 μm.

The resulting half width of the focused spot is large due to an insufficient index change or depth of the GRIN region. The depth of the GRIN region is limited by the extremely low thermal conductivity of the pure silica glass and the laser densified spot is made at one shot of the laser pulse in this study. In the future, the depth of the GRIN region may be increased by increase the frequency of the input laser pulse. The resulting depth could be increased due to a larger penetration depth of the laser-induced heat.

6.3.6 Characterization of M-III Microlenses

In this study, surface depressions are formed on a pure silica plate by laser heating at various laser processing conditions. Table 6.2 shows the results of laser densification for fabricating negative microlenses. The variables of the laser densification conditions are laser power (in watts) and L2 (shown in Figure 4.2). Other parameters like pulse width

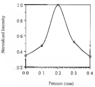

Figure 6.13 The intensity profile of the focused spot formed by a GRIN planar gel silica microlens

Table 6.2 Optical property of the negative microlens at various processing parameters.

Power (mA)	L2(inches)	Depth d(μm)	Diameter D (μm)	|R1|	|Focal Length|(mm)
14	2.88	2.0	480	14.40	32.00
14	3.00	1.0	400	20.00	44.45
15	2.88	56.0	760	1.36	3.06
15	3.00	34.0	700	1.82	4.04
15	3.13	16.0	540	2.26	5.08
15	3.28	5.8	530	8.39	14.19
15	3.38	1.5	480	17.63	39.16
15	3.50	1.0	420	22.05	49.00
16	2.88	77.0	870	1.27	2.62
16	3.00	88.0	840	1.37	3.04
16	3.13	49.0	800	1.88	3.68
16	3.25	26.0	720	2.25	5.00
16	3.38	20.5	640	2.51	5.57
16	3.50	7.0	600	6.43	14.29
16	3.63	1.0	440	24.20	53.78

(~1.5 seconds), humidity (~25%), surrounding temperature (~ 26°C) are used during the laser treatment. The row number represents the sequence of the laser irradiated spots. The columns show the resulting experimental data and the calculated focal length of the negative microlens.

The diameter of laser irradiated spots range from 0.40 mm to 0.92 mm (±0.02mm). The range of the surface depressions are from ~1mm to 110 mm. The calculated focal length of the negative microlenses is around few millimeters as the depth of the depression is above 40 μm. This short focal length is usable in the applications of micro-optics or acousto-optics.

It is found that as L2 increases, both the diameter and the depression of the irradiated region decreases. A higher incident laser power results in a shorter focal length of the negative microlens. The shortest focal length of the fabricated negative microlens is ~ 3 mm due to the large curvature of the surface depression. The size of the depression can be modulated by using different laser powers and the distance L2.

6.4 Conclusions

The variations in the IR reflectance spectra across the surface of the laser densified spot indicate a gradually enhanced densification. The periphery of the spot is still porous whereas the center is fully densified. The densification of the cross section of the laser densified spot at the same depth is also gradually enhanced from the periphery to the center.

The index profiles of the laser densified planar microlens at 0.633 μm and 3.57 μm show a gradient index change. The estimated index changes induced by CO_2 laser heating at 0.633 μm and at 3.57 μm are 0.09 and 0.08, respectively.

The focal length of M II planar microlens is a little large due to the extremely low thermal conductivity of the pure silica substrate. The focal length can be reduced by increasing the index change or the depth of the GRIN region. The coupling efficiency is excellent due to the high transmittance of the gel-silica glass at 0 633 μm. The numerical aperture can also be enlarged by increasing the index change or the depth of the GRIN region The resulting half width of the focused spot is large which is also due to the insufficient index change and depth of the GRIN region

The shortest focal length of the laser irradiated negative microlens is ~ 3 mm due to the large curvature of the surface depression. The size of the depression can be modulated by using different laser power and varying the distance L2.

CHAPTER 7
LASER DENSIFICATION MODELINGS

7.1 Thermal Model of a Laser Densified Track

7.1.1 Abstract

A three dimensional transient model for heat conduction in silica glass is developed. The model simulates a three-dimensional temperature distribution in a silica glass irradiated by a moving CO_2 laser. Both the reflectivity of the glass surface and the strong attenuation of the laser energy in the glass medium are accounted for by a detailed radiation analysis. The energy absorbed by the glass is determined to be confined in a 10 μm thickness; the laser irradiation is thus treated as a boundary condition. The heat diffusion equation is solved by using an alternating-direction implicit method.

7.1.2 Introduction

Many models have been developed for predicting the temperature distribution inside materials treated with laser heating[Cal82][Cha84][Rap87]. In this study, the temperature rise in the material is analyzed. The results are useful to determine the effect of applying a CO_2 laser on a porous gel-silica glass monolith. Previous studies report the processing and properties of the alkoxide derived gel silica investigated in this study[Pw86][Hen86][Hen88]

The laser energy is assumed to be absorbed and totally transformed into heat. Based on the high absorption coefficient[Hsi79] of the glass, the laser energy is determined to be absorbed primarily within a very thin layer (~10 μm) of the glass surface. The

Gaussian distribution of this energy is integrated within the absorption layer, and the absorbed energy is treated as a boundary condition in the analysis.

The model developed in this study simulates the three dimensional heat transfer in the silica glass irradiated by a moving CO_2 laser. Relative temperature distributions at various laser power settings and travelling velocities are evaluated numerically. Parametric studies for the effects of the heat transfer coefficient on the glass surface and the thermal physical properties of the glass medium are also investigated. It is well known that the properties of gel-silica glasses are strongly related to their processing temperature. The results presented in this study can thus be used to evaluate the property changes due to the temperature rise in the gel-silica glass.

7.1.3 Formulation of the Physical Model

The physical system under investigation is shown in Figure 7.1. A focused CO_2 laser beam is travelling in the x direction. The thickness of the glass substrate is in the z direction, and because of the motion of the beam, the temperature distribution in glass is symmetrical with respect to the x-z plane; only one half of the medium is needed for analysis.

The thermal conductivity of the glass is extremely low that the heat affected zone is highly localized and represented by the shaded lines in the figure. The irradiated energy is transformed into heat and diffused into the glass medium by conduction while the surface of the glass dissipates heat by convection and radiation to the surroundings[Bat82]

The thermal effect of the laser irradiation can be evaluated by a detailed radiation analysis. Accounting for the reflectivity of the glass surface as well as the absorption of the glass medium, the heat generated by the laser can be derived as

$$Q = \int I_0 * (1-R) * \exp(-2r^2/w^2) * [1-\exp(-\alpha\Delta z)]\ 2\pi r dr \qquad (7.1)$$

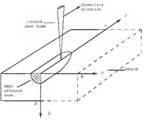

Figure 7 1 Physical system of laser densification under investigation

Here all notations have been defined in Table 7.1. For the CO_2 laser (at wavelength of 10.6 μm) used in this work, the generated heat is determined to be confined to a depth of 10 μm measured from the glass surface, where the laser energy is attenuated to 0.15% of its surface value. This depth is small to the extent that the laser heating can be treated as a boundary condition. On the back side of the glass($z=d$), an adiabatic condition prevails because of the low thermal conductivity of glass. The problem can then be formulated mathematically as follows[Ozi80]

$$\rho c(\partial T/\partial t) = \nabla\cdot(k\nabla T),\ T(x,y,z,t),\quad \begin{array}{l} 0<x<a \\ -b<y<b,\ t>0 \\ 0<z<d \end{array} \tag{7.2}$$

Initial Condition

$$T(x,y,z,0) = T_\infty \tag{7.3}$$

Boundary Conditions

$$k\partial T(0,y,z,t)/\partial x = h[T(0,y,z,t)-T_\infty] \tag{7.4}$$

$$T(a,y,z,t) = T_\infty \tag{7.5}$$

$$T(x,\pm b,z,t) = T_\infty \tag{7.6}$$

$$q(vt,y,0,t)+k[\partial T(vt,y,0,t)/\partial z] - h[T(vt,y,0,t)-T_\infty] = 0 \tag{7.7}$$

Table 7.1 Calculational variables and values.

	Nomenclature	Values
a	Sample length	0.4 cm
b	Sample width	0.2 cm
c	Specific heat[Tou70a]	10.5 J/g°C
d	Sample thickness	0.3 cm
D	Heat Diffusivity	6.5×10^{-4}(=k/ρc) cm^2/sec
h	Heat transfer coefficient	7.1×10^{-3} W/cm^2°C
I_0	Laser intensity	3.3×10^{4} W/cm^2
k	Thermal Conductivity[Tou70b]	1.5×10^{-2} W/cm°C
q	Heat flux	
Q	Absorbed laser power density	10^7(=q/Δz) W/cm^3
$\underline{Q}$	Absorbed laser power	
R	Reflectivity	0.17
T	Temperature	
T_∞	Room temperature	24°C
t	Time	
Δt	Time step	0.01 second
v	Travelling Velocity	0.04 cm/sec
w	Half width of laser beam	0.01 cm
Δz	Depth	
α	Absorption Coefficient	6.5×10^{-1} 1/μm
ρ	Density	2.2 g/cm^3

$$\partial T(x,y,d,t)/\partial z = 0 \qquad (7\ 8)$$

The problem as given can only be solved exactly for a special case in which the laser beam has travelled a long distance to the extent a quasi-steady state is reached. At that time the glass temperature is invariant with time in a coordinate system that is travelling along with the beam. For the general case of a short time or a small sample size in a fixed coordinate system, the temperature is time dependent, and the problem must be solved numerically[Ros46]

For the present work, a finite-difference, alternating-direction implicit (ADI) method is used to solve the problem[Ozi80]. The intense heat from the laser beam requires the use of a very thin surface layer together with short time steps in order to assure a convergent solution The criterion for stable solution is found to be $D\Delta t/(\Delta z)^2<0\ 5$, which governs the selection of time steps and spatial increments in the numerical solution. An IBM Converted Monitor System (CMS) was used for the computation

7.1.4 Results and Discussion

Values of the parameters used in the computation are summarized in Table I. Of those listed in the table, the values of D, H, Q, and v are also changed in order to examine their effects on the temperature changes. For graphical presentation of results, composite diagrams (see Figure 7 2 through Figure 7 5) are constructed so that the temperature profiles in both x and |y| directions can be viewed simultaneously All temperatures are plotted for the distributions at the surface (z=0), and they are normalized by using the peak values evaluated at the beam center in all instances those evaluated with the tabulated parameters are used for control It is noted that in each of these plots, the laser beam has moved to x equal to 0 32 cm and the temperature profiles in the y direction are those of T evaluated at this x position.

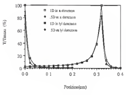

Figure 7 2 Relative temperature profiles at different heat diffusivities.

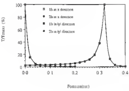

Figure 7.3 Relative temperature profiles at different heat transfer coefficients.

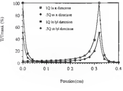

Figure 7 4 Relative temperature profiles at different laser power settings

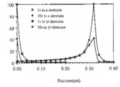

Figure 7 5 Relative temperature profiles at different travelling velocities

As shown in Figure 7 2, a reduction of the thermal diffusivity by one half has a minor effect of lowering the peak temperatures. For the temperature distributions in the x direction, the temperature gradients at the leading sides(x>0 32 cm) are always greater than those at the trailing sides(x<0.32 cm), a typical phenomenon for the problem investigated. In fact, the trailing side temperatures are practically unchanged with the diffusivity changes Physically, the temperature decreases at low thermal diffusivities can be attributed by the large heat capacitance, which permits more heat to be stored in the glass medium

Doubling the heat transfer coefficient (h) has a negligible effect in changing the surface temperature; see Figure 7 3 The h value quoted in the table accounts for both free convection and radiation Notice that, while the peak surface temperature at the beam center is high, the area over which this temperature is found to be small. As a result, the heat transfer coefficient has negligible effect on the surface temperature.

We expect that a reduction of laser power and an increase of the laser velocity would lower the peak temperatures found on the surfaces; see Figure 7 4 and Figure 7.5 The major difference between Figure 7 4 and Figure 7 5 , however, is in the trailing sides A reduction of the power is shown to have a dominant effect in lowering the trailing side temperatures

The temperature attenuation in the z direction are shown in Figure 7 6 and 7 7 In these figures, the values of the parameters are listed in Table 7 1 Those peak temperatures at z=0 correspond to peak curves presented earlier in the composite plots in Figure 7.2 through 7.5.

To complete this study, a numerical experiment was performed to test the convergence of the numerical solution The time steps were successively reduced by half and the peak temperatures are compared for convergence As shown in Figure 7 8 the temperatures converged to within 0 4% for time steps changing from 0.002 to 0 001 second. The results presented in this paper were obtained by using a time step of 0 002 second, a compromise between accuracy and economy

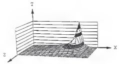

Figure 7 6 Three-dimensional temperature distribution on X-Z plane

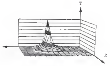

Figure 7 7 Three dimensional temperature distribution on Y Z plane

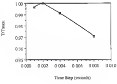

Figure 7.8 Convergence of the solution of equation (7.2).

7.1.5 Conclusions

Parametric effects on the calculated temperature distribution in the silica glass are investigated. The results show that the laser irradiated area is highly localized for an assumed condition. The accuracy of the method depends mainly on the number of elements used, and the computing time available[Gar88]. The results presented in this study are useful to correlate the laser treatment with the property changes in the irradiated area of the gel-silica glass.

7.2 Thermal Model of a Laser Densified Spot

7.2.1 Introduction

A three-dimensional transient model for the temperature distribution of a laser heated region is developed. This model is used to simulate a three-dimensional temperature distribution produced by the localized laser heating on a pure porous silica glass. In a previous study[Chi90], the laser energy absorbed by the glass is determined to be confined to a ~10 μm thickness. The laser intensity in the silica glass attenuates rapidly to 0.15% of its initial value at the depth of 10 μm. The absorbed energy is assumed to be totally transformed into heat. The generated heat within the thin layer, approximately 10 μm, is subsequently conducted into the glass substrate and results in a gradient temperature distribution. The heat loss on the glass surface is also considered in the simulation[Chi90]. The heat transfer equation is solved by using an alternating-direction implicit method. The strengths of this method are also discussed.

The importance of the thermal modeling is to predict the three-dimensional temperature distribution within a limited region. It is technically difficult to measure the temperature distribution in the heated region of 1 mm in diameter and 0.1 mm in depth. In order to determine a temperature distribution experimentally, arrays of thermocouples would be needed for instrumentation within that small region inside the glass substrate to record the temperature distribution. In this study, a thousand temperature data points in the irradiated region of a volume of 2x2x2 mm^3 are computed.

The other motivation of developing this thermal model is that the properties of the gel silica glass are strongly affected by the processing temperature, as discussed in Chapter 3. As the processing temperature increases, the bulk density and the refractive index of the porous gel silica glass increase till the gel-silica glass is fully densified(bulk density = 2.2 g/c.c.). In this effort, a CO_2 laser serves as a heat source to enhance the densification locally on the porous gel-silica glass. And the resulting property variations of the laser irradiated region on the partially densified gel-silica glass is controlled by the temperature distribution. Thus, the results of this thermal model can be used to predict or compare with the property distributions of the laser-irradiated region on the gel-silica substrate.

In this study, there is no relative motion of the glass sample and the CO_2 laser source. A round-shape spot on the glass surface is observed after the laser heating. The heating rate and the cooling rate of the laser heating are analyzed. Three-dimensional temperature distributions of the laser irradiated region are obtained numerically.

The property variations of the laser densified spots were characterized by using a FTIR reflectance microspectroscopy and a microhardness tester discussed in Chapters 4 and 6. Profiles of the Vickers hardness number and the peak maximum position(PMP) of the laser irradiated spot are obtained. Comparisons of the property profiles with the calculated three-dimensional temperature distributions of the laser irradiated region are also shown.

7.2.2 Computation Method

There are three approaches to solve a problem of heat transfer using (1) experimental (2) theoretical and (3) numerical methods[And84]. If the investigated region is too small, it is difficult to use the experimental method. The theoretical method is usually restricted to a simple geometry, idealized conditions and linear problems. There are many advantages of using the numerical method which include

(a)it is not restricted to linearity,

(b)it can be applied to complicated geometry, and

(c)the time evolution of heat transfer can be obtained.

A fictitious ordinary differential equation solved by using the numerical method is used as an example to show the relationship between the spatial step(Δx or Δy or Δz) for the calculations and the resulting solutions. Figure 7.9 illustrates the exact solutions($\Phi(x)$) and the numerical solutions(Φ_i, $i=1$ to n) of a fictitious ordinary differential equation(i.e.heat transfer) discussed by Shih[Shi84]. $\Phi(x)$ represents the exact solutions, Φ_1 to Φ_n give the finite difference solutions. It is found that as Δx(spatial step) decreases, the finite difference solutions are closer to the exact solutions. And the accuracy of the solution can be increased by reducing the spatial step, however at an increasing computing cost and time. In this study, Δx is selected as 0.20 mm, a compromise between the accuracy and the computing cost.

The alternating-direction implicit method(ADI) used in this study was developed by Peaceman and Rachford in 1955 and Douglas and Rachford in 1956[And84]. The ADI method is one of the finite-difference numerical methods where the allowed spatial step is unrestricted to ensure numerical stability[Shi84]. Some assumptions are made and a high-speed digital computer is used to solve the governing heat transfer equation[And84].

The heat governing equation (7.2) is discretized using the ADI method according to Figure 7.10.

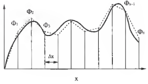

Fig 7.9 A fictitious exact solution and an approximate solution from a finite-difference method, after [Shi84]

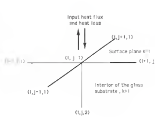

Figure 7.10 A mesh structure of the glass substrate designed for the computations of the three-dimension temperature distribution by laser irradiation each point in the mesh represents a data point.

$$\rho c\frac{\Delta T}{\Delta t}(\Delta x\Delta y\Delta z)=k\frac{\Delta T}{\Delta x_{i+0.5}}\Big|_{i+0.5}(\Delta y\Delta z)\ k\frac{\Delta T}{\Delta x_{i-0.5}}\Big|_{i-0.5}(\Delta y\Delta z)+$$

$$k\frac{\Delta T}{\Delta y_{j+0.5}}\Big|_{j+0.5}(\Delta x\Delta z)\ k\frac{\Delta T}{\Delta y_{j-0.5}}\Big|_{j-0.5}(\Delta x\Delta z)+$$

$$k\frac{\Delta T}{\Delta z_{k+0.5}}\Big|_{k+0.5}(\Delta x\Delta y)-k\frac{\Delta T}{\Delta x_{k+0.5}}\Big|_{k+0.5}(\Delta x\Delta y)+$$

$$q\Delta x\Delta y\Delta z-h(T_{i,j,1}\ T_{\infty})(\Delta x\Delta y) \qquad (7\ 9)$$

where

$$\Delta x=\frac{\Delta x_{i+1}-\Delta x_{i\ 1}}{2}$$
$$\Delta y=\frac{\Delta y_{j+1}\ \Delta y_{j\ 1}}{2}$$
$$\Delta z=\frac{\Delta z_{k+1}\ \Delta z_{k\ 1}}{2}$$

$$\Delta x_{i+0.5}=\Delta x_{i+1}\ \Delta x_i$$

$$\Delta x_{i-0.5}=\Delta x_i\ \Delta x_{i\ 1}$$

$$\Delta y_{j+0.5}=\Delta y_{j+1}\ \Delta y_j$$

$$\Delta y_{j-0.5}=\Delta y_j\ \Delta y_{j\ 1}$$

$$\Delta z_{k+0.5}=2\Delta z=z_2\ z_1$$

(i, j, k), where i, j, k=1 through n. Parameters h, k, q, t and T are given in Table 7 2 This discretized equation is then programmed by using FORTRAN written by Qin and listed in Appendix II. The temperatures are computed by using a IBM Converted Monitor System(CMS)

A convergence check is needed as the thermal model is solved using the ADI method. In Figure 7 11, it is shown that the maximum temperature obtained from the

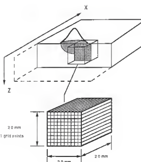

Figure 7.11 A three-dimensional temperature profile produced by laser irradiation on the surface of a silica glass with more than 1000 data points per volume

simulations increases and levels off when the time step Δt is decreased from 0.05 to 0.001 seconds. Thus, the convergence of the solution is verified. A time step of 0.01 second is used for the temperature simulation in this study which is also a compromise between the accuracy and economy.

7.2.3 Computation Results

Figure 7.12 shows the physical system for the laser densification. A focused CO_2 laser beam is incident on a partially densified gel-silica glass. The shaded region represents the heat affected zone produced by laser irradiation. a(length), b(width), and d(depth) are the dimensions of the sample. In Figure 7.13, a three-dimensional cubic mesh is used to frame the temperature distribution in the heat affected zone. More than 1000 grid points in the heat affected zone are investigated within a volume of 2x2x2 mm^3. (i, j, k) in Figure 10 represents the positions of the grid points in the cubic mesh.

The temperature profiles investigated in this study are illustrated in Figure 7.14. One is the surface temperature distribution of the laser irradiated region on the X-Y plane; see (a) in Figure 7.14. The other is the temperature profile of the cross section of the heat affected zone on the X-Z plane; see (b) in Figure 7.14. In addition, the heating rate and cooling rate can also be obtained from this transient thermal model.

The physical parameters of the gel-silica glass are assumed to be close to that of a commercial silica glass because the bulk density of the gel-silica substrate used for the laser densification is larger than 1.90 g/c.c., which is larger than 85% of full density of fused silica(2.2 g/c.c.). The other parameters used in the computations are listed in Table 7.2.

The operating conditions(laser power, pulse width and the laser beam width) of laser densification are used to simulate the temperature distributions. The diameter(=2w) of the laser beam used in the computation is 1.0 mm which is determined by measuring the diameter of the laser irradiated spot on an alumina plate. From Figure 4.3, if the laser pulse

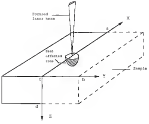

Figure 7.12 Physical system of laser densification under investigation.

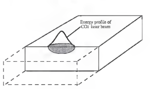

(a) Top view of the heat affected zone

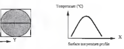

(b) Cross section view of the heat affected zone

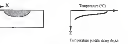

Figure 7 13 Schematic of the heat affected zone and the temperature profiles on the surface(a) and the cross section(b) of a laser irradiated spot.

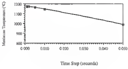

Figure 7.14 A relationship between the calculated maximum temperature and the time step.

Table 7.2 Calculated variables, sample specifications, and property values.

	Nomenclature	Values
a	Sample length	0.4 cm
b	Sample width	0.2 cm
c	Specific heat	10.5 J/g°C
d	Sample thickness	0.3 cm
D	Heat Diffusivity	6.5×10^{-4}(=k/ρc) cm^2/sec
h	Heat transfer coefficient	7.1×10^{-3} W/cm^2°C
k	Thermal Conductivity	1.5×10^{-2} W/cm°C
Q	Absorbed laser power density	7.3×10^{5}(=q/Δz) W/cm^3
q	Heat flux	
R	Reflectivity	0.17
T	Temperature	
T_∞	Room temperature	24°C
t	Time	
Δt	Time step	0.01 second
v	Traveling Velocity	0 cm/sec
w	Half width of laser beam	0.05 cm
Δz	Depth	
α	Absorption Coefficient	6.5×10^{-4} 1/μm
ρ	Density	2.2 g/cm^3

is equal to 1.5 seconds and the power setting is 16 mA, the input laser energy is 20 watts. The input laser power density Q used in the computations is estimated to be 7.30×10^5 W/cm^3 when the input laser power is set at 20 watts. The absorbed 20 watts is confined in a hemisphere of ~ 0.10 cm in diameter and 10 μm in depth. Thus, the energy is dissipated in a volume of approximately 2.73×10^{-5} cm^3 resulting in a calculated power density of 7.30×10^5 W/cm^3

The surface temperature profiles on the X-Y plane at different time steps are shown in Figure 7.15. This figure compares the resulting profiles if the time step is changed. The temperature profile elevates as the time step Δt decreases. It is found that there is little difference between the temperature profiles with time steps equal to either 0.01 or 0.001 seconds. In addition, Figure 7.16 shows the comparison of the temperature profiles on the X-Z plane(cross section) at different time steps. There is little difference between the temperature profiles with time steps equal to either 0.01 or 0.001 seconds. Consequently it is acceptable to use 0.01 second to be the time step for the computations.

Figure 7.17, a three-dimensional diagram, shows the temperature profile on the surface(on the X-Y plane in Figure 7.12) of the laser irradiated region. The T-axis represents the calculated temperature. X and Y axes give the position of the laser irradiated region, the maximum length is 2 mm in Y and 1.8 mm in X direction. The center of the profile shows the highest temperature which follows the laser beam profile is of a Gaussian distribution. The temperature rises to a maximum of about 1150°C in the middle of the laser irradiated region, a value equivalent to the temperature needed to fully densify the gel silica glass by furnace heating, as discussed in Chapter 3. The diameter of the heat affected zone(from 1150°C to 24°C) evaluated from Figure 7.17 on the surface is 2.0 mm.

Figure 7.18 shows a 'contour map' of the temperature distribution in Figure 7.17. The temperature values for each pattern are provided by the key on the right margin. The heat affected zone with temperature greater than 600°C seems to be confined to 1 mm in diameter. Since the cross section of the incident laser beam is 1 mm in diameter, the

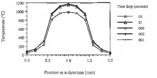

Figure 7 15 Surface temperature profiles on the X Y plane at different time steps.

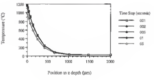

Figure 7 16 Temperature profiles on the cross section of a laser irradiated region at different time steps.

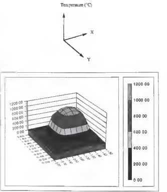

Figure 7.17 A three-dimensional diagram shows the temperature profile on the surface of a laser densified spot, dimensions and temperature range are also indicated

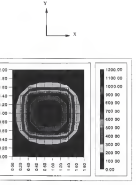

Figure 7.18 A contour map of the temperature profile on the surface of a laser densified spot. Dimensions and temperature range are also indicated.

induced temperature in the heat affected zone(with diameters >1 mm and < 2 mm) should be a result of heat transfer The temperature contour can be made smooth if the spatial step is reduced However, the cost of the computation will be too high.

Figure 7.19 illustrates a three-dimensional temperature distribution on the X Z plane Again, the absorbed energy in the middle of the laser irradiated region reaches a maximum and it decreases as the depth increases Clearly in Figure 7 19 the depth of the heat affected zone(from 1150°C to 24°C) is ~ 1.0 mm. Figure 7.20 illustrates a contour map of the temperature distribution in Figure 7 19 Again the right margin provides the key to the temperature distribution. The dimension of the depth is not equally divided in the calculations in order to get a detailed temperature information within a thin layer(five data points within a depth of 200 µm). The temperature distributions along the depth will be discussed in Figures 7.24 and 7.25

Heating rate and cooling rate of the glass substrate by laser irradiation can also be obtained from the simulation The laser heating time(=laser exposure time) is 1 5 seconds. After that the irradiated region cools due to heat transfer by radiation, convection and conduction. The temperature change is composed in the middle of the surface laser irradiated region, the heating and cooling curve at the investigated point are shown in Figure 7 21 At the end of the heating time the temperature reaches a maximum of about 1150°C and it drops as soon as the heat source is removed. Clearly the heating and cooling rates are nonlinear The heating rate from 0 to 0 25 second is calculated to be ~2200°C/sec(=550°C/0.25 sec) which is quite high From 0 25 to 1.5 seconds the heating rate drops to ~460°C/sec(=575°C/1 25 sec). The cooling rate is calculated to be ~1200 °C/sec(=(1150-550)°C/0.5 sec) during the first half second(1.5-2 0 second) after removal of the heating source The cooling rate for the remainder of the cooling curve is reduced to ~300°C/sec(=(550-250)°C/1 sec) As expected, the heating rate and cooling rate are high during the initial heating and cooling periods. The lower heating rate during 0.25 1.50 seconds minimizes the crack or foaming of the laser irradiated region

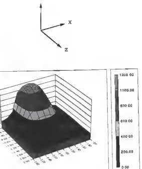

Figure 7 19 A three dimensional diagram shows the temperature profile on the cross section of a laser densified spot Dimensions and temperature range are also indicated

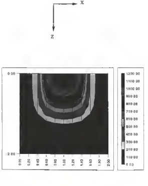

Figure 7.20 A contour map of the temperature profile on the cross section of a laser densified spot, dimensions and temperature range are also indicated.

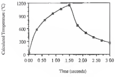

Figure 7.21 The calculated heating and the cooling curves by laser irradiation on a pure silica glass

The changes of the surface temperature profiles during heating and cooling period are shown in Figure 7.22 and Figure 7.23, respectively. The time steps are taken to be 0.5 second. In Figure 7.22, the temperature increases rapidly upon inception of laser heating as shown by the large distance between the temperature profiles. During cooling, as shown in Figure 7.23, the cooling rate is high in the first 0.5 second of the cooling. The wings of the temperature profile at 1.5 second are raised to be higher than those of the initial at 0 second, a result of the heat conduction in the glass substrate during cooling.

Figure 7.24 and Figure 7.25 give the temperature history in the center of the irradiated region at different depths. Time steps are taken to be 0.5 second for each temperature plot. The same conditions occur in the temperature profiles of the cross section during heating and cooling. In Figure 7.24, the temperature rises rapidly at the beginning of the laser heating and reaches a maximum at the end of 1.5 second. During cooling, as shown in Figure 7.25, the cooling rate is high in the first 0.5 second. And the wings of the temperature profile at 1.5 second are higher than those of initial wings at 0 second, a result of the heat transfer through conduction during cooling. It is also found that at 1.5 second the heat affected zone with temperature higher than 700°C is confined at depth smaller than 140 μm. Deeper heat penetration requires lower laser energy densities with continuous irradiation until ultimately thick layers are obtained[Mor90]. For our studies only concentrated heating zones are required.

Clearly the heating and cooling rate of laser heating is quite high. Therefore, annealing of the irradiated region is indicated for future studies to relieve any residual stress. However, there is no indication of stress birefringence around densified spots, so this may not be a problem.

In Figures 7.22 and 7.23, the diameter of the heat affected zone on the surface is 2.0 mm. At the region with diameter smaller than 1.0 mm, the induced temperature is higher than 600°C. In Figures 7.24 and 7.25, the depth of the heat affected zone is 1.0

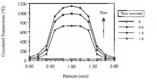

Figure 7.22 The temperature profiles on the surface of the glass substrate upon heating

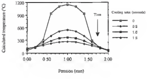

Figure 7.23 The temperature profiles on the surface of the glass substrate upon cooling

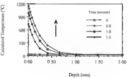

Figure 7 24 The temperature profiles on the cross section of the glass substrate upon heating.

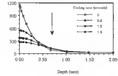

Figure 7.25 The temperature profiles on the cross section of the glass substrate upon cooling

mm. At depth smaller than 140 μm, the calculated temperature is higher than 700°C. These results are consistent with the furnace densification of the gel-silica glasses that the temperature higher than 600°C results in further densification of a porous gel silica substrate.

7.2.4 Comparisons

The simulated temperature distributions are comparable with the experimental results obtained for the laser densified spots. VHN profile and PMP(peak maximum position) profile on the surface and the cross section of the densified region were shown in Chapters 4 and 6. VHN and PMP increases as the densification temperature increases till they reach a maximum of 812 ± 18 and 1122 cm^{-1}, respectively. Both the VHN and PMP of the gel-silica glasses can be taken as an indication of the localized densification, as demonstrated earlier.

In Figure 7.26 (a), the calculated temperature profile is compared with the VHN profile on the surface of the laser densified spot. The maximum temperature and maximum VHN in the profile are located at the same position of 1.0 mm. The highest laser induced temperature(=1146°C) corresponds to a maximum VHN(=802). The laser generated heat effectively enhances the densification of the gel-silica substrate and produces an increase in VHN when the calculated temperature is higher than 300°C. In Figure 7.26 (b), normalized temperature and VHN at different positions are also shown. Clearly, these two profiles based on the same scale are matched in width and shape of the profiles. The laser-induced property changes follow the calculated temperature distribution. Normalized temperature or normalized VHN is obtained from the following equations.

$$\text{normalized temperature} = \frac{\text{calculated temperature}}{\text{maximum temperature}(=1146^{\circ}\text{C})} \qquad (7.10)$$

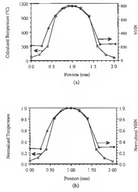

Figure 7 26 Comparison of the calculated temperature profile with the VHN profile on the surface along the diameter of the laser densified spot as shown in (a), normalized temperature and VHN varied with position are shown in (b)

$$\text{normalized VHN} = \frac{\text{measured VHN}}{\text{maximum VHN}(=812)} \tag{7.11}$$

Figure 7.27 (a) shows the calculated temperature profile and the PMP profile on the surface of the laser densified spot. The PMP is obtained from the IR reflectance microscope spectra of a laser densified spot using the IR microscope, as discussed in Chapters 4 and 6. PMP at each position is an average of a region with 100 µm in diameter shown in Figure 4.15. The maximum temperature(=1146°C) and the maximum PMP(1122 cm^{-1}) in the profile is located at the same position of 1.0 mm. The laser generated heat effectively enhances the densification of the gel-silica substrate and produces an increase in PMP when the calculated temperature is higher than 100°C. In Figure 7.27 (b), normalized temperature and PMP at different positions are shown. These two profiles based on the same scale are matched in width and shape of the profiles. This thermal model successfully predicts the dimensions of the heat affected zone. Normalized PMP is obtained from the following equation due to the large value of the PMP(up to 1122 cm^{-1})

$$\text{normalized PMP} = \frac{\text{maximum PMP measured PMP}}{\text{maximum PMP minimum PMP}} \tag{7.12}$$

In Figure 7.28 (a), the calculated temperature profile is compared with the VHN profile on the cross section of the laser densified spot at increasing depth. The depth of the heat affected zone is estimated to be <200 µm. The VHN drops sharply to ~500 from surface to the depth of 1.40 mm where the corresponding temperature is ~ 700°C. The generated heat enhances the densification of the gel-silica substrate and produces an increase in VHN when the calculated temperature is > 500°C. Comparing the calculated temperature of the base lines of the VHN profiles, the calculated temperature of the cross section is 200°C higher than that of the surface(in Figure 7.26 (a)). It indicates that the cross section of the glass sample has higher mechanical strength and higher calculated

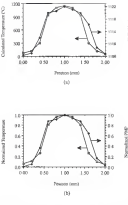

(a)

(b)

Figure 7.27 Comparison of the calculated temperature profile with the PMP profile on the surface along the diameter of the laser densified spot as shown in (a), normalized temperature and PMP varied with position are shown in (b)

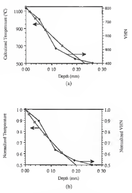

Figure 7 28 Comparison of the calculated temperature profile with the VHN profile in the middle and along the cross section of the laser densified spot as shown in (a) normalized temperature and VHN varied with depth are shown in (b) temperature than those of the surface In Figure 7 28 (b), normalized temperature and VHN at different positions are shown These two profiles based on the same scale are matched in the shape of the profiles

Figure 7 29(a) shows the calculated temperature profile and the PMP profile on the cross section of the laser densified spot as a function of increasing depth. In Figure 7 29 (b), normalized temperature and PMP at different positions are shown. These profiles in (a) and in (b) based on the same scale are decreased at increasing depth, however, they are not matched in the shape of the profiles. The discrepancy may be attributed to the fact that the PMP at each depth is an average of a investigated region with diameter of 100 μm and the depth of the heat affected zone is very small which is 140 μm.

Figure 7 30 (a) shows the calculated temperature profile and the PMP profile along the cross section at the same depth The temperature profile at a depth of 37 μm is illustrated at the left side of the figure. The PMP profile is obtained from the FTIR reflectance spectra at a depth equal to 50 μm shown in Figure 6.8 The diameter of the region investigated using FTIR microspectroscopy is 100 μm shown in Figure 4.15 The PMP increases to a maximum at the center of the cross section This maximum(=1118 cm^{-1}) of the profile at a depth of 50 μm is lower than the surface PMP(=1122 cm^{-1}) In Figure 7.30 (b), normalized temperature and PMP at different positions are shown These two profiles based on the same scale are matched in width and shape of the profiles.

Above comparisons from Figures 7 26 to 7 30 show that the calculated temperature profiles are in good agreement with experimental results The width depth, and the shape of the temperature profile match well with the property profiles on the surface or the cross section of the laser densified spot. It is found that the densification of the gel silica glass is effectively enhanced by laser-induced high temperature On the surface of the laser irradiated spot, the calculated temperature higher than 300°C(or 100°C) results in an increase in VHN(or PMP) Along the cross section of the laser irradiated spot, the calculated temperature higher than 500°C results in an increase in VHN

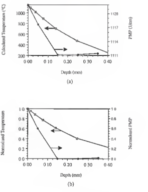

Figure 7.29 Comparison of the calculated temperature profile with the PMP profile in the middle and along the cross section of the laser densified spot as shown in (a), normalized temperature and PMP varied with depth are shown in (b)

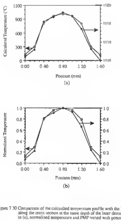

Figure 7.30 Comparison of the calculated temperature profile with the PMP profile along the cross section at the same depth of the laser densified spot as shown in (a), normalized temperature and PMP varied with position are shown in (b)

7.2.5 Conclusions

A transient model simulating the three-dimensional temperature distribution of a laser densified spot is demonstrated. The input parameters for the computations are close to the real laser operating conditions. The heating rate and cooling rate are evaluated. The maximum temperature of ~1150°C in the center of the spot obtained from the calculations is near the temperature needed for fully densifying the gel-silica glass using furnace heating. On the surface of the irradiated spot with calculated temperature higher than 600°C is confined in a region with 1.0 mm in diameter. The calculated temperature of the cross section of the irradiated spot higher than 700°C is confined within a depth smaller than 140 μm. The simulated temperature profiles are in good agreement with VHN or PMP profiles on the surface and the cross section of the laser densified spot.

CHAPTER 8
SUMMARY AND CONCLUSIONS

8.1 Summary

This study explored the optical applications of the laser densified gel-silica glasses. The modern technologies of sol-gel processing and laser processing were combined and compared with the current optical fabrication methods, as shown in Table 2.1 A new method for making microlenses and micro-optical arrays resulted from the study

Lasers are high technology tools for modifying the surface property of the materials by direct heating. The difference in the bulk density between Type VI porous and Type V full density gel-silica glasses gives rise to the development of optical devices with a higher refractive index than the substrate. This concept becomes a reality by using a laser to locally densify the Type VI porous gel silica glasses[Hen85][Ram88] Thus, optical devices can be directly "written" on the surface of the porous gel-silica substrates

Advantages of using laser heating to make microlenses on Type VI gel-silica glass are speed(mass production), cleanliness, stability, high optical quality, multichromatic source compatible, index matching with fiber optics, ease of fabrication and design, and wide optical applications in integrated optics or micro-optics. Laser writing is a direct technique that simultaneously improves the optical performance of the laser irradiated area and produces the focusing lens in the substrate

In this study, gel silica substrate glasses are densified up to 1000°C using thermal and chemical stabilizations. The product is termed a Type VI porous gel silica glass. Type VI gel-silica glass has a unique homogeneous pore texture with average pore radii of 1.2 nm. These structural features make it possible to control laser densification and therefore it is selected as the substrate for laser densification in this study.

The properties of the gel-silica glasses during densification are demonstrated. The final product, a Type V full density gel-silica glass, has superior thermal and optical properties[Hen88] The property changes of gel-sillica glasses during furnace densification support the concept of enhancing the densification of porous gel-silica glasses by using laser heating. Mechanisms of the physical, thermal, mechanical and optical properties of the gel silica glasses are discussed.

FTIR normal reflectance micro-spectroscopy provides a feasible mean for structural investigations of the gel silica glasses during furnace densification. As the densification temperature increased from 150°C to 1150°C, it was observed that the AS Si-O-Si stretching vibration mode is intensified as a result of increasing concentration of the vibrational species The wavenumber of the AS peak is also shifted towards higher frequencies as a result of polycondensation and densification of the silica network.

Refractive indices of the gel-silica glasses can be calculated from the normal reflectivities in the visible range using equation (3.16). Or, the refractive indices of the gel silica glasses in the infrared range can be obtained from a normal reflectance spectrum using the Kramers Kronig method. The linear relationships in Figures 3 15 and 3 19 can be used to evaluate the refractive index at 0.633 nm of the Type VI porous gel-silica glasses if the bulk density or the peak maximum position of the AS vibration mode is known This method was developed due to the fact that the refractive index of porous glass is difficult to obtain by using a conventional refractometer

As discussed in Chapter 4 fully densified regions can be produced on porous gel-silica glasses directly, using a CO_2 laser without masks, diffusion, or other intermediate processing steps The evaluated diameter and depth of the fully densified region in the center of the laser densified spot are ~300 µm, and ~10 µm. The dimensions of the heat affected zone were ~1400 µm diameter and 140 µm depth respectively The laser irradiated region is highly densified with a GRIN characteristic which can be used to manipulate optical rays for focusing or imaging

Laser irradiated spots on gel silica samples with bulk density > 1.8 g/c.c show environmental stability and the capability of attaining a full density(2.2 g/c c.) region in the center of the laser densified spot. This is the best result for laser densification on Type VI porous gel-silica glass that can possibly be achieved.

The stability of the laser irradiated spot can be assured if the following requirements are met:

(a)Use of a gel-silica sample with high starting density(>1.8 g/c.c) as a substrate,

(b)Use of proper laser densification conditions to achieve full density,

(c)Predesorption of adsorbed water in the gel-silica substrate prior to exposure to the laser beam,

(d)Providing a low humidity environment during laser densification.

Conditions (c) and (d) are required to prevent the deleterious effects of water on the laser densified region and increase the efficiency of laser densification.

Mechanisms of laser densification on Type VI porous gel-silica glasses are proposed, which include (I) Elastic densification(reversible), (II) Viscoelastic densification(reversible, and irreversible), and (III) Plastic densification(irreversible). These mechanisms are consistent with the experimental results, such as gradient property changes and the phenomena of relaxation of the laser densified region on a substrate with low bulk density.

Slight surface depressions and/or GRIN regions are formed on the surface layer of the gel-silica glasses after laser irradiation. The optical applications of these laser densified regions are discussed in Chapter 5. There are three types of microlenses that can be fabricated on Type VI porous gel-silica substrates and Type V full density gel-silica substrates. They are (a) M-I microlenses, a geodesic lens or a combined lens, (b) M-II microlenses, a planar GRIN lens, and (c) M-III microlenses, a negative microlens. These microlenses can be used in integrated-optics or micro-optics, as described in Chapter 2.

It is demonstrated that a M-I GRIN geodesic lens can be used to focus an optical ray parallel to the surface, with a focal length feasible for use in integrated-optics or acoustic-optics. An M-II GRIN planar gel-silica microleases arrays can be used to magnify an image or focus optical rays incident perpendicularly on the surface in micro-optics or stack planar optics discussed in Chapter 2. Arrays of the M-III negative microlens can be used to defocus an optical ray as a component of a compound microleases. In order to obtain a low loss GRIN surface channel waveguide, control of translational speed of the gel sample, densification in a dry environment, use of a gel sample with density >1.8 g/c.c., use of high quality surface and laser densification conditions of proper pulse energy are important.

Optical properties of the laser densified microlenses are discussed in Chapter 6. It is demonstrated that micro-IR spectroscopy is a fast and nondestructive technique for characterization GRIN optics. This technique allows an immediate investigation of the structural changes of laser densified spots and tracks. The variations of the AS Si-O-Si stretching vibration mode in the IR reflectance spectra across the surface of the laser densified spot indicates a gradient in the densification region. The periphery of the laser densified spot is porous(BD=1.8 g/c.c.) whereas the center is fully densified(BD=2.2 g/c.c.).

The refractive index profiles of the laser densified planar microlens at 0.633 μm and at 3.57 μm also show a gradient index change. Thus, the laser densified region can be used as a GRIN microlens. The estimated index changes induced by CO_2 laser heating at 0.633 μm and at 3.57 μm are 0.09 and 0.08, respectively.

The coupling efficiency is excellent due to the high transmittance of the gel-silica glass at 0.633 μm. The focal length of a laser densified M-II planar microlens is a little large which is limited by the extremely low thermal conductivity of the pure silica substrate. The focal length can be reduced by increasing the index change or the depth of GRIN region. The numerical aperture can also be enlarged by increasing the index change or the depth of the GRIN region. The resulting half width of the focused spot is large which is also due to the insufficient index change and depth of the GRIN region.

The shortest focal length of the laser irradiated M-III negative microlens is – 3 mm due to the large curvature of the surface depression. The size of the depression can be modulated by using different laser power and varying the distance L2 of the laser focusing lens.

Theoretical analyses of the optical properties of the GRIN planar microlenses show that the focal length decreases drastically at decreasing radius of the microlens, increasing index change or increasing GRIN depth. The minimum focal length can be reduced to 0.25 mm if the radius of the microlens is reduced to 0.05 mm. The calculated focal length of 5.14 cm is consistent with the measured focal length of 5.26 cm.

In Chapter 7, transient models simulating the dynamic three-dimensional temperature distributions of a laser densified track or spot are demonstrated. Temperature distributions of the laser densified spot are simulated within a computational volume of 2x2x2 mm^3, with 1000 data points per volume. The input parameters for the computations of the temperature distributions are close to the real laser operating conditions. The heating rate and cooling rate are evaluated. The maximum temperature of ~1150°C in the center of the laser irradiated region obtained from the calculations is close to the temperature needed for furnace densification. The simulated temperature profiles are in good agreement with the microhardness(VHN) and the IR peak maximum position(PMP) profiles on the surface and the cross section of the laser densified spots.

8.2 Conclusions

The significant accomplishments of the laser densification of gel-silica glasses and optical applications achieved in this study are summarized.

(a)Developed a new method of fabricating optical devices on gel-silica substrates using laser heating

(b)Developed a method of measuring the refractive index of the porous gel-silica glass from optical reflectivities.

(c)A process was developed for producing gel-silica substrates for further laser densification with high bulk densities > 1.8 g/c.c and < 2.2 g/c.c and low hydroxyl content. The process used a combination of thermal and chemical stabilization

(d)Special methods were developed to avoid the relaxation of the laser densified region

(e)Demonstrate that substrate densities >1.8 g/c.c. produced stable optical elements by using localized laser densification.

(f)Established the necessary laser densification conditions for fabricating optical transparent spots on the porous gel-silica substrates.

(g)Proved that the laser densified region has a higher refractive index than of the gel-silica substrate, and showed that the index change can be modified up to 0.09 which is larger than the index change(=0.05) of a GRIN rod made from sol-gel process[Yam90]

(h)Demonstrated that the shape of the laser densified region is hemispherical, the dimensions are ≤ 1.500 mm in diameter and ≤ 150 μm in depth

(i)Showed that a full density(2.2 g/c.c.) region in the center of the laser densified spot was achieved on a substrate with bulk density > 1.80 g/c.c., the dimensions of the full density region is ~0.300 mm in diameter, and ~10 μm in depth.

(j)Characterized the laser densified region to have a GRIN property which can be used to manipulate optical rays such as focusing, imaging, guiding and directing.

(k)Demonstrate the feasibility of using micro-IR spectroscopy to characterize the laser densified region which is a fast and nondestructive technique.

(l)Demonstrated unique features of laser-written optical devices such as controllable dimensions(≤ 1.5 mm) and patterns of the laser irradiated regions.

(m)Showed several optical applications of the laser densified optical devices such as GRIN microlenses, geodesic microlenses, and micro-optical arrays, some of which cannot be made easily by any other means

(n)Established that the focal length of a geodesic microlens made by laser densification can focus optical rays along the surface due to the sufficient index change and GRIN depth

(o)Demonstrated that the coupling efficiency of a laser densified lens is excellent due to the high transmittance of the gel silica glass at 0.633 μm.

(p)Identified the variables(the radius or the GRIN depth of the microlens) which can lead to producing short focal lengths of the GRIN planar gel-silica microlenses

(q)Developed a 3-D thermal model which successfully predicts the dimensions of the heat affected zone of the laser densified gel silica glasses.

(r)Showed that the calculated results of the temperature distributions from the theoretical model are in good agreement with the property distributions of the laser densified region

This work also showed that the focal length of M-II planar microlens is a little large for use in micro-optics due to the limitation of the extremely low thermal conductivity of the pure silica substrate. However, the focal length can be reduced by increasing the index change or the depth of the GRIN region The numerical aperture can also be enlarged by increasing the index change or the depth of the GRIN region. The resulting half width of the focused spot is large which is also due to the insufficient index change and depth of the GRIN region.

8.3 Future Work

Future work which can be extended from these studies include

(a)The focal length of the GRIN planar gel-silica microlens can be increased by reducing the radius the the microlens

(b)The index change of the microlens can be increased by doping or diffusion of heavy ions on the surface layer of the gel-silica substrate prior to laser densification

(c)The wavelength range of the optical transmittance can be increased by using a porous flouride gel-silica substrate for further laser densification.

(d)Laser densification is feasible to produce a stable and fully densified multimode channel waveguide if the processing conditions are properly controlled before and during the laser densification.

APPENDIX A
KRAMERS KRONIG METHOD

Galeener et al derived expressions in the harmonic approximation to relate the first-order IR spectra of a disordered solid to a common set of vibrational densities of states[Pet73] Infrared derived quantities $\omega\varepsilon_2$ and $\omega \mathrm{Im}(-\varepsilon^{-1})$ are equivalent as IR spectra. ω is equal to $(2\pi f)$ where f is the frequency(1/second) $\varepsilon^*(=\varepsilon_1 + i\varepsilon_2)$ is the complex dielectric constant of the isotropic material where the real (ε_1) and imaginary (ε_2) parts of ε can be computed from the reflectivity(=R) at normal incidence using Kramers Kronig techniques, if R is measured over a sufficiently large frequency range Studies of Kramers-Kronig methods are discussed elsewhere[Gas76][Gas76][Obt88]

Since n and k are related to the aforementioned ε, the reflection spectrum also depends on the fundamental optical constants n(real part) and k(imaginary part) of a complex refractive index n^* The relationships between ε, n, and k are listed as follows[Alm90]

$$n^*=\sqrt{(\varepsilon^*)}=n-ik \tag{A.1}$$

$$\varepsilon_1=n^2-k^2 \tag{A.2}$$

$$\varepsilon_2=2nk \tag{A.3}$$

$$\mathrm{Im}(-1/\varepsilon^*)=2nk/(n^2+k^2)^2 \tag{A 4}$$

$$k=\alpha\lambda/4\pi \tag{A 5}$$

n is the index of refraction and k is related to the absorption coefficient α and the wavelength λ. These constants can be obtained by a deconvolution of specular reflectivity results by using Kramers-Kronig analysis. The percentage reflectivity(=R) from one surface is equal to

$$R=|(n^*-1)/(n^*+1)|^2 \qquad \text{(A 6)}$$

The complex amplitude r* of the reflected wave is given as a function of the phase difference θ between the incident and reflected waves

$$r^*=|r|\exp(i\theta) \qquad \text{(A 7)}$$

Since $R=|r|^2$, the following expressions of n and R are easily derived as follows(Alm90)

$$n=\frac{1-R}{1+R-2R^{1/2}\cos\theta} \qquad \text{(A 8)}$$

$$k=\frac{2R^{1/2}\sin\theta}{1+R-2R^{1/2}\cos\theta} \qquad \text{(A 9)}$$

Where R is experimentally measured and θ is obtained from the experimentally reflectivity R(ω) via the Kramers Kronig transformation $\theta(\omega_i)$

$$\theta(\omega_i)=\frac{2\omega_i}{\pi}\int_0^{\infty}\frac{\ln[R(\omega)]^{1/2}-\ln[R(\omega_i)]^{1/2}}{\omega_i^2-\omega^2}d\omega \qquad \text{(A.10)}$$

Above integral has computed for each angular frequency of interest ω_i over a sufficiently large frequency range In this study, n and k from (A 8-A.10) through

Kramers-Kronig method are obtained by using a software called LABCALC from Galactic Industries Corporation[Lab90] In addition, the reflection spectrum obtained in this study is at normal incidence which is consistent with the assumption of the Kramers Kronig analysis

APPENDIX B

COMPUTER PROGRAM OF THE LASER DENSIFICATION MODELING

```
c**********************************************************************
c*          This program models temperature                           *
c*                                                       *
c*                                                       *
c**********************************************************************
      program laser
      DIMENSION s(43,12,11),m(12,11),
     1          t(43,12,11),x(43),y(12),z(11),a(43),b(43) apb(43)
c
      ia = 43
      jo = 12
      ke = 11
c
c
      write(*,*) choose
      write(*,*)
     1'    1. 2-D case (x-z plane, maximum grid points = 41*11)'
      write(*,*)
     1     2. 3-D case (x-y-z domain, maximum grid points = 41*11*11)
      read(*,*) idir
c
c********** list grid system of three directions  **********
      if(idir.eq.2) then
      write(*,*)
      write(*,*)          X Z plane represents plane of symmetry'
      write(*,*)                      * X'
      write(*,*)                     *'
      write(*,*) '        imax  ********************************'
      write(*,*) '           * *                        * *'
      write(*,*) '          * *                        *  *'
      write(*,*) '       m * *                        *   *'
      write(*,*) '        * *                        *    *'
      write(*,*)         * *                        *     *'
      write(*,*) ' 1 ************************************  Y *'
      write(*,*) '    * *                       * jmax    *'
      write(*,*) '    * *                       *        *'
      write(*,*) '    * *                       *        *'
      write(*,*) '    * *                       *        *'
      write(*,*) '    * *                       *       *'
      write(*,*) '    * *                       *      *'
      write(*,*) '    * *                       *     *'
      write(*,*) '    * *                       *   *'
      write(*,*) '    * *                       * *'
      write(*,*) 'kmax*******************************'
      write(*,*)        *'
      write(*,*) '      *  Z'
      write(*,*) ' Fig.  3-D computational domain
      write(*,*) continue (1 - yes, 2 - no) ?
      read(*,*) ic
      if(ic.eq.2) stop
      endif
      if(idir.eq 1) then
      write(*,*)
      write(*,*) '
      write(*,*)
      write(*,*)
      write(*,*)
      write(*,*)
      write(*,*)      1                   imax'
      write(*,*)      ************************************  X'
      write(*,*)      *                   *
      write(*,*)      *                   *
      write(*,*)      *                   *
      write(*,*)      *                   *
      write(*,*)      *                   *'
      write(*,*) '    *                   *'
      write(*,*) '    *                   *
      write(*,*) '    *                   *
      write(*,*)      *                   *
      write(*,*)      *                   *'
      write(*,*)  kmax*****************************
      write(*,*)      *
      write(*,*)      *
      write(*,*)      Z'
      WRITE(*,*)    Fig.  2-D computational domain
      write(*,*) 'continue (1 = yes, 2 = no) ?
      read(*,*) ic
      if(ic.eq.2) stop
      ENDIF
c
c  ... data in x-direction ...
c
      xmax = .5
      imax = 41
      write(*,*) '******
 303  write(*,331) xmax,imax
 331  format(/
     2 1x,'maximum length in x-direction (cm)           =' f9.4/
     4 1x,'total grid-point number in x-direction       =',i3/1x)
c
      write(*,*)' '
      write(*,*)'Do you want to change these data? (1 = yes, 2 = no)'
      read(*,*) it
      if(it.eq.1) then
      write(*,*) 'Please input:
      write(*,*) 'maximum length in x-direction (cm) =
      read(*,*) xmax
      write(*,*) 'total grid-point number in x direction =
      read(*,*) imax
      write(*,*)
      write(*,*) '* Input data have been changed to the following:
      goto 303
      endif
      write(11,*) '******
      write(11,331) xmax,imax
c
      dx = xmax/(imax-1)
      imax = imax+2
```

```
c
      x(2) = 0
      do 333 i = 3,imax
 333   x(i) = x(i-1)+dx
       x(1) = -dx/5
c       x(imax) = x(imax-1)+dx
c
c .... data in z-direction ....
c
      z0=0.
      zmax = .08
      kmax = 11
      beta = 1.01
      write(*,*) '******'
 323  write(*,321) zmax,kmax,beta
 321  format(/
     4 1x,'maximum depth in z-direction (cm)      =',f8.4/
     8 1x,'total grid point number in z-direction = ',i3/
     3 1x,'stretching function                    = ',f18.6/1x)
c
      write(*,*) ' '
      write(*,*) 'Do you want to change these data? (1 = yes, 2 = no)'
      read(*,*) it
      if(it.eq.1) then
      write(*,*) 'Please input: '
      write(*,*) 'maximum depth in z-direction (cm) ='
      read(*,*)  zmax
      write(*,*) 'total grid-point number in z-direction ='
      read(*,*) kmax
      write(*,*) 'stretching function                    ='
      read(*,*) beta
      write(*,*) ' '
      write(*,*) '* Input data have been changed to the following.'
      goto 323
      endif
      write(11,*) '******'
      write(11,321) zmax,kmax,beta
c
      call stretch(beta,ko,z,0.,zmax,1,kmax)
c
c .... data in y-direction ....
c
      y(1)= -.5
      y(2)=0
      y(3)=.5
      ymax=.5
      jmax=3
      if(idir.eq.1) goto 1
c
      jmax = 11
      beta = 1.01
      write(*,*) '******'
  313 write(*,311) ymax,jmax,beta
  311 format(/
     2 1x,'maximum width in y-direction (cm)        = 'f8.4/
     4 1x,'total grid-point number in y-direction = 'i3/
     3 1x,'stretching function                    = ',f18.6/1x)
c
      write(*,*) '
      write(*,*) Do you want to change these data? (1 = yes, 2 = no)'
      read(*,*) it
      if(it.eq.1) then
      write(*,*) Please input.'
      write(*,*) maximum width in y-direction (cm) ='
      read(*,*) ymax
      write(*,*) total grid-point number in y-direction ='
      read(*,*) jmax
      write(*,*) stretching function                    ='
      read(*,*) beta
      write(*,*) '
      write(*,*) ' Input data have been changed to the following: '
      goto 313
      endif
      write(11,*) '******'
      write(11,311) ymax,jmax,beta
c
      y(2) = 0
      ymax = jmax+1
      call stretch(beta,je,y,0.,ymax,2,jmax)
c
      y(1) =  y(3)
      WRITE(*,*) ''
      WRITE(*,315) (J,Y(J),J = 2,JMAX)
  315 FORMAT(1X,'J = ',I3,'  Y(J) = ',F10.7)
c
c********** input physical properties  **********
c
c  .... input thermal properties ..
c
    1  qlaser = 22100000
      dck = .008
       eck = .015
      dch = .0071
      tair = 24.
      write(*,*) '******'
 403  write(*,*)
      write(*,*) ' laser power (W/cm**3)                  = ',qlaser
      write(*,*) ' heat diffusivity (cm**2/sec)          = ',dck
      write(*,*) ' thermal conductivity (W/cm*degree C)      = ',eck
      write(*,*) ' convective coefficient (W/(cm**2*degree C)) = ',dch
      write(*,*) ' air temperature (degree C)             = ',tair
      write(*,*)'
      write(*,*)'Do you want to change these data? (1 = yes, 2 = no)
      read(*,*) it
      if(it.eq.1) then
      write(*,*) Please input.
      write(*,*) ' laser power (W/cm**3) = '
      read(*,*) qlaser
      write(*,*) ' heat diffusivity (cm**2/sec) = '
      read(*,*) dck
      write(*,*) ' thermal coductivity (W/cm*degree C) = '
      read(*,*) eck
      write(*,*) ' convective coefficient (W/(cm**2*degree C)) = '
      read(*,*) dch
      write(*,*) ' air temperature (degree C) = '
      read(*,*) taur
      write(*,*) ' '
      write(*,*) ' Input data have been changed to the following.'
      goto 403
      endif
c
      write(11,*) '******'
      write(11,*) ' '
      write(11,*) ' laser power (W/cm**3)                   = ',qlaser
      write(11,*)' heat diffusivity (cm**2/sec)             = ',dck
      write(11,*)' thermal coductivity (W/cm*degree C)      = ',eck
      write(11,*) ' convective coefficient (W/(cm**2*degree C)) = ',dch
      write(11,*) ' air temperature (degree C)              = ',taur
      write(11,*)
c
      u = 5.
      w = .02
      write(*,*) '******'
 433  write(*,*) '
      write(*,*) ' moving velocity (cm/sec) = ',u
      write(*,*) ' half laser width (cm)    = ',w
      write(*,*)'
      write(*,*)'Do you want to change these data? (1 = yes, 2 = no)'
      read(*,*) it
      if(it.eq.1) then
      write(*,*) ' Please input'
      write(*,*) ' moving velocity (cm/sec) = '
      read(*,*) u
      write(*,*) ' half laser width (cm) = '
      read(*,*) w
      write(*,*) ' '
      write(*,*) ' Input data have been changed to the following:'
      goto 433
      endif
c
      write(11,*) '******'
      write(11,*) ' '
      write(11,*)' moving velocity (cm/sec)  = ',u
      write(11,*) ' half laser width (cm)     = ',w
      write(11,*) ' '
c
c********** set time step **********
c
      dtt = 1
      dt0 = .01
      dtint = .01
      write(*,*) '******'
```

```
473  write(*,*)
     write(*,*) ' total time              = ',dtt
     write(*,*) ' time step               = ',dt0
     write(*,*) ' time interval in output = ',dtint
     write(*,*) '
     write(*,*)'Do you want to change these data? (1 = yes, 2 = no)
     read(*,*) it
     if(it.eq.1) then
     write(*,*) ' Please input
     write(*,*) ' total time =
     read(*,*) dtt
     write(*,*) ' time step =
     read(*,*) dt0
     write(*,*) ' time interval in output =
     read(*,*) dtint
     write(*,*) '
     write(*,*) '* Input data have been changed to the following:
     goto 473
     endif
c
     write(11,*) '*****
     write(11,*) '
     write(11,*) ' total time              = ',dtt
     write(11,*) ' time step               = ',dt0
     write(11,*) ' time interval in output = ',dtint
     write(11,*) '
c
c**********  set initial temperature  **********
c
c ....  input uniform initial temperature  ..
c
     tair = 24
     do 111 j = 1,jmax
     do 111 k = 1,kmax
      ts(j,k) = tair
     do 111 i = 1,imax
 111 t(i,j,k) = tair
c     call unsta(ie,je,ke,imax,jmax,kmax,t,tsi)
c
c**********  storage of initial data  for plot  **********
c
c  14 OPEN(21,FILE= 'plot.out',STATUS= 'NEW')
c
c     write(21,*) idir
c
c     write(21,*) imax,jmax,kmax
c     write(21,900) (x(i),i= 1,imax)
c     write(21,900) (y(j),j= 1,jmax)
c     write(21,900) (z(k),k= 1,kmax)
 900  format(f8.4)
c
c**********  calculation begins  **********
c
     dt = dt0
```

```
c      dt = 0
      itmax=dtt/dt0+1
      if(dt0*itmax.lt.dtt+dt0/2.) itmax=itmax+1
      int = dtint/dt0
      if(dt0*int.lt.dtint-dt0/2.) int=int+1
c
      do 200 it = 1,itmax
c
      dt = dt+dt0
      if((it-1).eq.(it-1)/int*int.or.it.eq.itmax) then
       write(*,201) dt
       write(11,201) dt
 201   format(//1x,78('*')//1x,'second = ',f8.5)
      endif
c
c********** calculate temperature **********
c
c .... calculate the right hand side of difference equation ....
c
c      w = f12
      call rhs(ie,je,ke,imax,jmax,kmax,x,y,z,
     1            s,t,dck,cck,dch,tair,a,b,aph,dt0,dt,n,w,qlaser)
c
c .... calculate along x-direction ....
c
c      write(*,*) 'calculate along x direction  m=1'
      do 140 j=2,jmax-1
       do 140 k=1,kmax-1
        call coefab(ie,je,ke,1,1,imax,jmax,kmax,ie,imax
     1            ,i,j,k,x,dck,cck,dch,tair,a,b,aph,dt0,u,z)
        call trid(ie,je,ke,1,imax,a,b,aph
     1           ,i,j,k,imax,jmax,kmax,s,t)
      do 140 i=1,imax
c      if(k.le.1) write(*,*) 'i,j,s1(i,j,1) = ',i,j,s(i,j,k)
 140  continue
c
c .... calculate along y-direction ..
c
      if(jmax.le.3) goto 125
c      write(*,*) 'calculate along y-direction  m=1
      do 130 i=2,imax-1
       do 130 k=1,kmax-1
        call coefab(ie,je,ke,1,2,imax,jmax,kmax,je,jmax
     1            ,i,j,k,y,dck,cck,dch,tair,a,b,aph,dt0,u,z)
        call trid(ie,je,ke,2,jmax,a,b,aph
     1           ,i,j,k,imax,jmax,kmax,s,t)
      do 130 j=1,jmax
c      if(k.eq.1) write(*,*) 'i,j,s2(i,j,1) = ',i,j,s(i,j,k)
 130  continue
c
c .... calculate along z-direction ....
c
 125  k=1
      do 120 i=2,imax-1
      do 120 j= 2,jmax-1
       call coefab(ie,je,ke,1,3,imax,jmax,kmax,ke,kmax
     1             i,j k,z,dck,cck,dch,tair,a,b,aph,dt0 u,x)
       call trid(ie,je ke,3,kmax,a,b,aph
     1            i,j k,imax,jmax,kmax,s,t)
c     write(*,*) 'i,j,s3(i,j,1) = ',i,j,s(i,j,k)
 120  continue
c
c  .. get the new values of temperature ....
c
 150 do 160 i= 2,imax-1
     do 160 j= 2,jmax-1
     do 160 k= 1,kmax-1
c     if(k.eq.1) write(*,*) 'i,j,to(i,j,1) = ',i,j t(i,j,k)
     t(i,j,k)=t(i,j,k)+s(i,j,k)
c     if(k.eq.1) write(*,*) 'i,j tn+1(i,j,1) = ',i,j,t(i,j,k)
 160 continue
c
     call tbc(ie,je,ke,t,it,dck,
    1          imax,jmax,kmax,u,x,y,z,cck,dch,tair,dt0,dt)
c
c .... output temperature data ....
c
      if((it-1).eq.(it-1)/int*int.or.it.eq.itmax)
    1   call pr(idir,ie,je,ke,dt,x,y,z,3,imax,jmax,kmax,t)
c
 200 continue
C     CLOSE(11,STATUS='KEEP')
c     CLOSE(21,STATUS='KEEP')
c
     stop
     END
c**************************************************************
c* subroutine:  stretching fuction routine                    *
c**************************************************************
c
     subroutine stretch(beta,lmax,a,amin,amax,ixil,ixih)
     dimension a(lmax)
     xhmal=(amax-amin)*2.
     xhmxl=float((ixih-ixil)*2)
     bp1= beta+1
     bm1= beta-1
     bd=bp1/bm1
     do 10 i=ixil,ixih
      be= bd**((2.*(i-ixil)-xhmxl)/xhmxl)
      xa= ixil+xhmxl*(bp1*be-bm1)/(2.*(1.+be))
      a(i)= amin+xhmal*(xa-ixil)/xhmxl
 10    continue
      A(IXIL) = AMIN
      A(IXIH) = AMAX
     return
     end
c
c**************************************************************
```

```
c* subroutine:  give the initial data for dependent variable          *
c***********************************************************************
c
      subroutine initn(ie,je,ke,imax,jmax,kmax,t,tini)
c
      dimension t(ie,je,ke)
c
c  ... set uniform initial tempreture field ....
c
      do 10 i=1,imax
      do 10 j=1,jmax
      do 10 k=1,kmax
  10  t(i,j,k) = tini
c
      return
      end
c
c***********************************************************************
c* subroutine:          output results                                 *
c***********************************************************************
c
      subroutine pr(idir ie,je,ke,dt,x,y,z,ic,imax,jmax,kmax,a)
c
      dimension a(ie,je,ke),x(ie),y(je),z(ke)
c
      do 50 j=2,jmax
c
       write(11,*) ' '
       write(11,*) ' '
c       write(21,*) dt
c       write(21 100) ((a(i,j,k),i=1,imax),k=1,kmax)
 100   format(f7 1)
 110   format(f7.2)
c
       if(idir eq.2) write(11 1) y(j)
   1   format(1x,'x - z plne at y = ',f9 4,  cm )
       write(11,*)                            T(degree C)
c
       i1=2
       i2=8
       if(i2.gt.imax 1) i2=imax-1
       i3=1
   3   write(11,*) ' '
       do 5 k =1,kmax
         write(11 10) z(k),(a(i,j k),i=i1,i2,i3)
   5   continue
  10   format(1x,'z = ',f7.4,' cm  ',7F9.0)
c
       write(11 20) (x(i),i=i1,i2,i3)
  20   format(15x,64(  )/8x,'x(cm) = ',7f9.5)
c
       if(i2.lt.imax-1) then
        i1=i1+7
        i2=i2+7
        if(i2.gt.imax-1) i2=imax-1
        goto 3
       endif
c
  50 continue
c
      do 200 i=2,imax-1
       write(*,150) x(i),s(i,2,1)
 150  format(1x,'x = ',f8.5,'  T(x,y=0,z=0) = ',f7.0)
 200 continue
c
      return
      end
c
c****************************************************************
c* subroutine,  calculate the right hand side of difference equation *
c****************************************************************
c
      subroutine rhs(ie,je,ke,imax,jmax,kmax,x,y,z
     1              ,s,t,dck,cck,dch,taur,a,b,aph,dt0,dt,u,w,qlaser)
c
      dimension s(ie,je,ke),t(ie,je,ke)
     1          ,x(ie),y(je),z(ke),a(43),b(43),aph(43)
c
      call source(ie,je,ke,imax,jmax,kmax,
     1                  x,y,z,s,dt0,dt,u,w,qlaser,dck,cck,dch)
c
c ... calculate rhs along x-direction ...
c
      do 30 k=1,kmax-1
      do 30 j=2,jmax-1
       call coefab(ie,je,ke,2,1,imax,jmax,kmax,ie,imax
     1            ,i,j,k,x,dck,cck,dch,taur,a,b,aph,dt0,u,z)
      do 30 i=2,imax-1
       s(i,j,k)=s(i,j,k)+a(i)*t(i-1,j,k)+b(i)*t(i+1,j,k)
     1          +aph(i)*t(i,j,k)
  30  continue
c
c ... calculate rhs along y-direction ...
c
      if(jmax.le.3) goto 15
      do 20 k=1,kmax-1
      do 20 i=2,imax-1
       call coefab(ie,je,ke,2,2,imax,jmax,kmax,je,jmax
     1            ,i,j,k,y,dck,cck,dch,taur,a,b,aph,dt0,u,z)
      do 20 j=2,jmax-1
       s(i,j,k)=s(i,j,k)+a(j)*t(i,j-1,k)+b(j)*t(i,j+1,k)
     1          +aph(j)*t(i,j,k)
c      if(k.eq.1) write(*,*) 'v-d, i,j,s(i,j,1) = ',i,j,s(i,j,1)
  20  continue
c
c ... calculate rhs along z-direction ....
c
  15  do 10 i=2,imax-1
```

```
      do 10 j= 2,jmax-1
       call coefzk(ie,je,ke,2,3,imax,jmax,kmax,ke,kmax
     1             i,j,k,z,dck,cck,dch,tair,a,b,apb,dt0,u,z)
      do 10 k= 1,kmax-1
       if(k.eq.1) then
        ac = 1 +2.*dch*dck/cck/(z(2)-z(1))*dt0
        s(i,j,k) = s(i,j,k)+b(k)*t(i,j,k+1)+apb(k)*t(i,j,k)
     1           2.*dch*dck/cck/(z(2)-z(1))*(t(i,j,k)-tair)*dt0/ac
c     1          b(k)*dch/cck*(z(2)-z(1))*tair
       else
        s(i,j,k)=s(i,j,k)
     1         +a(k)*t(i,j,k-1)+b(k)*t(i,j,k+1)+apb(k)*t(i,j,k)
       endif
c      if(k.eq.1) write(*,*) 'z-d, i,j,s(i,j,1) =  i,j,s(i,j,1)
 10   continue
c
      return
      end
c
c*********************************************************************
c* subroutine,  calculate the heat generation internal source        *
c*********************************************************************
c
      subroutine source(ie,je,ke,imax,jmax,kmax,
     1                 x,y,z,s,dt0,dt,u,w,qlaser,dck,cck,dch)
c
      dimension s(ie,je,ke),x(ie),y(je),z(ke)
c
      do 40 i = 1,imax
      do 40 j = 1,jmax
      do 40 k = 1,kmax
       s(i,j,k) = 0
 40   continue
c
      Qsum = 0
      rhoC = cck/dck
      Qtotal = qlaser*(3.14159265*w**2*.001)
c
      do 100 j= 2,jmax-1
       if((y(j-1)+y(j))/2..ge.w) goto 100
c
       yd = .5*(y(j+1)-y(j-1))
       if((y(j)+y(j+1))/2..ge.w) yd = w-.5*(y(j-1)+y(j))
       if(j.ne.2) then
        yd = yd*2.
       endif
c
       xloc = u*dt
       xloch = xloc + w
       xlocl = xloc - w
c
       xm2 = (x(1)+x(2))/2.
       xmm = (x(imax-1)+x(imax))/2.
c
```

```
      do 10 i=2,imax-1
c       s(i,j,1) = 0.
        xmh = (x(i+1)+x(i))/2.
        xml = (x(i-1)+x(i))/2.
        if(xlocl.lt.xm2) i1 = 2
        if(xlocl.ge.xml.and.xlocl.lt.xmh) i1 = i
        if(xloch.gt.xml.and.xloch.le.xmh) i2 = i
        if(xloch.gt.xmm) i2 = imax-1
 10     continue
c
      do 20 i=i1,i2
        xd = (x(i+1)-x(i-1))/2.
        if(i.eq.i1) xd = (x(i+1)+x(i))/2.-xlocl
        if(i.eq.i2) xd = xloch-(x(i-1)+x(i))/2.
        if(i1.eq.i2) xd = 2.*w
c
        vv = .125*(x(i+1)-x(i-1))*(y(j+1)-y(j-1))*(z(2)-z(1))
        IF(I.EQ.2)
     1  VV = .25*(X(I+1)-X(I))*(Y(J+1)-Y(J-1))*(Z(2)-Z(1))
        if(j.ne.2) then
         vv = vv*2.
        endif
        ratio = xd/(2.*w)*yd/(2.*w)
        s(i,j,1) = Qtotal*ratio/vv*(dt0/rhoC)
c        write(*,*) 'xd,yd,ratio,vv = ',xd,yd,ratio,vv
C        WRITE(*,*) 'I,J,Q(I,J,1) = ',I,J,S(I,J,1)
        Qsum = Qsum+s(i,j,1)*vv/(dt0/rhoC)
c
 20     continue
100   continue
c
      aa = Qtotal/Qsum
C      WRITE(*,*)
C      WRITE(*,*) 'QTOTAL,QSUM,AA = ',QTOTAL,QSUM,AA
C      WRITE(*,*) '
c
      do 200 i = 2,imax-1
      do 200 j = 2,jmax-1
       if(s(i,j,1).ne.0.) then
        ac = 1.+2.*dch*dck/ack/(z(2)-z(1))*dt0
        s(i,j,1) = aa*s(i,j,1)/ac
C        WRITE(*,*) 'I,J,S(I,J,1) = ',I,J,S(I,J,1)
       endif
200   continue
c
      return
      end
c
c***********************************************************************
c* subroutine:  calculate coefficients of difference equations         *
c***********************************************************************
c
      subroutine coefsh(ie,je,ke,ica,icc,imax,jmax,kmax,mc,mmax
     1                  ,i,j,k,m,dck,ack,dch,tair,a,b,aph,dt0,u,z)
```

```
      dimension xi(mc),z(kc),a(43),b(43),aph(43)
c
c ica is a choice.
c     ica = 1 the subroutine is called by main program
c     ica = 2 .. ....... ......... subroutine RHS
c
c ioc is a choose of direction
c     ioc = 1  xi = x
c     ioc = 2  xi = y
c     ioc = 3  xi = z
c
c      write(*,*) 'ica(1=main, 2=sub) = ',ica
c      write(*,*) 'ioc(1=x, 2=y, 3=z) = ',ioc
c
      mmin = 2
      if(ioc.eq.3) mmin = 1
c
      do 20 m=mmin,mmax-1
c
       if(m.eq.1) then
        a(m)=0.
        b(m)=2.*dck/(xi(2)-xi(1))**2*dt0
       else
        a(m)=2.*dck/(xi(m+1)-xi(m-1))/(xi(m)-xi(m-1))*dt0
        b(m)=2.*dck/(xi(m+1)-xi(m-1))/(xi(m+1)-xi(m))*dt0
       endif
c
       ac = 1
       if(k.eq.1.or.m.eq.1) ac = 1+2.*dch*dck/cck/(z(2)-z(1))*dt0
       a(m)=a(m)/ac
       b(m)=b(m)/ac
c
c       if(ioc.eq.1) b(m)=b(m)+1./(xi(m+1)-xi(m))*dt0*u
c
       if(ioc.eq.2.and.m.eq.2) then
        b(2)=a(2)+b(2)
        a(2)=0.
       endif
       aph(m)=-(a(m)+b(m))
c       if(m.eq.1) aph(m) = -b(m)*(1.-dch/cck*(xi(m+1)-xi(m)))
c
       if(ica.eq.1) then
        a(m)=-a(m)
        b(m)=-b(m)
        aph(m)=1.-aph(m)
       endif
c
c      write(*,*) 'm,a,aph,b = ',m,a(m),aph(m),b(m)
 20   continue
      return
      end
c
c*****************************************************************
c* subroutine:  establish boundary conditions of temperature equations *
```

```
c*****************************************************************
c
      subroutine tbc(ie,je,ke,t,tx,dck,
     1               imax,jmax,kmax,u,x,y,z,cck,dch,tair dt0,dt)
c
      dimension tx(je,ke),t(ie,je,ke),x(ie),y(je) z(ke)
c
c*********  set boundary conditions at z-direction (k=kmax)  *********
c
      do 40 i= 2,imax 1
      do 40 j= 2,jmax 1
       t(i,j,kmax)= t(i,j kmax 1)
 40    continue
c
c*********  set boundary conditions at y-direction (j=1 and j=jmax)  *********
c
      do 30 i= 1 imax
      do 30 k= 1 kmax
      t(i 1 k) = t(i,3 k)
 30   t(i,jmax,k) = t(i,jmax 1 k)
c
c*********  set boundary conditions at x-direction (i=1 and i= imax)  *********
c
      if(imax.le.3) goto 5
      do 10 j=1,jmax
      do 10 k= 1,kmax
       X1 = X(2) X(1)
       Z1 = Z(2)-Z(1)
       T(1,J K) = (CCK/X1*T(2,J,K)+DCH*TAIR)/(CCK/X1+DCH)
       IF(K.EQ 1) T(1,J 1) = (CCK/X1*T(2,J 1)+CCK/Z1*T(1,J 2)+DCH*TAIR)
     1                /(CCK/X1+CCK/Z1+DCH)
C      T(1,J,K) = T(2,J,K)
       t(imax,j k) = tx(j,k)
       TX(J K) = T(IMAX,J,K)
     1 (T(IMAX,J,K)-T(IMAX 1,J,K))*(U*DT0)/(X(IMAX)-X(IMAX 1))
 10    CONTINUE
c
  5    return
      end
c
c*****************************************************************
c* subroutine    solve tri-diagonal matrix                    *
c*****************************************************************
c
      subroutine trid(ie,je,ke,icc,mmax,a,b,aph
     1               ,g,k,imax,jmax,kmax,s,t)
c
      dimension a(43) b(43) aph(43),g(43),s(ie,je ke),t(ie,je,ke)
c
c      write(*,*) 'in TRID icc =  icc
      mmin = 2
      if(icc.eq.3) mmin = 1
c
      do 10 m= mmin,mmax-1
      if(iec.eq.1) g(m)=s(m,j,k)/apb(m)
      if(iec.eq.2) g(m)=s(i,m,k)/apb(m)
      if(iec.eq.3) g(m)=s(i,j,m)/apb(m)
c      write(*,*)
c     1  'm a,b,apb,s = ',m,a(m),b(m),apb(m),g(m)
  10  continue
c
     do 15 m=mmin,mmax,1
      a(m)=a(m)/apb(m)
      b(m)=b(m)/apb(m)
  15  apb(m)=1
c
     b(mmin)=b(mmin)/apb(mmin)
     g(mmin)=g(mmin)/apb(mmin)
     do 20 m=mmin+1,mmax-1
      dj=apb(m)-a(m)*b(m-1)
  20  g(m)=(g(m)-a(m)*g(m-1))/dj
c
     do 30 m=mmax-1,mmin,-1
  30  g(m)=g(m)-b(m)*g(m+1)
c
     do 40 m=mmin,mmax,1
      if(iec.eq.1) s(m,j,k)=g(m)
      if(iec.eq.2) s(i,m,k)=g(m)
      if(iec.eq.3) s(i,j,m)=g(m)
c      write(*,*) 'result: m,s = ',m,g(m)
  40  continue
c
     return
     end
```

LIST OF REFERENCES

Acc90 Accordi P., C. P. Basola, G. P. Bava, G. Chiaretti and I. Montrosset, 1990, Applied Optics 29, 37

Alm90 Almeida R. M., T. A. Guiton, and C. G. Pantano, 1990, Journal of Non-Crystalline Solids 121, 193

And84 Anderson D. A., J. C. Tannehill, and R. H. Pletcher, 1984, Computational Fluid Mechanics and Heat Transfer, Hemisphere Publishing Corp., Washington, 599

Asa86 Asahara Y., H. Sakai, S. Ohmi, S. Nakayama, Y. Yoneda, and T. Izumitani, 1986, Applied Optics 25, 3384

Atk84 Atkinson L. G. III, J. D. Downie, D. T. Moore, J. M. Stagaman, and L. L. Voci 1984 Applied Optics 23, 1735

Atk82 Atkinson L. G., S. N. Houde-walter, D. T. Moore, D. P. Ryan, and J. M. Stagaman 1982, Applied Optics 21, 993

Bar91 Bartley J. and W. Goltsos 1991 SPIE, San Diego, to be published

Bat82 Batteh J. H., 1982, J. Appl. Phys. 53, 7537

Bec64a Beck A. C., 1964 Bell Sys. Tech. J. 43, 1818

Bec64b Beck A. C., 1964 Bell Sys. Tech. J. 43, 1821

Bel90 Belforte D. A., 1990, SPIE 1276, 2

Ber90 Bergmann H. W., R. Kupfer and D. Muller, 1990, SPIE 1276, 375

Ber64a Berreman D. W., 1964 Bell Sys. Tech. J. 43, 1469

Ber64b Berreman D. W., 1964, Bell Sys. Tech. J. 43, 1476

Ber82 Bertoluzza A., C. Fagnano, M. A. Morelli, V. Gottardi, and M. Guglielmi, 1982, Journal of Non-Crystalline Solids 48, 117

Bor88 Borrelli N. F. and D. L. Morse, 1988, Applied Optics 27, 476

Bri88a Brinker C. J. Journal of Non-Crystalline Solids 100, 31

Bri88b Brinker C. J., R. K. Brow, D. R. Tallant and R. J. Kirkpatrick, 1988, Mat. Res. Soc. Symp. Proc. 105, 289

Bri82 Brinker C J K D Keefer D W Schaefer and C. S Ashley, 1982, Journal of Non Crystalline Solids 48, 47

Bri88c Brinker C. J R J Kirkpatrick, D R. Tallant, B C Bunker and B Montez 1988 Journal of Non Crystalline Solids 99, 418

Bri85a Brinker C J and G W Scherer, 1985, Journal of Non-Crystalline Solids 70, 301

Bri84 Brinker C J G W Scherer 1984, in Ultrastructure Processing of Ceramics Glasses and Composites edited by Hench L. L , and D R Ulrich Wiley Interscience, New York 564

Bri90 Brinker C J , G W Scherer, 1990, Sol-Gel Science, Academic Press Inc San Diego, 908

Bri85b Brinker C. J G W Scherer and E P Roth, 1985, Journal of Non-Crystalline Solids 72, 345

Bri85c Brinker C. J G W Scherer, E. P Roth and D R. Tallant, 1985, Journal of Non Crystalline Solids 71, 171

Bri82 Brinker C. J D R Tallant E. P Roth and C. S Ashley, 1982, Journal of Non-Crystalline Solids 48, 47

Bri86 Brinker C J , D R Tallant E P Roth and C S Ashley, 1986, Mat. Res. Soc. Symp. Proc. 61, 387

Bru38 Brunauer S P H Emmett, and E Teller, 1938 J. Amer. Chem. Soc. 60, 309

Cal86a Caldwell J B , L R. Gardner, S N Houde-Walter, M T Houk, D S Kindred, D T Moore D P Naughton, and C B Wooley, 1986, Applied Optics 25, 3345

Cal86b Caldwell J B and D T Moore, 1986, Applied Optics 25, 3351

Cal82 Calder I D and R. Sue, 1982, J. Appl. Phys. 53, 7545

Car91 Carts Y A., 1991, Laser Focus World 27, No 6, 93

Cha84 Chang C Y , Y K. Fang, B S Wu, and R M Chen, 1984, Mat. Res. Soc. Symp. Proc. 23, 497

Che90 Che T M , J B Caldwell, and R M Mininni, 1990, SPIE 1328, 145

Che79 Checcacci V R., 1979 in Fiber and Integrated Optics, Edited by D B Ostrowsky Plenum Press New York 417

Che87 Chen B., 1987 in Integrated Optical Circuits and Components, Edited by L. D Hutcheson Marcel Dekker Inc New York, 403

Che76 Chen D B Koepke, J D Zook and E G Bernal , 1976, Applied Physics Letters, 29, 657

Che77 Chen B , E. Marom and A Lee, 1977 Applied Phys. Lett. 31, 263

Che91 Cheng Y, 1991, Ph.D Dissertation University of Florida, Gainesville

Chi92a Chia T , and L. L. Hench 1992 Chemical Processing of Advanced Materials L. L. Hench and J K West, eds. Chapter 83 J Wiley and Sons New York

Chi92b Chia T and L. L. Hench, 1992 SPIE, to be published

Chi90 Chia T L. L. Hench Chuobin Qin, and C K Hsieh, 1990, Mat. Res. Soc. Symp. Proc. 180 819

Chm85 Chmel A , and S B Eronko, 1985, Journal of Non-Crystalline Solids 70, 45

Chu89 Chuang T J , 1989 in Laser Microfabrication edited by D J Ehrlich and J Y Tsao, Academic Press New York, 587

Coh74 Cohen L. G. and M V Schneider, 1974 Applied Optics 13, 89

Col90 Colthup N B , L. H Daly, and S E Wiberley, 1990, in Introduction to Infrared and Raman Spectroscopy, Academic Press Inc New York, 547

Cou82 Coutaz J L , and P C. Jaussaud, 1982, Applied Optics 21, 1063

Cra76 Crawford B , 1976, in Infrared and Raman Spectroscopy Part A, edited by E. G Brame Jr , J G Grasselli, Marcel Dekker Inc New York, 345

Cul64 Cullom J H and R W Waynant 1964 Applied Optics 3, 989

Dai84 Daimon M M. Shinoda, and T Kubo, 1984, Applied Optics 23, 1790

Dav68 Davit J , 1968 J. Applied Physics 39, 6052

Dev88 Devine R A B , 1988, J. Vac. Sci. Technol. A6(6), 3154

Dia87 Diadiuk V , J N Walpole and Z L. Liau 1987, Topical Meeting on Semiconductor lasers(Optical Society of America, Washington, DC) Technical Digest 6, 91

Dis83 Dislich H. 1983 Journal of Non-Crystalline Solids 57, 371

Dor90 Dore S., 1990, Applied Optics 29, 4026

Dun90 Dunn B , J D Mackenzie, J I Zink, and O M Stafsudd, 1990 SPIE 1328, 174

Dur86 Duran A , C Serna, V Fornes and J M Fernandez Navarro, 1986, Journal of Non Crystalline Solids 82, 69

Elm83 Elmer T H Ceramic Bulletin 62 513

Fab90 Fabes B. D., D. J. Taylor, L. Weisenbach, M. M. Stuppi, D. L. Klein, L. J. Raymond, B. J. J. Zelinski, and D. P. Birnie III, 1990, SPIE 1328, 319

Fei88 Feitelson D. G., 1988, Optical Computing, The MIT Press, Cambridge MA, 393

Fio86 Fiorо C. and R. A. B. Devine, 1986, Physical Review B33, 2972

For83 Forer J. D., S. N. Houde-Walter, J. J. Miceli, D. T. Moore, M. J. Nadeau, D. P. Ryan, J. M. Stagaman and N. J. Sullo, 1983, Applied Optics 22, 407

Fos90 Fosmoe A. G., 1990, Mat. Res. Symp. Proc. 180, 1112

Fra91 Frank M., M. Kufner, S. Kufner, and M. Testorf, 1991, Applied Optics 30, 2666

Gal83 Galeener F. L., A. J. Leadbetter and M. W. Stringfellow, 1983, Physical Review B27, 1052

Gal84 Gallo T. A., C. J. Brinker, L. C. Klein and G. W. Scherer, 1984, Mat. Res. Soc. Symp. Proc. 32, 85

Gar89 Garrett I., 1989, in Principles of Modern Optical Systems, edited by I. Andonovic and D. Uttamchandani, Artech House Inc. MA, 608

Gas76a Gaskell P. H., and D. W. Johnson, 1976, Journal of Non-Crystalline Solids 20, 153

Gas76b Gaskell P. H., and D. W. Johnson, 1976, Journal of Non-Crystalline Solids 20, 171

Góm86 Gómez-Reino C., J. Liñares, 1986, Applied Optics 25, 1096

Gra88 Grant W. O., 1988, Understanding Lightwave Transmission, Harcourt Brace Jovanovich, New York, 366

Gre80 Gregorka Lisa, and D. T. Moore, 1980, Applied Optics 19, 3418

Hai67 Hair M. L., 1967, in Infrared Spectroscopy in Surafce Chemistry, Marcel Dekker Inc. New York, 315

Hal87 Hall D. G., L. D. Hutcheson., 1987, in Integrated Optical Circuits and Components, edited by L. D. Hutcheson, Marcel Dekker Inc. New York, 403

Ham90a Hamanaka K., H. Nemoto, M. Oikawa, E. Okuda, and T. Kishimoto, 1990, Applied Optics 29, 4064

Ham90b Hamilton M. C., A. E. Spezio, in Guided-Wave Acousto-Optics, 1990, edited by Chen S. Tsai, Springer-Verlag, Berlin Heidelberg, 253

Har90 Haruna M., M. Takahashi, K. Wakahayashi and H. Nishihara, 1990, Applied Optics 29, 5120

Hau90 Haun N. D. S. Kindred, and D. T. Moore, 1990 Applied Optics 29, 4056

Hea83 Heaney J. B. K. P. Stewart, and G. Hass, 1983 Applied Optics 22, 4069

Hec87 Hecht J. 1987 Understanding Fiber Optics Howard W. Sams & Company Indianapolis 450

Hec74 Hecht E. and A. Zajac 1974 Optics Addison-Wesley, Reading MA, 565

Hen85 Hench L. L. 1985 U. S. Patent Application Serial No 07/333, 742

Hen86 Hench L. L. in Science of Ceramic Chemical Processing edited by L. L. Hench and D. R. Ulrich, 1986 Wiley Interscience, New York, 594

Hen88 Hench L. L., S. H. Wang, and J. L. Nogues, 1988, SPIE 878, 76

Hen90a Hench L. L., and J. K. West, 1990 Chem. Rev. 90, 33

Hen89 Hench L. L. M. J. R. Wilson C. Balaban and J. L. Nogues, Feb. 1989, in the Proceedings of the 4th International Conference on Ultrastructure Processing of Ceramics Glasses and Composites, Tucson, AZ

Hen84 Hench L. L., and D. R. Ulrich eds, 1984, Ultrastructure Processing of Ceramics, Glasses, and Composites, Wiley-Interscience, New York, 564

Hen90b Hench L. L., and W. Vasconcelos, 1990, Annu. Rev. Mater. Sci. 20, 269

Hsi79 Hsieh C. K. and K. C. Su, 1979 Journal of Solar Energy Science and Technology 22, 37

Hut87 Hutcheson L. D., 1987, in Integrated Optical Circuits and Components, edited by L. D. Hutcheson, Marcel Dekker Inc. New York, 403

Iga82a Iga K., 1982 Applied Optics 21, 1024

Iga84 Iga K., Y. Kokubun, M. Oikawa, 1984 Fundamentals of Microoptics, 22

Iga82b Iga K., Masahiro Oikawa S. Misawa, Junichi Banno, and Y. Kokubun, 1982 Applied Optics 21, 3456

Ile79 Iler R. K. 1979, The chemistry of Silica, Wiley New York, 729

Ile86 Iler R. K. 1986 in Science of Ceramic Chemical Processing, edited by L. L. Hench and D. R. Ulrich, 1986, Wiley Interscience New York, 594

Ish90 Ishikawa A. M. Izutsu, and T. Sueta, 1990, Applied Optics 29, 5064

Jah89 Jahns J. and A. Huang 1989 Applied Optics 28, 1602

Jah90 Jahns J. and S. J. Walker 1990 Applied Optics 29, 931

Jew90 Jewell J. L. S. L. McCall Y. H. Lee, A. Scherer, A. C. Gossard and J. H English, 1990 Applied Optics 29, 5050

Kaw80 Kawazu M., and Yukio Ogura 1980 Applied Optics 19, 1105

Kin90a Kindred D. S. 1990 Applied Optics 29, 4051

Kin90b Kindred D. S., J. Bentley, and D. T. Moore, 1990 Applied Optics 29, 4036

Kin88 Kindred D. S., and D. T. Moore, 1988 Applied Optics 27, 492

Kin90c King T. A., 1990 SPIE 1328, 474

Kin92 King T. A. 1992 Chemical Processing of Advanced Materials, L. L. Hench and J. K. West, eds., Chapter 90 J. Wiley and Sons, New York

Kir88 Kirk C. T., 1988, Physical Review B 38 No. 2, 1255

Koi86 Koike Y., Y. Sumi, and Y. Ohtsuka 1986, Applied Optics 25, 3356

Koi88 Koike Y., Y. Takezawa, and Y. Ohtsuka, 1988, Applied Optics 27, 486

Kok82 Kokubun Y. and K. Iga 1982 Applied Optics 21, 1030

Kon90 Konishi S., 1990, SPIE 1328 160

Kro84 Krol D. M. and J. G. van Lierop, J. Non-Cryst. Solids 63, 131

Lam82 Lama W., 1982 Applied Optics 21, 2739

Leg88 Leger J. R. M. L. Scott, and W. B. Veldkamp, 1988, Appl. Phys. Lett. 52, 1771

Lei91 Lei S., Dounan Zhuang, and Kewu Wang, 1991, SPIE OE Reports No. 94, 3

Li91a Li H., and R. C. Bradt 1991, Materials Science and Engineering A142, 51

Li91b Li H., and R. C. Bradt, 1991, Proceedings of International Symposium on Ceramics Yokohama Japan, to be published

Lia88 Liau Z. L., V. Diadiuk, J. N. Walpole, and D. E. Mull, 1988, Appl. Phys. Lett. 52, 1859

Lia89 Liau Z. L., V. Diadiuk, J. N. Walpole and D. E. Mull 1989, Appl. Phys. Lett. 55, 97

Liu91 Liu S. 1991, Ph.D. Dissertation, University of Florida, Gainesville

Liu89 Liu Y. S., 1989 In Laser Microfabrication edited by D. J. Ehrlich and J. Y. Tsao, Academic Press New York 587

Luc87 Lucovsky G., M. J. Mantini, J. K. Srivatsa, and E. A. Irene 1987, J. Vac. Sci. Technol. B5(2), 530

Mac82 Mackenzie J. D., 1982, J. Non-Cryst. Solids 48, 1

Mac84 Mackenzie J. D., 1984, In Ultrastructure Processing of Ceramics, Glasses, and Composites, edited by Hench L. L. and D. R. Ulrich, Wiley-Interscience, New York, 564

Mac88 Mackenzie J. D., 1988, J. Non-Cryst. Solids 100, 167

Mac90 Mackenzie J. D., 1990, SPIE 1328, 2

Mag89 Magdich L. N., and V. Y. Molchanov 1989, Acoustooptic Devices and their Applications, Gordon and Breach Science Publishers, New York, 160

Mat80 Matsushita K., and Minoru Toyama, 1980, Applied Optics 19, 1070

Mat84 Matsuyama I., K. Susa, S. Satoh and T. Suganuma, 1984, Ceramic Bulletin 63, 1408

Mer83 Mergerian D., and E. C. Malarkey, Acousto-Optic Signal Processing, 1983, Edited by Norman J. Berg, John N. Lee, Marcel Dekker Inc., New York und Basel, 481

Mes88 Messerschmidt R. G., and M. A. Matthew, 1988, Infrared Microspectroscopy, Marcel Dekker Inc., New York, 282

Mil69 Miller S. E., 1969, The Bell System Technical Journal 48, 2059

Mis88 Misawa S., and K. Iga, 1988, Applied Optics 27, 480

Mis84 Misawa S., M. Oikawa, and K. Iga, 1984, Applied Optics 23, 1784

Miy80 Miyazawa T., K. Okada, T. Kubo, K. Nishizawa, I. Kitano, and K. Iga, 1980, Applied Optics 19, 1113

Miz85 Mizuno T., J. Phalippou and J. Zarzycki, 1985, Glass Technology 26, 39

Mor90 Moriake B. L., SPIE 1276, 332

Muk88 Mukherjee S. P., 1988, in Sol-Gel Technology for Thin Films, Fibers, Preforms, Electronics and Specialty Shapes, edited by L. C. Klein, Noyes Publications NJ, 407

Nis86 Nishi H., H. Ichikawa, M. Toyama, and I. Kitano, 1986, Applied Optics 25, 3340

Nis80 Nishizawa K., 1980, Applied Optics 19, 1052

Oht88 Ohta K. and H. Ishida, 1988, Applied Spectroscopy 42, 952

Oht74 Ohtsuka Y., T. Senga and H. Yasuda, 1974, Applied Physics Letters 25, 659

Oik82a Oikawa M. and K. Iga, 1982, Applied Optics 21, 1052

Oik82b Oikawa M., K. Iga, and S. Misawa, 1982, Electronics Letters 17, 452

Oik84 Oikawa M., K. Iga, M. Morinaga, T. Usui, and T. Chiba, 1984, Applied Optics 23, 1787

Oik81 Oikawa M. K. Iga, and T. Sanada, 1981, Electronics Letters 18, 316

Oik90 Oikawa M., H. Nemoto, K. Hamanaka, and E. Okuda, 1990, Applied Optics 29, 4077

Ono78 Onoda G. Y., and L. L. Hench eds. 1978 Ceramic Processing Before Firing, John Wiley and Sons New York, 490

Ozi80 Ozisik M. N., 1980, in Heat Conduction Wiley-Interscience, New York, 687

Par86 Park S. C., and L. L. Hench, in Science of Ceramic Chemical Processing, edited by L. L. Hench and D. R. Ulrich, Wiley-Interscience, New York, 1986 594

Par89 Parson N.,1989 in Principles of Modern Optical Systems, edited by I. Andonovic and D. Uttamchandani, Artech House Inc., Norwood MA, 608

Pau84 Pauleau Y. R. Stawski P. Lami, and G. Auvert 1984 in Laser Controlled Chemical Processing of Surfaces, edited by A. W. Johnson, D. J. Ehrlich, and H. R. Schlossberg North-Holland New York, 425

Pav74 Pavlopoulos T. G., and K. Crabtree, 1974 Journal of Applied Physics 45, 4964

Pea69 Pearson A. D., W. G. French, and E. G. Rawson, 1969 Applied Physics Letters 15, 76

Per91 Perry C. C. and X. Li, Feb 1991, 5th Internation Conference on Ultrastructure Processing Orlando, to be published

Pet73 Peterson C. W. B. W. Knight, 1973, Journal of the Optical Society of America 63, 1238

Pha82 Phalippou J. M. Prassas, and J. Zarzycki, 1982, Journal of Non Crystalline Solids 48, 17

Pop88 Popovic Z. D. R. A. Sprague, and G. A. Neville Connell, 1988, Applied Optics 27, 1281

Pra90 Prasad P. N. 1990 SPIE 1328, 168

Rab85 Rabinovich E. M., 1985, Journal of Non Crystalline Solids 71, 187

Ram88 Ramaswamy R. V. T. Chia, R. Srivastava, A. Miliou and J. West, SPIE, Multifunctional Materials 878, 86

Rap87 Rappaz M. B. Carrupt, M. Zimmermann and W. Kurz, 1987, Helvetica Physica Acta 60, 924

Ree84 Rees J D and W Lama 1984, Applied Optics 23, 1715

Rig73 Righini G C V Russo S Sottini and G Toraldo di Francia, 1973, Applied Optics 12, 1477

Ros46 Rosenthal D , 1946 Trans. Am. Soc. Mech Engrs 68, 849

Roy56 Roy R 1956 J. Am. Ceram. Soc. 39, 145

Roy69 Roy R 1969, J. Am. Ceram. Soc. 52, 344

Rud78 Rudolf Kingslake Lens Design Fundamentals, Academic Press, New York 1978

Sak85 Sakka S 1985, Am. Ceram. Soc. Bull. 64, 1463

Sak88 Sakka S H Kozuka and S Kim in Ultrastructure processing of advanced ceramics, edited by J D Mackenzie and D R. Ulrich, John Wiley & Sons New York, 1014

Sam90 Samuels J E., and D T Moore, 1990 Applied Optics 29, 4042

San74 Sanders D M W B Person and L L. Hench 1974 Applied Spectroscopy 28 No. 3, 247

Sar80 Saruwatari M., and T Sugie 1980 Electronics Letters 16, 955

Sat85 Satoh S , K Susa, I Matsuyama, and Suganuma, 1985, J. Am. Ceram. Soc. 68, 399

Sch86 Scherer G W , J. of the American Ceramic Society 69, 473

Sch87a Scherer G W , Journal of Non Crystalline Solids 87, 199

Sch87b Scherer G W Journal of Non Crystalline Solids 89, 217

Sch88 Scherer G W in Ultrastructure processing of advanced ceramics, edited by J D Mackenzie and D R Ulrich, John Wiley & Sons New York, 1014

Sch86 Scherer G W C J Brinker, and E P Roth, Journal of Non Crystalline Solids 82, 191

Sch90 Schmidt H and M Popall 1990 SPIE 1328, 249

Sha89 Shaw D J A J Berry, and T A King 1989, Inst. Phys. Conf. Ser. No.103 Part I, 85

Sha90 Shaw D J , and T A King, 1990, SPIE Vol 1328 474

Shi84 Shih T , 1984 Numerical Heat Transfer, Hemisphere Publishing Corp., Washington 563

Shi90a Shimano T , A Arimoto, and K Muraoka, 1990, Applied Optics 29, 5060

Shi90b Shingyouchi K., and S Konishi, 1990 Applied Optics 29, 4061

Shi87 Shiono T K Setsune O Yamazaki, and K Wasa, 1987, Applied Optics 26, 587

Sim53 Simon I and H O McMahon, 1953, The Journal of Chemical Physics 21, 23

Sla89 Slaoui A F Foulon M Bianconi L. Correra, R Nipoti R. Stuck, S Unamuno E Fogarassy, and S Nicoletti 1989 Materials Research Society Symposium Proceedings 129, 591

Slo90 Slocumb R. W JR. 1990 Master Thesis, University of Florida, Gainesville

Sny66 Snyder L. R.,and J W Ward The Journal of Physical Chemistry 70, 3941

Soc86 Sochacki J., 1986, Applied Optics 25, 235

Sop78 Sopori B., and W S C. Chang, 1978, IEEE J. of Quantum Electronics QE 14, 323

Str91 Streibl N U Nolscher, J Jahns, and S Walker, 1991, Applied Optics 30, 2739

Sus86 Susa K I Matsuyama S Satoh and T Suganuma, 1986 Journal of Non-Crystalline Solids 79, 165

Swa85 Swanson G J, and W B Veldkamp, 1985, Optical Engineering 24, 791

Tak86 Takada H, and K Masuno, 1986, Optical Fiber Transmission, edited by K Noda, Elsevier Science Pub North-Holland, Amsterdam The Netherlands 307

Tal86 Tallant D R B C Bunker, C J Brinker, and C. A Balfe 1986 Mat. Res. Soc., Symp. Proc. 73, 261

Tat84 Tatsumi K. T Saheki T Takei and K. Nukai, 1984 Applied Optics 23, 1742

Ter87 Teruhiro Shiono Kentaro Setsune, Osamu Yamazaki, and Kiyotaka wasa, 1987, Applied Optics 26, 587

Tom80 Tomlinson W J 1980 Applied Optics 19, 1117

Tou70a Touloukian Y S and E. H Buyco 1970, in Thermophysical Properties of Matter, The TPRC Data Series 2, 202

Tou70b Touloukian Y S, R W Powell, C Y Ho and P G Klemens, 1970, in Thermophysical Properties of Matter The TPRC Data Series 2, 922

Toy82 Toyama M and M Takami, 1982 Applied Optics 21, 1013

Uch69	Uchida T., M. Furukawa, I. Kitano, K. Koizumi, and H. Matsumura, 1969, IEEE J. of Quant. Electron. QE-5, 331
Uch70	Uchida T., M. Furukawa, I. Kitano, K. Koizumi, and H. Matsumura, 1970, IEEE J. of Quant. Electron. QE-6, 606
Ulr85	Ulrich D. R., Ceramic Bulletin 64, 1444
Ulr88	Ulrich D. R., in Ultrastructure processing of advanced ceramics, edited by J. D. Mackenzie and D. R. Ulrich, John Wiley & Sons New York, 1014
Vas89a	Vasconcelos W. L., 1989, Ph.D. Dissertation, University of Florida, Gainesville
Vas89b	Vasconcelos W. L., R. T. DeHoff, and L. L. Hench, Feb. 1989, in the Proceedings of the 4th international Conference on Ultrastructure Processing of Ceramics, Glasses and Composites, Tucson, AZ
Vei90	Veiko V. P., E. B. Iakovlev, G. K. Kostyuk, V. A. Chuiko, P. A. Fomichov, V. S. Kozhukharov, 1990, SPIE 1328, 201
Vei91	Veiko V. P., Feb. 1991, 5th Internation Conference on Ultrastructure Processing, Orlando, to be published
Wad81	Wada O., S. Yamakoshi, M. Abe, Y. Nishitani, and T. Sakurai, 1981, IEEE J. of Quant. Electron. QE-17, 174
Wal91	Wallace S., 1991, Ph.D. Dissertation, University of Florida, Gainesville
Wal86	Walrafen G. E., and M. S. Hokmabadi, 1986, in Structure and Bonding in Noncrystalline Solids, edited by G. E. Walrafen and A. G. Revesz, Plenum Press New York, 449
Wan88	Wang S., 1988, Ph.D. Dissertation, University of Florida, Gainesville
Wes90a	West J. K., and S. Wallace, 1990, Mat. Res. Soc. Symp. Proc. 180, 255
Wes90b	West J. K., B. F. Zhu, Y. C. Cheng, and L. L. Hench, 1990, Journal of Non-Crystalline Solids 121, 51
Whi90	Whitehurst C., D. J. Shaw, and T. A. King, 1990, SPIE 1328, 183
Wil89a	Wilson M. J. R., 1989, Master Thesis, University of Florida, Gainesville
Wil89b	Wilson M. J. R., and L. L. Hench, Feb. 1989, in the Proceedings of the 4th International Conference on Ultrastructure Processing of Ceramics, Glasses and Composites, Tucson, AZ
Woo88	Wooton D. L., and D. W. Hughes, 1988, edited by Messerschmidt R. G., and M. A. Matthew, Infrared Microspectroscopy, Marcel Dekker Inc. New York, 282
Yam85	Yamada Y., M. Kawachi, M. Yasu, and M. Kobayashi, 1985, Applied Optics 24, 454

Yam83 Yamagishi T K. Fujii and I Kitano, 1983 Applied Optics 22, 400

Yam80 Yamamoto N , and K. Iga, 1980, Applied Optics 19, 1101

Yam82 Yamamoto N, H Nishi K Nishizawa and I Kitano, 1982, Applied Optics 21, 1021

Yam88 Yamane M , 1988 in Sol Gel Technology for Thin Films, Fibers, Preforms Electronics, and Specialty Shapes, edited by L. C. Klein, Noyes Publications NJ, 407

Yam91 Yamane M Feb. 1991 5th International Ultrastructural Processing Conference, at Orlando FL, to be published

Yam86 Yamane M , J B Caldwell and D T Moore, 1986, Journal of Non-Crystalline Solids 85, 244

Yam90 Yamane M A Yasumori, M Iwasaki and K. Hayashi, 1990, SPIE 1328, 133

Yol75 Yoldas B E , 1975, Bull. Am. Ceram. Soc. 54, 286

Yon58 Young G J , J. of Colloid Science 13, 67

Zar84 Zarzycki J 1984 in Ultrastructure Processing of Ceramics, Glasses, and Composites, edited by Hench L L., and D R Ulrich, Wiley-Interscience, New York 564

Zel91 Zelinski B J J , B D Fabes, L Weisenbach, and T C Zaugg Feb 1991, 5th Internation Conference on Ultrastructure Processing, Orlando, to be published

Zhu88 Zhu X., and K. Iga, 1988, Applied Optics 27, 468

Zhu89 Zhu B F , G F Wang and L L. Hench Feb. 1989, to the Proceedings of the 4th international Conference on Ultrastructure Processing of Ceramics, Glasses and Composites, Tucson, AZ

BIOGRAPHICAL SKETCH

Taipau Chia was born on January 13, 1962, in Keelung, Taiwan, Republic of China. She graduated from Municipal Chung-Shan Senior High School in June 1979 She attended National Taiwan Normal University from 1979 to 1984 with a physics major Before graduation, she entered Taipei Ho-Pin Junior Middle School as a practice teacher from August 1983 to June 1984 In June 1984 Taipau received her Bachelor of Science degree. She worked as a teaching assistant in the Department of Physics of National Taiwan Normal University from July 1984 to July 1986.

Taipau married Shanshin Ton on June 8, 1986, in Hsin-Chu, Taiwan R O C.

She began her graduate studies at the University of Florida since August 1986. She earned a Master of Science degree in materials science and engineering, and she is now working to fulfill the requirements for the doctorate degree.

She is a member of Materials Research Society, The International Society for Optical Engineering, and the International Honorary Metallurgical Society

I certify that I have read this study and that in my opinion it conforms to acceptable standards of scholarly presentation and is fully adequate, in scope and quality, as a dissertation for the degree of Doctor of Philosophy

Larry L. Hench, Chairman
Graduate Research Professor of Materials
Science and Engineering

I certify that I have read this study and that in my opinion it conforms to acceptable standards of scholarly presentation and is fully adequate, in scope and quality, as a dissertation for the degree of Doctor of Philosophy

David E Clark

David E Clark
Professor of Materials Science and Engineering

I certify that I have read this study and that in my opinion it conforms to acceptable standards of scholarly presentation and is fully adequate, in scope and quality, as a dissertation for the degree of Doctor of Philosophy

Rolf E Hummel
Professor of Materials Science and Engineering

I certify that I have read this study and that in my opinion it conforms to acceptable standards of scholarly presentation and is fully adequate, in scope and quality, as a dissertation for the degree of Doctor of Philosophy

Joseph H. Simmons

Joseph H Simmons
Professor of Materials Science and Engineering

I certify that I have read this study and that in my opinion it conforms to acceptable standards of scholarly presentation and is fully adequate, in scope and quality, as a dissertation for the degree of Doctor of Philosophy.

Chung K. Hsieh
Professor of Mechanical Engineering

This dissertation was submitted to the Graduate Faculty of the College of Engineering and to the Graduate School and was accepted as partial fulfillment of the requirements for the degree of Doctor of Philosophy.

August 1992

Winfred M. Phillips
Dean, College of Engineering

Madelyn M. Lockhart
Dean, Graduate School